Development of a Standard Small Satellite Research Platform for Life Sciences Research

Senior Design 2
Final Project Document and Group Identification
University of Central Florida
CREOL, the College of Optics and Photonics
Department of Electrical Engineering and Computer Science

Group 9

John Semmen	Photonics
Brandon Triplett	Photonics
Nicholas Hubbard	Electrical Engineering
Jennifer Starling	Computer Engineering
NASA	Sponsor

April 27, 2021

Contents

1 Executive Summary

The goal of this project is the development of a standard small satellite research platform for Life Sciences research. Our project will be to develop a module that is in the CubeSat range of sizes. This will be a sensor suite designed to fit a 6U CubeSat platform which measures 60cm x 10cm x 10cm. We will not be launching the final prototype and so our demonstration will be based around what can be accomplished on land and within our budget. The prototype itself will contain an ecosphere which is a closed self-sustaining ecological environment consisting of active micro-organisms, small shrimp, algae, and bacteria. With cooperation from NASA, the final prototype should have features that demonstrate technical and economically feasible ways to maintain thermal balance, observe, and characterize the reaction to and survival of the contained life in a space radiation environment.

This device will be researched as if the end product would be launched and monitored in orbit by NASA but developed and built within the realistic time and budgetary constraints of a senior design project. Even though the budget is beyond a typical project with the financial and advisory support from Kennedy Space Center, we are not in the same range of an actual research project that could use the radiation shielding, solar panels, or top level components. Since the project is designed to be used by NASA who already have extensive experience in operating satellites in space, sacrifices will be made by keeping our main focus on the sensors themselves.

The prototype will be shaped in an elongated, rectangular cuboid. Each face will have a different set of sensors, camera, power, or other component part of the sensor suite. These sensor filled faces will be built around our ecosphere that contains the living organisms. Our primary challenge will be fitting all of our proposed sensors into such a small, contained space. It will be powered by a battery, contain a heater to prevent the ecosphere from reaching life threatening temperatures, and a transmitter to report our data back to an earth station.

The data collected by the sensor suite will be based on biological and chemical components that have been determined to be vital to the survival of the ecosphere. The selected members of the ecosystem are based on NASA's goal to develop habitats and flight systems capable of producing high yield plants. Algae and other living organisms can be valuable fertilizer and allowing this life to survive in space is vital to the future of human kind spending extended time off planet without as much of a need for constant resupply.

The satellite will be using an on-board computer in order to coordinate the use of the sensors, monitor the temperatures, take the readings, log the data, and transmit back to our earth station. Since there is no launch involved, our earth station will be a member of our team located 500 meters away from the satellite in order to test its communication capabilities. A successful demonstration will be for the device to run through a reading of every component, log the measurements, and then transmit

through the antenna to be read on the so called earth station. FCC regulations require the ability to cease transmissions when requested and so a terminate transmissions program will be written into the computer and demonstrated as well.

Transmission of the sensor readings is paramount to the project being useful for research. Heating the ecosphere to avoid the freezing of the organisms may be even more important as dealing with the in-space radiation environment is the true goal of NASA. Although radiation hardened components and radiation shielding is outside of our budget, we can still attempt to demonstrate a way to deal with the extreme cold while in Earth's shadow. During the loop of sensor readings, the temperature will also be measured. If the temperature reaches a dangerous level, the sensors will be shut off by the computer and the heater will be turned on until a safe temperature is reached. For the purposes of our project, this will be tested and demonstrated by surrounding the satellite in a tub of ice or placed in a freezer. A successful demonstration will be proving the device can avoid life threatening freezing temperatures.

2 Project Description

Here we present the overview of our project including: our motivation, what we wish for to achieve with the project, a summary of each component that we will develop for the project.

2.1 Motivation

Our platform will be designed and built with the intention of being a remote controlled research vessel. It seeks to gain an understanding of how animals react to micro gravity environments. This is essential to understanding how humans will react to micro-gravity environments, which is the key take away from the potential research. Additionally, the research platform could potentially be used to gather data on algal-based aquatic regenerative systems. This is important for understanding biomass production, which can be used as food or fertilizer sources in space.
Our motivation then is to pursue a high effort senior design project, for educational purposes, that may also serve the purpose of providing a foundation for a real NASA experiment. This device will be researched as if the end product would be launched and monitored in orbit by NASA but developed and built within the realistic time and budgetary constraints of a senior design project. Even though the budget is beyond a typical project with the financial and advisory support from Kennedy Space Center, we are not in the same range of an actual research project that could use the radiation shielding, solar panels, or top level components. Since the project is designed to be used by NASA who already have extensive experience in operating satellites in space, sacrifices will be made by keeping our main focus on the sensors themselves.

For our project to succeed at being useful for NASA, the overall size and body of the package will be designed to fit the dimensions of a typical CubeSat range small satellite. Remotely enabled imaging will be done to consider the color, particulate settling, bubbles, and culture medium transparency in an effort to infer the state of the system and the changes to the health of the Ecosphere while exposed to an extraterrestrial environment. The data will be collectively monitored to determine whether the sustainability is being affected by in-house dependency of the various water quality parameters or the external factors of the microgravity and radiation environment. Upon completion of our project we hope the information obtained will give a better baseline of what research needs to be done to develop a sustainable and thriving closed microalgal-based microcosm that can be used by astronauts.

2.2 Goals & Objectives

Understanding how animals react to microgravity environments is essential to understanding how humans will react to microgravity environments. NASA is interested in using animals to study living species that react in space, so that experiments can be

conducted without having to interfere with astronauts' daily activities. Algal-based aquatic regenerative systems produce a higher biomass per square meter than do terrestrial plant systems [77]. This is ideal for efficient biomass production, which can be used as food or fertilizer sources, in space. Additionally, aquatic regenerative systems reuse a limited volume of water and are already isolated from the atmosphere [32]. Our goal is to develop a sensor suite that monitors a self-sustaining, hypersaline, Closed Ecological Life Support System (CELSS) of brine shrimp, algae, and possibly other microorganisms.
This suite will use electronic and optical sensors to observe the following:

- dissolved oxygen
- specific gravity/salinity
- ammonia (NH_3)
- average temperature
- algae color

The accuracy and precision to which these measurements are expected to be taken will be outlined in the next section. Based on our research, these characteristics are vital to understanding the health of the CELSS. They will be most informative to biologoical researchers learning about the artemia's expereience in a zero gravity environment. This information will be fundamental to understanding how humans, or living organisms in general, survive in space.

Our choice for the measurement of dissolved oxygen is the optode sensor. We chose this sensor over the electrochemical oxygen sensor because optodes are less sensitive to fowling than electrochemical sensors are. Although their response is influenced by salinity, the response is linear and can be compensated with a formula given the current salinity and temperature of the water [82]. Optodes are based on a phenomena called luminescence quenching, where the luminescence exhibited by a material is influenced by the presence of a quencher, which results in more rapid depletion of its excited state population. The optics and electronics required to build such a sensor are low cost [27]. The sensor simply consists of blue LEDs, silicon photodiodes, a glass substrate, a gas-permeable silicon black layer [81], blue and red filters, and a sensing material. Such sensing materials, being oxygen-quenchable luminophores, which are commercially available, may be highly luminescent ruthenium(II) complexes with diimine ligands, and phosphorescent platinum and palladium porphyrins [48]. These materials can be obtained from Frontier Scientific [55] and sigma aldrich [4] [13].

We are going to develop our prototype optode sensor based off of the design of optode as presented by Tengberg et al.[81] and as seen in figure 52, however we will consider ruthenium-based sensors [10]. We expect that the sensing material will ultimately determine the cost and quality of our sensor.

Our choice to measure salinity will be a refractometer. Although salinity of the water is conventionally measured by using a hydrometer to find the specific gravity of the water [41], because a hydrometer is based off of buoyancy, such a device is not considered for use in microgravity conditions. Methods of measurement of the salinity of water including the optical refraction method, the use of an optical fiber grating, a technique involving optical interference, and a technique that takes advantage of the surface plasmon effect [72]. We have chosen to use a refractometer, as we expect such an approach to be both within our budget, viable to build ourselves, and lightweight enough to package with the rest of the sensor suite. A custom design involving a laser, series of prisms, and a detector will be used. The detector will ideally be position-sensitive detector (PSD).

The refractometer is a tool used to measure refractive indices of some materials. For this application, we will exploit the fact that water's salinity and it's refractive index have a linear relationship. The more salt in the water, the higher it's refractive index. The proposed design is to pass water through a filter and into an external chamber where it will sit meet the interface of the prism. The higher refractive index of the water at the prism interface will slightly alter the angle at which a laser beam refracts through it. The displacement of that laser beam can then be measured with a one-dimensional CCD line array sensor, which can be used to calculate the water's refractive index, and thus it's salinity.

The ammonia and algae color will be measured via camera monitoring of a passive sensor or the algae itself, respectively. The temperature will be taken with a thermometer.

Ultimately, our goal of this project is to show a proof of concept for all of these goals and requirements, that can be built into a smaller, more efficient and robust system for a real experiment.

2.3 Specifications

2.3.1 Overall platform

- Should fit the dimensions of a 6U cubesat (approximately 60x10x10 cm).
- Should weigh less than: 10kg.
- Should operate off of battery power.
- Should transmit data.
- Should take measurements of dissolved oxygen, salinity, ammonia, water temperature, and images.
- Should cost less than $1600 to build.

Component	Requirement Specifications
Ammonia sensor	• Should be able to detect ammonia levels at a 0.5 mg/L concentration. • Should cost less than $35.
Temperature sensor	• Should have a minimum temperature resolution of 0.25 °C. • Should be accurate within 0.25 °C. • Should cost less than $25.
Refractometer	• Overall: Distinguish fresh water from salt water. Far-reach goal: reach 5 PPT. salinity resolution (about 0.001 change in refractive index). • Detector: Minimum pixel size of about 10 micron. • Laser: 650 micron laser module with a minimized spot size. • Prism: Refractive index of 2+ (ZnSe).
Optode	• Should cost less than $200 to build. • The optode will detect the oxygen levels within 100 nanomoles.
Camera	• Should be smaller than $64cm^3$. • Should be able to interface with the MCU. • Should cost less than $100 to build.
Thermal Camera	• Should have 0.25 °C temperature sensitivity resolution. • Should have 720p resolution to distinguish shrimp. • Should cost less than $150 to build.

Table 1: Ammonia strip indicators to be interpreted by colormetry

Component	Requirement Specifications
Microcontroller	• Should be able to encode data and images for transmission. • Should have enough Input/Output pins for the sensor array. • Should be able to hold data from sensors and camera in storage before transmission.
Transmitter	• Should operate with less than 1 Watt. • Should transmit 500 meters. • Should cost less than $50 to build.
Receiver	• Should operate with less than 1 Watt. • Should have sensitivity of -140dBm or better. • Should cost less than $50 to build.
Battery	• Should provide 12 Volts or better. • Should be able to operate the system for 1 hour. • Should cost less than $50 to build.
Heater	• Should be able to prevent freezing in ecosphere. • Should be able to operate under battery power. • Should cost less than $50 to build.

Table 2: Ammonia strip indicators to be interpreted by colormetry

For the refractometer, we showed though calculation in section 3.6.3 and experiment in section 7.2 that with a single prism setup a change in deviation that results from a change in 0.001 refractive index, will be hard to notice. A change of 5 PPT salinity will result in only approximately 0.075°deviation. For this reason, a change of about 5 PPT salinity will be a far-reach goal for this measurement. Many limiting factors such as ”noise” from particles in the water and movement will also disturb the beams placement on the detector. For the sake of proof of concept, the required specification

will be to demonstrate ability to distinguish salt water from freshwater.

2.3.2 Selected Demonstrations

For Senior Design 2 demonstrations we will show the following:

- We will demonstrate the ability to take the five suggested measurements (dissolved oxygen, salinity, ammonia (NH_3), average temperature, algae color) by demonstrating a working refractometer, optode, thermometer, and camera and record that data to the systems computer.
- The refractometer will distinguish saltwater from freshwater (an estimated 0.006 difference in refractive index).
- The prototype will be placed in a freezer where the computer will detect freezing temperatures and turn on the heater to prevent the aquarium from freezing, at environment temperatures below 0°C.
- The transmitter will successfully send and receive data at a range of 100 meters.

Additionally, the following demonstrations will be attempted as an added bonus:

- The prototype will be placed in a freezer where the computer will detect freezing temperatures and turn on the heater to prevent the aquarium from freezing, at environment temperatures below 0°C.
- The computer will receive a cease transmissions signal and shut off the transmitter as required by the FCC.
- The optode will detect the oxygen levels within 100 nanomoles.

2.4 House of Quality

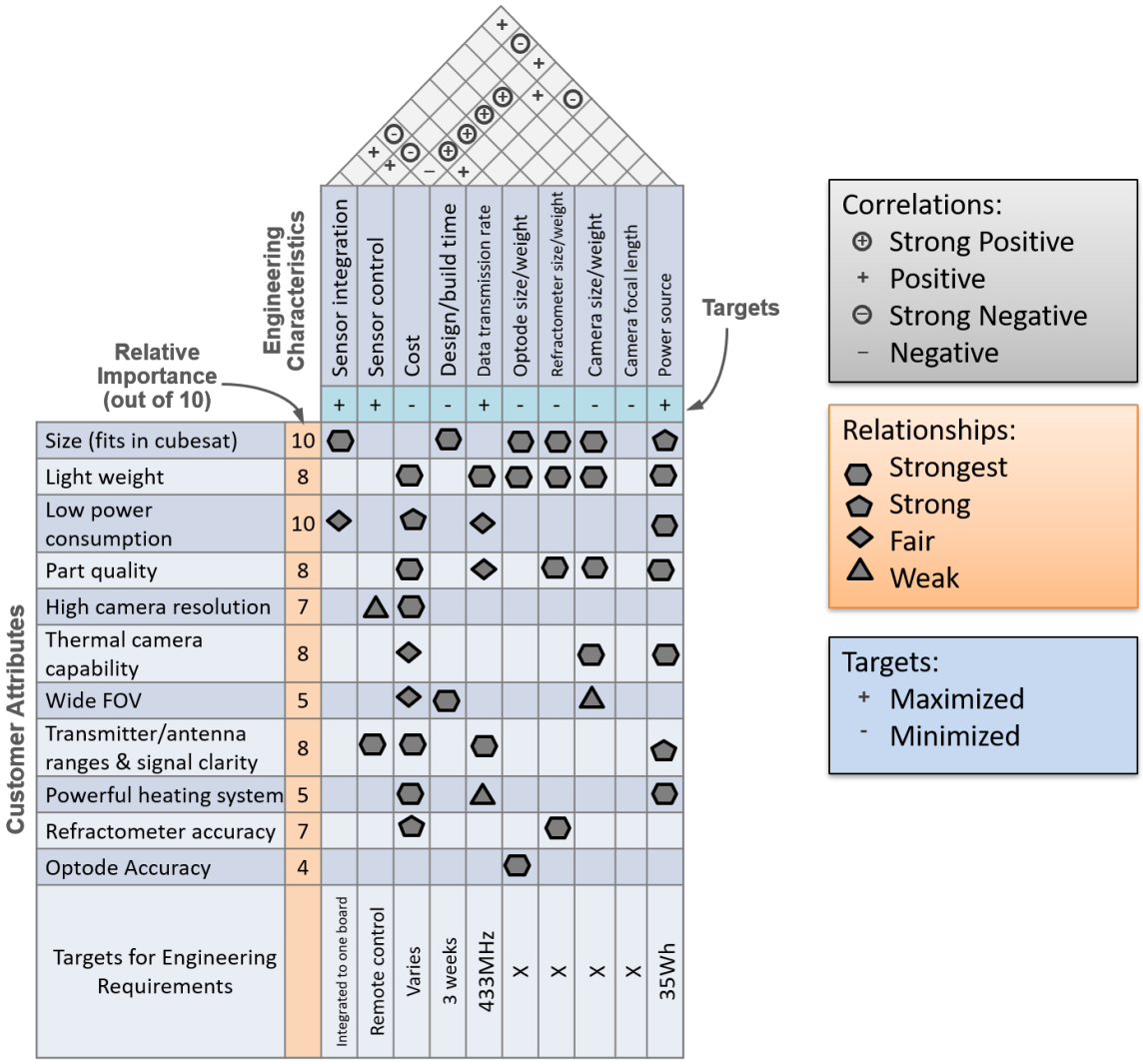

Figure 1: Quality of House

Figure 1 is our current House of Quality diagram. As this is an interdisciplinary project we will be working with our customer and sponsor, NASA, throughout the time frame. The initial ask from NASA is intentionally very open ended to allow for our group to come up with a more imaginative solution. We are currently operating under the goal of fitting the project into a 6U style sat cube. As we cannot test in space orbit, we are developing the prototype for realistic testing ranges. The listed engineering specifications are based on current research and are subject to change as per feedback from NASA.

3 Research and Parts Selection

3.1 Background: Artemia and Ecosystem

We begin with a description of the system that we wish to monitor. It is imperative to understand every element of a marine ecosystem that may indicate its overall health, in order to design a suite of sensors that successfully serves its purpose of characterizing the system as a whole. We must also understand the implications that our system parameters have on the health of our brine shrimp and algae when the parameters are above or below their target value by a certain margin. By knowing this, we may also observe the shrimp and algae directly, in order to see their response as corresponding to the changes in the system parameters that we have monitored. A discrepancy between our parameters relating to an expected response by the shrimp and algae, and the observed response of the shrimp and algae, may serve as a tool for identifying unique effects that the extraterrestrial environment has on the marine ecosystem. Understanding the test subject is key to understanding the design requirements of our customer.

3.1.1 Importance of Artemia in an Extraterrestrial Environment

As occupation of non-earth locations will no doubt become more and more common in the future, a system in which a bio-regenerative food source is available must be established [90]. Any raw materials available will be recycled waste. Algae may double as a way of converting carbon dioxide into oxygen while also processing waste into more usable forms, by allowing the algae itself to be consumed, or by serving as a food source for Artemia. Artemia may then serve as a food source for fish in a aquaponics system, allowing for biomass to be converted to a state that is once again edible. The nutritional value of Artemia will vary among strains, especially for marine organisms [54]. Due to their versatility however, Artemia are commercially exploited in the Great Salt Lake in Utah, chiefly for aquaculture purposes [40].

3.1.2 Flora & Fauna in a Marine Environment

We must consider how various elements of a marine ecosystem are parametrized. This is so that we may later measure these parameters in order to characterize it. The underlying processes in a marine ecosystem are quite complex. However, we may describe the next contributions of these processes in terms of the movements of organic materials, dissolved gasses, and salts within the system.

3.1.3 The Nitrogen Cycle

Nitrogen in the atmosphere is an inert gas that cannot be utilized by all but a few organisms who have the ability to convert it into a chemical compound that can be used by plants and animals [26]. Nowadays, we observe algae blooms as a result of excessive runoff of organic nitrates and lead to an imbalance of oxygen as a result of excessive microbial activity. These excessive runoffs are due to the large-scale

manufacturing of synthetic fertilizers that has made nitrogen highly available in its plant-ready form, and are a great example of how a system can be imbalanced by the excessive concentration of one component of the system.

Nitrogen and nitrification plays a critical role in any biological ecosystem on earth. Nitrification is a series of reactions in which certain microorganisms will oxidize ammonium (NH_4^+) to nitrite (NO_2^-) or nitrite into nitrate (NO_3^-). Ammonium ions result when microorganisms decompose dead plants an animals. Nitrates can then be consumed by organisms such as algae and higher plants to repeat the processes. This cycle is fundamental in any ecosystem on earth, and the presence of microorganisms, plants, and animals are all simultaneously required in order to allow the process to take place. An imbalance in the nitrogen cycle may lead to reduced oxygen levels [29], and the overproduction of free ammonia in the water, which is toxic to animals in the system. If the nitrogen cycle cannot take place, the mutual reliance that plants, animals and microorganisms all have on each other would not be satisfied, as this reliance is in part through the nitrogen cycle. Nitrogen is used as a fundamental ingredient to a great deal of biological compounds, thanks to its ability to bind with hydrogen, oxygen and a number of other atoms.

3.1.4 Dissolved Oxygen

Dissolved oxygen is a critical component of any aquatic ecosystem, as it serves as part of the life support for aquatic animals. However, dissolved oxygen will be related to the presence of oxygen-consuming animals, and an excess of biological material without a subsequent excess of oxygen production from CO2 thanks to plants will result in an excess of population in animals in the ecosystem [50]. This is imbalance will result in dangerously low concentrations of oxygen present in the water, and the ecosystem will become a hypoxic environment, effectively removing the animals' ability to breath, and killing them. Mass mortality of marine animals caused by the lack of oxygen has been reported in a number of systems, and is often related to a nutrient imbalance [30]. With that being said, oxygen is both an indicator of environmental imbalance, and safety of the environment for animals to live in. In a closed environment, compromise of the oxygen-dependent species will remove CO_2 production that the flora are dependent on, and this will sabotage the entire ecosystem.

3.1.5 Salinity

Osmoregulation is the control of water and salt concentrations in an organism, and it is critical for an organism's survival in an environment of a certain salt concentration. In aquatic organisms, osmoregulation is a fundamental limitation in the environment that they are able to inhabit, according the salinity of the aquatic environment.

Plants and animals have evolved to deal with environments in which salinity levels far exceed that of seawater, such that adaptations allow the plants and animals to

better regulate their internal osmotic pressure [44]. An environment in which the salt concentrations have exceeded that of seawater is termed hypersaline. Osmoregulatory mechanisms result as plants and animals naturally evolve in order to survive environments of high concentrations of salinity. These mechanisms are a result of complex interaction, and very few plants and animals have successfully developed the mechanisms necessary to survive in hypersaline environments. In hypersaline environments were Artemia (brine shrimp) have adapted to survive, the abundance of certain phytoplankton which serve as food for artemia will vary with salinity. The reduction of diversity of phytoplankton will reduce the nutrients available to the Artemia, having a significant affect on the ecosystem [52]. Also, despite their abilities to survive hypersaline environments, Artemia will still become stressed in hypersaline environments, and a part of their adaptation to survive the environment is to make cysts instead of live offspring, that will better survive the harsh environment until it becomes more survivable at a later time [85].

3.1.6 Artemia

Artemia (brine shrimp) are the sole macro-planktonic inhabitants of salty lakes, also known as brine shrimp [40]. They are a micro-crustacean that has adapted to harsh conditions resultant from a hypersaline environment: an aquatic environment who's salt concentration is higher than that of sea water. A harsh environment is defined in this context as an environment that has not existed long enough to allow for a wide variety of organisms to evolve and adapt to the environment [70]. As Artemia have adapted to the extremely harsh conditions of hypersaline environments, they are considered a model animal extremophile by virtue of satisfying the relevant definition of extremophile. They withstand up to 10 times the salt concentration of ordinary seawater, and are tolerant to extreme variations in oxygen concentrations [5]. As salinity increases, dissolved oxygen in the water is reduced [60]. High salinity in the water reduces the species diversity within the environment, and simplifies the structure of the system.

3.1.7 Cyst Production

Artemia possess the ability to produce highly resistant embryo under extremely critical conditions, called cysts. They are capable of surviving in harsh environments including anoxia, heat, cold, desiccation, UV radiation, and food deprivation. [58] Cysts will enter diapause, which is a reversible state of dormancy. [57] Artemia cysts effectively store the genetic memory of the artemia, and are arguably the most resistant of all animal life history forms to environmental stress. They aid as both genetic reservoirs to increase genetic variability, and as survival vehicles for surviving periods of extreme conditions.

The subsequent termination of diapause in Artemia is also mainly a response to environmental factors [85]. As such, cyst production serves as an excellent indicator of the presence of stressors in the environment.

3.1.8 Genetic Mutation

Artemia are distributed globally in hypersaline lakes, temporary desert ponds, coastal lagoons, saltern ponds, pools and saltmarshes. Accumulation of random variations due to genetic mutations eventually evolve Artemia [86]. These random mutations are sorted by natural selection out of necessity for survival, requiring favorable (or more survivable) traits pertinent to the environment that the Artemia exist within. This explains why Artemia isolated in hypersaline lakes that exhibit vastly different environmental variation from each other show considerable genetic differences. They will finely adapt to their local environment. [85] Genetic diversity is important for the fitness of the population, as low levels of genetic variation may result in a decrease in the population's ability to adapt to an environmental crisis [6]. Noticeable differences between distinct species of Artemia were found in their lifespan, lethal time, 21-day survival, and reproductive traits [15] Given their ability to maintain a high genetic variation, Artemia serve as a good model to study adaptation and speciation.

3.1.9 Indicators of their health

Presence of food, oxygen, high or low salinity, and temperature all play a role in stressing Artemia [40]. The most visible indicator from the Artemia themselves is the switching of females' reproductive mode between free-swimming nauplii and cysts.

Low brood sizes and lipid indices have been related to limitations in food availability of Artemia [60]. Increased salinity has been observed to inhibit cyst hatching. Below a threshold food concentrations, female Artemia have been found to be prevented from dedicating sufficient resources to reproduction, which will lead to a long inter-brood interval as the eggs are withheld in the brood sacs.

3.1.10 Food source, waste

The main food source of Artemia is algae scraped from the bottom of the water column [60]. The composition of this algae affects the growth, reproduction rates, brood size, density, lipid index, and cyst yield that is resultant. However, Artemia are non-selective filter feeders and will also feed on any article within the appropriate size range, including bacteria, detrius and other plankton [70].
The interaction between Artemia and phytoplankton population in hypersaline environments displays a reciprocal trend. [60]
Artemia have evolved to favor an abundance of bacteria, protozoa and algae which are the basis of the Artemia diet. [5]

3.1.11 Net contribution and dependence on nitrogen cycle

The nitrogen cycle as we see it in the Great Salt Lake consists of the use of inorganic nitrogen compounds resultant from algae, and the consumption primarily by brine shrimp [70]. Decomposition of the organic material via bacteria under anaerobic conditions will produce ammonia.

3.1.12 Use of Artemia in ecotoxicology

The adaptability, natural tolerance, short lifecycle, unique reproduction strategy and overall resistances of Artemia make it one of the most valuable organisms available in ecotoxicology research [65] Cysts are produced when female Artemia anticipate unstable environmental conditions, and thus begin to produce cysts instead of free-swimming nauplii. These organisms are also favoured for their low cost. A big factor contributing to the use of Artemia for ecotoxicology is the small scale of the test organisms, leading to a reduction in test volumes, produced waste, and space required for testing protocols. These improvements become extremely important when considering the ecotoxicology of an extraterrestrial environment [12] The use of cysts in ecotoxicology testing is helpful for early toxicity screening.

3.1.13 Chlorella and other algae

Salt concentration is thought to possibly affect the activity of nutrients needed for growth of microorganisms, however the lack of fixation of various nutrients may be a result of the absence of a variety of species available in the hypersaline environment [70]. A study in the great salt lake has found that inorganic nitrogen is the limiting factor for growth in algal culture there, as well as carbon.

3.2 pH and ORP sensors

Sensors for measuring the pH via colorimetry are commercially available in a small package, and some are coupled with sensors that also measure the free ammonia in the water by colorimetry. Due to the complexity of measuring pH by potentiometry, and the unreliability of doing so in a system that cannot see maintenance while in use, we have chosen to purchase a system that achieves the measurement by colorimetry.

3.3 Ammonia sensors

A most fundamental factor in maintaining a healthy system is to maintain the nitrogen cycle: the algae consumes nitrate, then either decomposes as organic material or is consumed by the artemia and then excreted as organic material. This is then broken down by microorganisms to produce ammonia, and further processed by other microorganisms to convert the ammonia to nitrite, and nitrite to nitrate. The health of these microorganisms is hugely dependent on the pH of the water. An imbalance in the nitrogen cycle may lead to reduced oxygen levels [29], and the overproduction of free ammonia in the water, which is toxic to the shrimp.

Ammonia is toxic to aquatic life and has been reportedly toxic at levels as low as 0.5 mg/L (approximately 0.5005 ppm). Ammonium generation depends on the pH, temperature, and concentration of dissolved salts in the water. We need to monitor the ammonia levels in the water to ensure the health of the ecosystem. We wish to keep the ammonia below the 0.5 ppm threshold. It is important to characterize the ammonia level to be above or below this level. It should also be a capability to

see when the ammonia levels begin approaching this level. For this application, a simple ammonia sensor is suitable. The sensor is passive and has four indicator for the environment's ammonia levels.

Indicator	**Ammonia (ppm)**	**Color**
SAFE	<0.02	Yellow
ALERT	0.05	Green
ALARM	0.2	Blue
TOXIC	0.5	Purple

Table 3: Ammonia strip indicators to be interpreted by colormetry

The sensor will be monitored by a camera. The camera will pick up the color of the strip to determine if the ammonia levels are at a safe level in post-process.

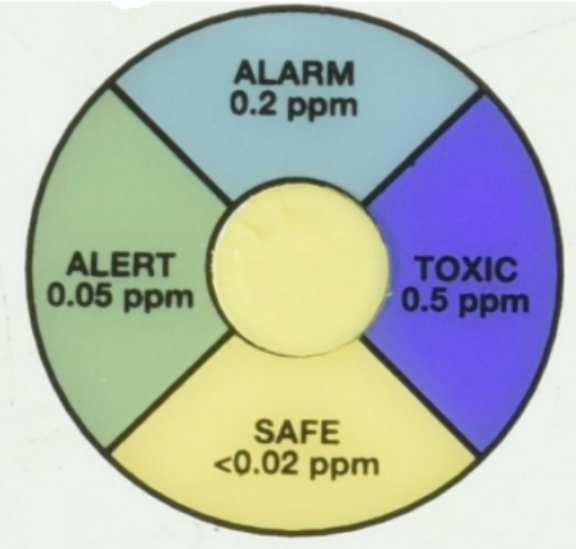

Figure 2: Ammonia Alert strip [79]

Based on this information, the best approach is to choose a cost effective ammonia alert strip from amazon for $10.

3.4 Temperature sensors

A temperature sensor will be used in conjunction with a heater to regular the temperature of the environment. Our temperature sensor will be a Thermocouple Amplifier MAX31855 breakout board (MAX6675 upgrade) +Thermocouple Type-K Glass Braid Insulated Stainless Steel Tip. This device will draw a relatively low amount of power and serve as an essential characterizing device for our ecosystem. The temperature sensor will interface seemlessly with our microcontroller. It provides good sensitivity (0.25 °C increments), and will easily cover the expected temperature range of our environment.

3.5 Optode Device

We discuss the phenomenon that is exploited in order to measure the concentration of dissolved oxygen in water. This phenomenon is the fluorescence of some materials to be reduced or "quenched" when oxygen is present, and the effect is increased with a higher concentration of oxygen present.

3.5.1 Luminescence quenching

When any substance sees transition from a higher electronically excited state to one which is lower, luminescence may occur [51]. The transition involves a drop in energy within the substance, and this energy must exit in some form. This may be in the form of phonons, that is, heat generation and other nonradiative processes. This may also be in the form of photonics, and such emission is termed luminescence. Luminescence may be separated into two categories: fluorescence and phosphorescence.

3.5.2 Fluorescence

Fluorescence is the emission of light by a substance that has absorbed light. The emitted light typically sees an effect known as the Stokes shift, an effect which describes the phenomena that the emitted light has a longer wavelength, and therefore lower energy, than the emitted light. Fluorescence is resultant from excited singlet state, s.t. the electron in the excited orbital is paired to an electron of opposite spin in the ground-state orbital, allowing the return to ground state to occur rapidly. These transitions occur on the order of 1-10 ns. Fluorescent substances are termed fluorphores. The absorption and emission spectra are distinct for a particular material due to it's electron energy levels which can absorb and emit photons at discrete values of energy equal to the energy difference between the excited and ground state levels of that electron. Based on this principle, we can excite materials with UV light, excite the atom's electrons (though absorption) and then observe the wavelength of light that is re-emitted to gain insight to the material's characteristics.

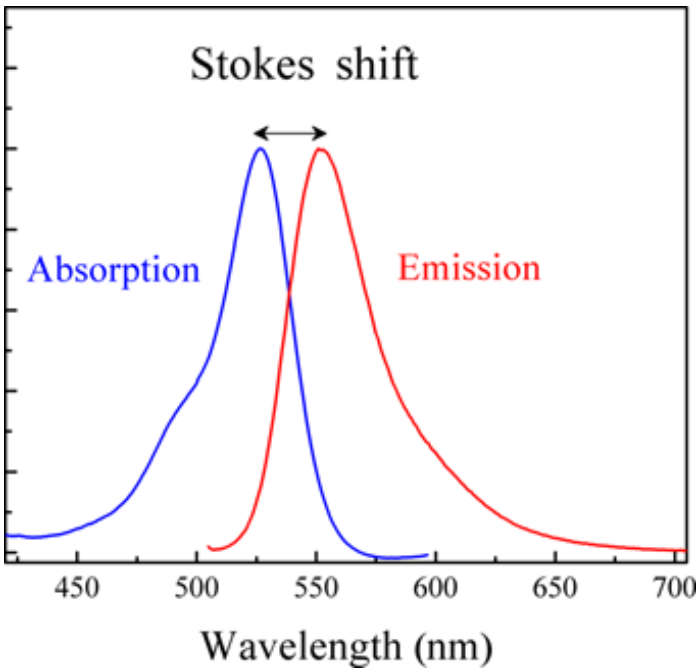

Figure 3: Stokes shift describes how the wavelength of emitted light is typically longer than the wavelength of absorbed light. [51]

3.5.3 Phosphorescence

Phosphorescence is the emission of photons as a result of electrons transitioning from triplet excited states: the electron in the excited orbital has the same spin orientation as the ground-state electron. Such transitions are forbidden, and thus take much longer: phosphorescence lifetimes are typically on the order of milliseconds to seconds.

3.5.4 Stokes' Shift

As seen in the example Jablonski diagram showing in Fig [JABLONSKI], the transition due to fluorescence or phosphorescence of a fluorophore is typically smaller than the transition due to absorption of a photon. This was first observed by Stokes [CITE Stokes 1852], who observed blue emission of quinine upon excitation by sunlight, despite quinine seeming to be a colorless liquid. Such losses in energy in-between absorption and emission are universal in fluorescent molecules in solution, commonly due to the rapid decay to the lowest vibrational level of S1 after excitation. Thermalization of excess vibrational energy may also allow fluorophores to lose excess vibrational energy after they have transitioned to a higher vibrational level of S_0, explaining another source of energy loss between excitation and emission.

3.5.5 Lifetime & Quantum Yield

Typically the most important characteristics of a fluorophore are its fluorescence lifetime and quantum yield. Quantum yield defines the number of photons emitted per photons absorbed: higher quantum yields result in brighter emissions. Fluorescence

lifetime is the defining characteristic that dictates how much time the fluorophore has to interact with its environment: environmental factors that interact with the fluorophore on a timescale longer than its lifetime will not be able to influence the fluorescent behavior of the fluorophore, and thus cannot be measured.

3.5.6 Luminescence Quenching

A number of processes can decrease the fluorescence emission of a fluorophore, inciting nonradiative transitions instead. This general phenomenon is termed quenching. One mechanism by which quenching can occur is collisional quenching: the excited-state fluorophore contacts another molecule in solution, and is deactivated. The other molecule is termed the quencher. Such a process does not chemically alter the fluorophore, however when a number of fluorophores are present, the intensity of their fluorescent emission may indicate the presence of a quencher. An alternative mechanism to collisional quenching that may also occur is static quenching, which is from the formation of nonfluorescent complexes between the fluorophores and quenchers. This occurs in the ground state and does not rely on diffusion or molecular collisions. However for the purposes of oxygen detection by luminescence quenching, collisional quenching will be the quenching mechanism of interest in this paper.

3.5.7 Upshot of these phenomena

Because fluorescent emission can occur over a relatively long period of time due to fluorescent molecules remaining in the excited state, collisional quenching from molecular oxygen will have enough time to have a noticeable effect on the fluorescent emission of a fluorophore. An oxygen molecule can diffuse about 7 nm in $10ns$, and for fluorophores feauturing fluorescent lifetimes on the order of 100s of ns, diffusion of oxygen may be observed over distances of 45 nm.

3.5.8 Types of Oxygen Quenchable Fluorescent Dyes and their Synthesis

The available dyes that are commonly used for oxygen sensors based off of fluorescence quenching by oxygen are presented. Our dye of choice is been PtTFPP. As presented below, this dye exhibits key characteristics that are helpful for an oxygen sensor for biological applications: high brightness, high molar absorption coefficients for reduction of power consumption from the light source, a large Stokes' shift for ease of distinguishing between source and fluorescence light with the use of a filter, and it can be excited with visible (blue) light, and its emission is also in the visible range (red). These perks make the dye a great candidate, however Ru(II) polypyridyl complexes have similar positive characteristics. The choice to use PtTFPP became clear when the availability, cost, and procedure for preparation was considered between metalloporphyrins and Ru(II) polypyridyl complexes. The PtTFPP requires minimal preparation after it has been synthesized, and it can be easily be immobilized in a polystyrene (PS) matrix by simply dissolving it in toluene with the PS. Whereas the Ru(II) polypyridyl complex competes only in other immobilization matrices which

are much more complicated to prepare, and many of which will dissolve in water and thus fail.

3.5.9 Polycyclic aromatic hydrocarbons (PAHs)

Polycyclic aromatic hydrocarbons are considered to be the first generation of oxygen-sensing materials. Although they exhibit a strong luminescence and many of them have a good photostability, their short lifetimes and insolubility in polymeric matrices greatly decrease their potential for use in sensing oxygen. They exhibit a relatively low sensitivity and require a more complex fabrication procedure due to the matrices in which they may be immobilized. No PAH is considered for our final comparison in dye selection. Common PAHs that have been utilized for oxygen sensors are listed in Table 4

Material	$\lambda_{exc,max}$**(nm)**	$\lambda_{em,max}$ **(nm)**	**Matrix**	**Solvent**	**Sensitivity**	τ
1-Pyrenebutyric acid	365	376/396/477	Oxidized alumina	Toluene	$I_0/I_{100} = 6.14$	200 ns
Pyrene	305/319/335	381/390	PDMS	Cyclohexane	$I_0/I_{100} = 6$	450 ns
Perylene dibutyrate	468	514	Silica	Toluene	$I_0/I_{100} = 1.67$	?
Decacyclene	385	510	PDMS	Toluene	$I_0/I_{100} = 7.8$	?

Table 4: Common PAHs & Sensitivities in given matrix

Pros:

1. Relatively high quantum yield ($\phi = 0.65$)
2. Good pressure sensitivity
3. Low temperature coefficient at ambient temperature
4. Some have a good photostability

Cons:

1. Tendency to to aggregate in polymer
2. Generally not very soluble in polymeric matrices
3. Short excitation wavelength will cause biological media to display strong background fluorescence
4. Very short fluorescence lifetimes of up to 200 ns: Highly gas-permeable polymers are required
5. Low molar absorption coefficient
6. Small Stokes' shifts

Immobilization Matrices:

1. Oxidized alumina

2. Silica

3. Sol-gel

4. Silicon rubber (PDMS)

5. Oxygen-permeable gel

6. Polystyrene

3.5.10 Ruthenium and Osmium Polypyridyl Complexes

Transition metal polypyridyl complexes are among the most commonly used indicators for sensing oxygen. This is due to their large Stokes' shift, photostability, their excitation and emission maxima being in the visible region, and their ease of preparation. Additionally, their solubility in silicon allows for them to be applied in high concentrations to create a highly luminescent layer with a short response time [49]. There are however drawbacks associated with this material, including a high susceptibility to thermal quenching, and a low sensitivity in the common polymeric matrices due to its short lifetimes [73]. Also, these materials have very broad excitation and emission bands, although this is accompanied by the drawback of exhibiting low molar absorption coefficients. Table 5 showcases the photophysical properties of commonly used transition metal polypyridyl Complexes. Because of its brightness and lifetimes being relatively higher than the other Ruthenium polypyridyl complexes, $[Ru(dpp)_3]^{2+}$ is considered as our dye of choice and will be compared with dyes from other categories.

Material	$\lambda_{exc,max}$**(nm)**	$\lambda_{em,max}$ **(nm)**	**Matrix**	Solvent	**Sensitivity**	τ
$[Ru(bpy)_3]^{2+}$	450	630	sol-gel	EtOH-MeOH	$I_0/I_{100} = 2.0$	$1.15\mu s$
$[Ru(phen)_3]^{2+}$	444	596	Nafion	MeOH	$I_0/I_{DO,8mM} \approx 1.4$	$0.28\mu s$
$[Ru(dpp)_3]^{2+}$	463	618	Ormosil	EtOH-MeOH	$I_0/I_{100} \approx 8.8$	$6.4\mu s$

Table 5: Common Polypyridyl Complexes & Sensitivities in given matrix

Pros:

1. Large Stokes' shifts

2. Excitation and emission maxima in visible region

3. Excellent photostability

4. Tunable luminescent properties

5. Fairly easy to prepare

Cons:

1. Mediocre molar absorption coefficients

2. They exhibit relatively short fluorescent lifetimes
3. Dependent on polarity of miroenvironment
4. Dependent on donor/acceptor character of surrounding medium
5. Rather low oxygen sensitivity in common polymeric matrices such as polystyrene.
6. Triplet states are subject to severe thermal quenching

Immobilization Matrices:

1. Sol-gels
2. Ethyl cellulose
3. PVC membranes
4. ORMOSILs
5. Polystyrene
6. Polysulfones
7. Poly(dimethylsiloxane) alone

3.5.11 Metalloporphyrins such as PdOEP, PtOEP, PdTFPP and PtTFPP

Pt(II) and Pd(II) porphyrins are the most popular luminophores in use, as a result of their strong phosphorescence, rather high absorption coefficients and large Stokes' shifts [73]. Although many of these indicators lack photostability, the metalloporphyrins PtTFPP and PdTFPP have a very high photostability, while retaining the other desireable characteristics that metalloporphyrins have as oxygen-quenchable fluorophores. Table 6 lists common metallophorphyrins and their photophysical properties. PtTFPP has been selected for consideration against dyes from other categories, due to its high performance and ease of fabrication, in part because of its high solubility in common polymeric matrices [73]. This was preferred due to its palladium counterpart, because the palladium complex is fully quenched far below oxygen levels that are typical in the environment that we wish to monitor, due to the dye's extraordinary sensitivity.

Material	$\lambda_{exc,max}$(nm)	$\lambda_{em,max}$ (nm)	Matrix	Solvent	Sensitivity	τ
PtOEP	382/536	649	Polystyrene	Toluene	$I_0/I_{100} = 4.5$	$75\mu s$
PdOEP	546	670	Polystyrene	Toluene	$I_0/I_{100} = 46$	$75\mu s$
PtTFPP	390/504/538	647/710	Polystyrene	Toluene	$I_0/I_{100} = 3$	$60\mu s$

Table 6: Common Metalloporphyrins & Sensitivities in given matrix

Pros:

1. Strong phosphorescence at room temperature
2. Moderate to high molar absorption coefficients
3. Large Stokes' shifts
4. Rather long and tunable phosphorescence lifetimes
5. Excitation and emission at visible wavelengths
6. High molar absorption coefficient in the soret band (near-UV and blue light)
7. Commercially available and very affordable

Cons:

1. Although PtOEP and PdOEP have a relatively low photostability, due to the high photostability of PtTFPP and PdTFPP, the only downside of these fluorophores is their lack of absorption in the 500 nm to 750 nm range. [89]

Immobilization Matrices:

1. Polystyrene
2. Sol-gels
3. Poly(aryl ether ketone)
4. Ethyl cellulose
5. Cellulose acetate butyrate
6. Polyvinylchloride

3.5.12 Cyclometallated complexes of Ir(III) and Pt(II)

Cyclometallated Ir(III) complexes are soluble in polymeric matrices, exhibit very high quantum yields and thus high luminescence, and have a large Stokes' shift. However, these indicators have very low molar absorption coefficients. To overcome this, coumarins may be introduced to the cyclometalated iridium(III) complexes, and other highly absorbant ligands are introduced to the cyclometalated Platinum(II) complexes in order to enhance the luminophore's absorption coefficient [73]. Table 7 features cyclometallated complexes that are commonly considered for use as an oxygen-quenchable luminophore. $Ir(ppy)_3$ is considered due to its strong green luminescence and acceptable quantum yield and lifetime while being more commercially available in comparison with the other cyclometallated complexes that may be synthesized for use as an indicator.

Material	$\lambda_{exc,max}$(nm)	$\lambda_{em,max}$ (nm)	Matrix	Solvent	Sensitivity	τ
$Ir(ppy)_3$	376	512	Polystyrene	Tetrahydrofuran	$I_0/I_{100} = 1.1$	$1.5\mu s$
$Ir(ppy - NPh_2)_3$	405	527	-	Ethyl cellulose	$\tau_0/\tau_{air} \approx 4.5$	$4.3\mu s$
$Ir(C_S)_2(acac)$	472/444	563	Polystyrene	Chloroform	$\tau_0/\tau_{air} \approx 1.51$	$11.3\mu s$
$Ir(C_N)_2(acac)$	450/421	545	Polystyrene	Chloroform	$\tau_0/\tau_{air} \approx 1.5$	$8.5\mu s$

Table 7: Common Cyclometallated Complexes & Sensitivities in given matrix

Pros:

1. Remarkably high luminescence quantum yields
2. Large stokes' shift
3. Photostable compounds

Cons:

1. Luminescence decay times are only on the order of several microseconds
2. Absorption in visible region is inefficient, with low molar absorption coefficients in this region

Immobilization Matrices:

1. Poly(styrene-co-trifluoroethylmetacrylate (TFEM))
2. Ormosil
3. Poly(dimethylsiloxane)
4. Polystyrene
5. pPEGMA
6. PDMS silicone

3.5.13 Polymeric Matrices and Supports

Polymers function as: A solid support in which the optical sensing material is immobilized, and as a material that is selectively permeable to oxygen, but not to other gasses [89]. Such a material is critical as to prevent the luminophores being used for sensing from leaching out of the sensor and into a fluid that the sensor is suspended in, which is especially important when using the device for measuring dissolved oxygen in a marine aquarium. Also, the choice of polymeric matrix, given its oxygen permeability, will allow the sensitivity of the sensing layer to be adjusted. This is because the oxygen permeability of the matrix will determine how quickly oxygen can diffuse into the material to interact with the indicator via collisional quenching. Because the sensing layer must be applied by dissolving the luminophore in some solvent with the polymeric matrix of choice, a certain combination between polymer, solvent and indicator must be found, based off of the compatibilies of each, the desired oxygen

permability of the matrix, and the environment that the sensor will be exposed to. A matrix which is water-soluble may not perform well for measuring dissolved oxygen in an aquarium, as the sensing layer would simply dissolve into the water unless some other oxygen-permeable material was coated over the top of it.

Other important factors that must be taken into consideration when selecting a polymeric matrix is: its optical transparency to the excitation and emission associated with the luminophore, other factors that may contribute to degradation of the matrix over time, and the effect that the matrix has on the indicator's photophysical properties.

The simplest method of immobilizing and indicator in a polymeric matrix is to dissolve the luminophore in a solvent, add the polymeric matrix to the solvent, or add a solution including the polymer, then spread the sensor cocktail onto a support and allow it to dry. The strength of interaction of the indicator with the polymeric matrix will determine how little leakage will occur. As such, it is optimal for the host polymer and the indicator to have a similar polarity. An alternative method is the adsorption of a charged indicator on the surface of a particle, such that this particle acts as a support. These particles may be alumina, silica, or porous glass beads, all of which possess a negative charge when suspended in a neutral solution. The resulting particles can then be incorporated into a host matrix without use of a solvent, or formed into a layer of any shape. A third method of immobilizing an indicator is to dissolve it in micro or nano-particles, and then incorporate these particles into a hose polymer without requiring that the original indicator can be dissolved into the host polymeric matrix. The latter two methods are superior for the negligible amount of leaching that will result, amongst other improvements. However, the first embodiment described may be preferred due to its simplicity. We have chosen to use this method for that reason, as our access to equipment common in a chemistry laboratory is limited in the lab that we will be performing the fabrication in. As such, we seek to avoid any steps in our fabrication that are in excess of simply mixing our materials in glassware, and coating it, while using a hotplate for temperature control, and a fumehood for safety around the toluene.

Table 8 lists common polymers that are used as matrices to immobilize oxygen-quenchable luminophores for use in oxygen optodes. P is the permeability, given in the following units:
$10^{-13} cm^3 cm (cm^2 s\ Pa)^{-1}$. This table was taken from Ref [89] as compiled by Wang et al. In maintaining a low budget, and acknowledging that the minimum quantity of any polymeric matrix that we purchase will by in great excess of what we require, we have chosen to use polystyrene. This polymer can be acquired at a very low cost, it provides and adequate oxygen permeability, has a good transparency in the visible wavelengths, and it is stable in aqueous solutions.

Polymer	P	Comments
Ethyl cellulose [EC]	11.0	Biocompatible; good optical transparency; good mechanical strength.
Poly(dimethyl siloxane) [PDMS]	695	Excellent gas permeability, high thermal stability, excellent chemical andmechanical stability, ease of handling, good adhesion to glass fibers,inertness to biological samples, optically transparent; hydrophobic; lowglass transition temperature; many commercially available prepolymerscontain solvents, fillers, low molecular weight cross-linkers, catalysts andother additives; need for curing.
Poly(methyl methacrylate) [PMMA]	0.116	Thermoplastic; easy to manufacture and reproducible; low cost; poor oxygen permeability; only useful for sensing oxygen at high partial pressure; photostable; good optical transparency; no need for curing.
Polystyrene [PS]	1.9	Easy to manufacture; low cost; moderate oxygen permeability; allows oxygen sensing at high concentration; may be sterilized; excellent shelf time and stability in aqueous solutions; good optical transparency;no need for curing; much lower sensitivity than PDMS.
Poly(1-trimethylsilyl-1-propyne)[PTMSP]	11251	High gas permeability; no need for crosslinking; good photostability; useful for trace oxygen sensing.
Poly(styrene)-co-(pentafluorostyrene)[poly-styrene-co-PFS]	n.d.	Extremely high gas permeability; excellent photostability; short response time; useful for trace oxygen sensing.
Poly(styrene)-co-(trifluoroethylmethacrylate) [poly-styrene-co-TFEM]	n.d.	Extremely high gas permeability; excellent photostability; short response time; useful for trace oxygen sensing.
Poly(isobutyl methacrylate)-co-(trifluoroethyl methacrylate)[poly-IBM-co-TFEM]	n.d.	Extremely high gas permeability; excellent photostability; short responsetime; useful for trace oxygen sensing.
Poly(4-tert-butylstyrene)-co-(trifluoroethyl methacrylate)[poly-tBS-co-TFEM]	n.d.	Extremely high gas permeability (even higher than poly-styrene-co-TFEM);excellent photostability; short response time; useful for trace oxygensensing.
Poly(hexafluoroisopropylmethacrylate)-co-(heptafluoro-n-butyl methacrylate) [FIB]	n.d.	Extremely high gas permeability; excellent photostability; short response time; small temperature dependence; suitable for application in wind tunnels with temperature compensation.
Poly(styrene-co-acrylonitrile) [PSAN]	0.0032	Moderate gas permeability that can be tuned by changing the ratio of monomers; good stability; easy to handle.
Nafion	0.81	Ionic polymer; chemically inert; good gas permeability; probes can be absorbed on the polymer; sensitivity depends on the swelling in different solvent.

Table 8: Common polymeric matrices and their permeability (P). n.d. indicates "no data". Taken from reference [89]

3.5.14 Fabrication

The procedure that will be followed in order to coat a glass substrate with PtTFPP immobilized in polystyrene is quite simple and follows a method akin to the procedure used in refs [9], [53] and [14]. The process requires that the PtTFPP is dissolved in toluene or chloroform with PS. It is then knife-coated onto a glass slide and allowed to dry in a fume hood. Variations of this procedure include:

1. Using and airbrush to coat
2. Dip-coating
3. Chloroform as a solvent instead of toluene

However our references including these alternative approaches do not seem to detail any improvements in performance, and the variations as such are based off of preference and whichever materials and tools are readily available in the lab. Already available to us in the lab is toluene, so it is practical to use this. We also have a doctor's knife available to us, which will allow us to knife-coat with good precision.

3.5.15 Light Source for Excitation

As detailed in Table 6, our PtTFPP has excitation maxima at 390 nm, 504 nm, and 538 nm. However the molar absorption coefficient at the 390 nm peak is significantly higher than that of the other peaks, as is indicated by figure 4.

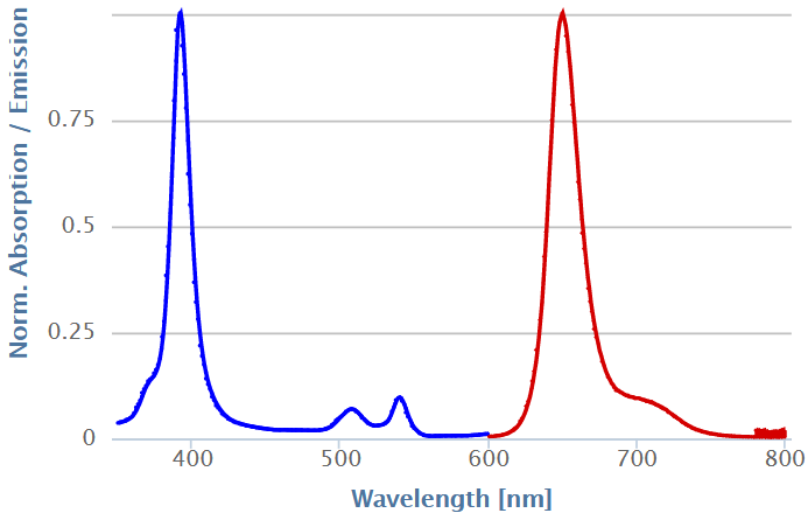

Figure 4: PtTFPP Excitation Spectrum (blue) and Emission Spectrum (red) [39]

We wish to find a light emitting diode who's peak emission matches that of our dye's peak absorption. Figure 5 shows the relative luminous intensity of UV LEDs made from Bivar according to their datasheet. A UV LED (LED A in Figure 5) who's peak intensity is at 395 is our LED of choice for our excitation source, as this matches up with the excitation peak of our dye. This is the UV5TZ-395-30 Bivar UV LED,

and it features an output of 40 mW at a 30° viewing angle (a solid angle of about 0.214 Steradians) at half-intensity. Further discussion of this LED's characteristics will take place later in this document, when we discuss the voltage vs current and light vs. current characteristics of the device, as well as our scheme for driving it.

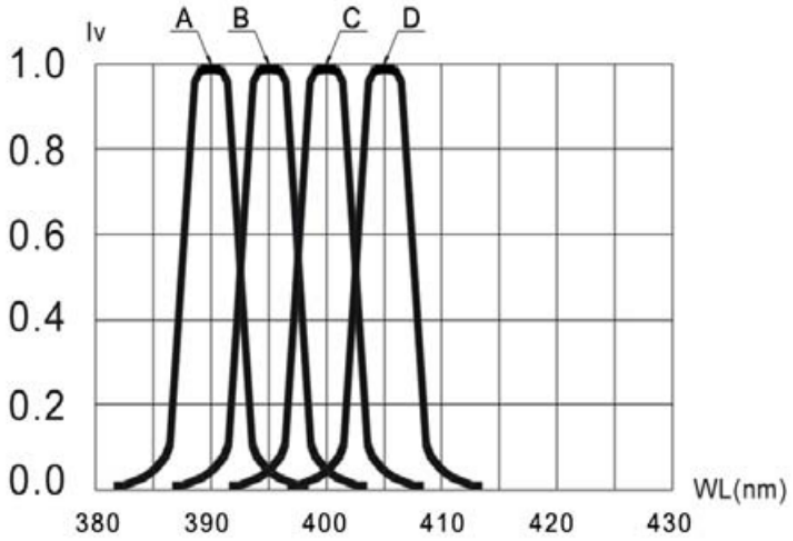

Figure 5: Emission Spectrums of Bivar's UV LEDs (Relative luminous intensity (unitless) vs. Wavelength (nm)) [11]

3.5.16 Photodiode and Measurement Scheme

As figure 4 and table 6 suggests, the peak emission of our luminophore PtTFPP is at 647 nm. In considering our options, we expect that our final design will feature the Hamamatsu S5973 IR + Visible Light Si PIN Photodiode. Its absorption spectrum is featured in figure 8. The S5973 will pick up the 647 nm emission from the PtTFPP, as well as the TSHG5510 Vishay 830nm IR LED. This will be our reference LED, its emission peak is at 830 nm at its relative radiant power vs. wavelength is featured in figure 6. As mentioned previously, a longpass filter is used to prevent light emitted from the UV LED from being picked up by the photodiode. Our longpass filter of choice is the 3mm SCHOTT OG570 longpass filter, and its transmission spectrum is featured in figure 7.

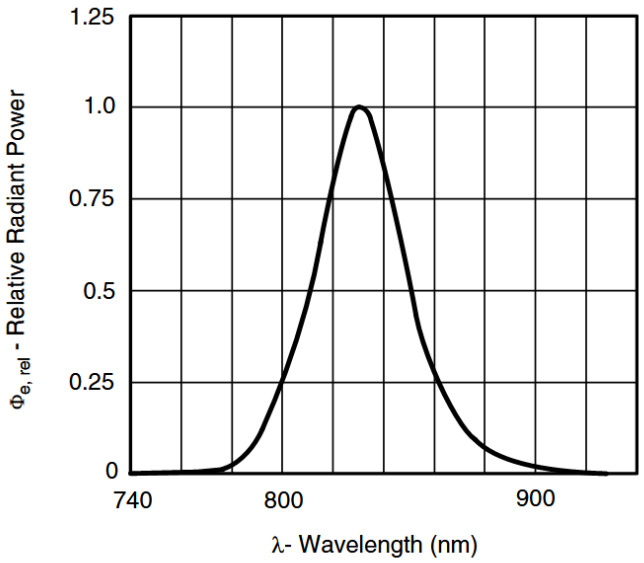

Figure 6: TSHG5510 Radiant Power vs. Wavelength (nm) [88]

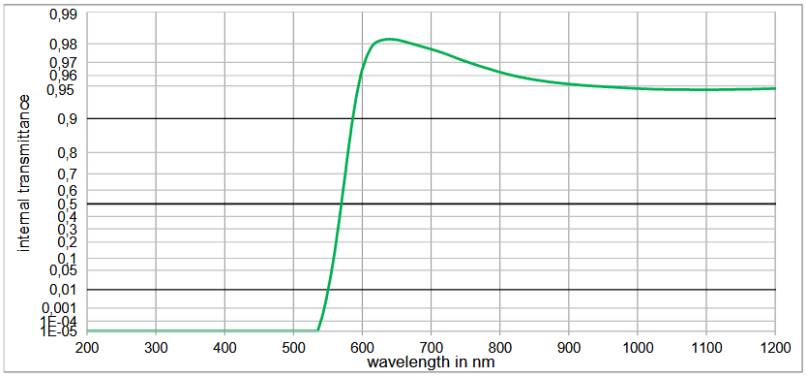

Figure 7: Relative Transmittance vs. Wavelength (nm) for the SCHOTT OG570 longpass filter [67]

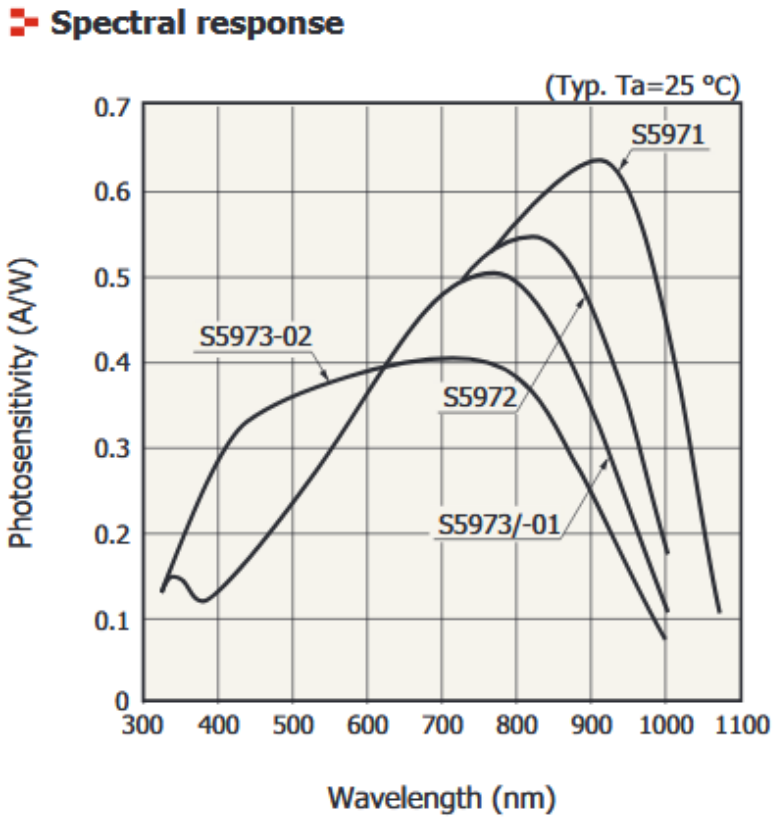

Figure 8: Hamamatsu S5970 series Photodiode Spectral Response [43]

3.5.17 Summary

The part selections are shown in the above sections. We find that given the materials that our optode device requires, a single oxygen optode effectively costs us $54.77 if we only consider the portion of materials it consumes. Because we are unable to purchase quantities of materials small enough to fabricate only one optode, the total cost out of our budget ($367.13) is much greater than the effective cost of a single optode ($54.77). The greatest contributor to this effect is the minimum quantity of PtTFPP that we could acquire: the PtTFPP was synthesized at our request, so we chose not to request an awfully small batch. This 100 mg batch of PtTFPP from PorphyChem is equivalent to the minimum quantity that is available at the other retailers who sell the luminophore. Our purchase of materials that will allow for an excess of one optode sensing layer will greatly benefit our prototyping of the device. We wish to fabricate a number of sensing layers, to allow for error in the process of mixing and knife-coating the PtTFPP/PS/Toluene coctail. We have enough PtTFPP to coat a 25x25 mm cover glass 33 times, with all other materials available in excess. This sensing layer will be inserted into a housing that holds our source & detection assembly. We will then be able to perform a number of tests on the sensing layer to verify that our mixture provides a high enough concentration of fluorophores. These tests, after completing a functional prototype optode that may be glued into our

aquarium after a 25x25 cm square hole has been cut, will allow us to experiment with further improvements in the compactness of our optode. We wish to apply our sensing layer coating directly onto the inside of the artemia and chlorella-containing test chamber that will be used when verifying the functionality of our sensor suit. Such an approach would eliminate the need for manually inserting the sensor, and it would increase the reliability of the device, as any chance of leakage into the electronics of the oxygen optode would thus be eliminated. Fabrication of the sensing layer is scheduled for mid-December 2020, given that our materials arrive on time. However due to shipping inconvenience as a result of the COVID-19 pandemic of 2020, it is possible that our materials arrive later, and require us to fabricate the sensing layer in early January. Later, we will verify its functionality by testing it with our LEDs and photodiode, biased from a breadboard. This will be after they have been mounted in their housing, and the photodiode isolated from the UV LED source with the use of the longpass filter.

3.6 Refractometer

A refractometer is a device that measures refractive index. The refractometer is implemented into our research platform for the purpose of measuring salinity of batches of the environment's water. We look to monitor the salinity of the environment to serve as another metric for characterizing the systems general health. Our refractometer works on the premise that the refractive index of the water holds a direct relationship to the salinity of the water. For example, the refractive index of freshwater is approximately 1.3325 and the refractive index of water containing 35 part per thousand salt has a refractive index of 1.3388 [8].

The refractometer, used to measure salinity of the water will be another custom-designed photonic component. Although salinity of the water is conventionally measured by using a hydrometer to find the specific gravity of the water [41], because a hydrometer is based off of buoyancy, such a device is not considered for use in microgravity conditions. Methods of measurement of the salinity of water including the optical refraction method, the use of an optical fiber grating, a technique involving optical interference, and a technique that takes advantage of the surface plasmon effect [72]. We have chosen to use a refractometer, as we expect such an approach to be both within our budget, viable to build ourselves, and lightweight enough to package with the rest of the sensor suite. A custom design involving a laser, prism (or series of prisms), and a detector will be used. If budget permits, the detector will ideally be a high resolution line array CCD. The refractometer will function by taking advantage of the fact that the salinity and refractive index of water have a direct relationship. Further research will have to be done to show exactly how much of a change in index results from a change in salinity and adjust for given the temperature of the sample. Preliminary research has shown that the changes are not negligible, which indicates this concept may be viable [83]. Thus, a design was pursued.

3.6.1 Background

It can be seen by the graph in figure 12, that the salinity of water and its refractive index share a linear relationship. For every 1 PPT increase in salt, the refractive index increases approximately 0.00018. Snell's law describes how light refracts through a boundary of two media. A refractive index can be measured using Snell's law. Snell's law:

$$n_1 \sin\theta_1 = n_2 \sin\theta_2 \tag{1}$$

Where n_1 and n_2 are the refractive indices of medium 1 and 2, respectively. θ_1 would be the angle of incidence onto the interface, and θ_2 is the angle of refraction out of the interface. The first refractometer was the Abbe refractometer. The abbe refractometer works off the principal of total internal reflection. Total internal reflection is the complete reflection of light that occurs when an angle, called the critical angle, is satisfied. In the abbe refractometer there is typically two prisms, one of which is called an illuminating prism and the other is a measuring prism. The sample is sandwiched in between the two prisms, then light enters the illuminating prism then is refracted at the critical angle at the bottom of the measuring prism. Then, a telescope is used to measure where the light/dark interface occurs, which is indicative of the critical angle. And as discussed, the critical angle is indicative of the refractive index, which is indicative of the salinity of the water. Therefore, the Abbe refractometer can be used to measure the salinity of the water [74].

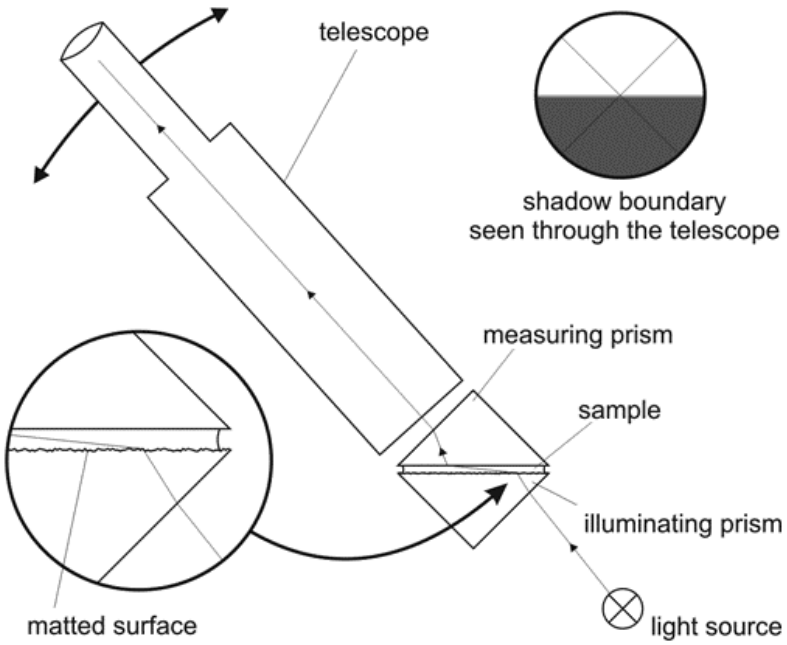

Figure 9: Illustration of an abbe refractometer.[76]

The abbe refractometer, however, requires adjustments of a telescope that cannot be made for this application. The design must be adapted to be remote control

compatible. A Pulfrich refractometer works on the same principal (critical angle) but uses a single prism. This design uses less parts, which is critical for our design.

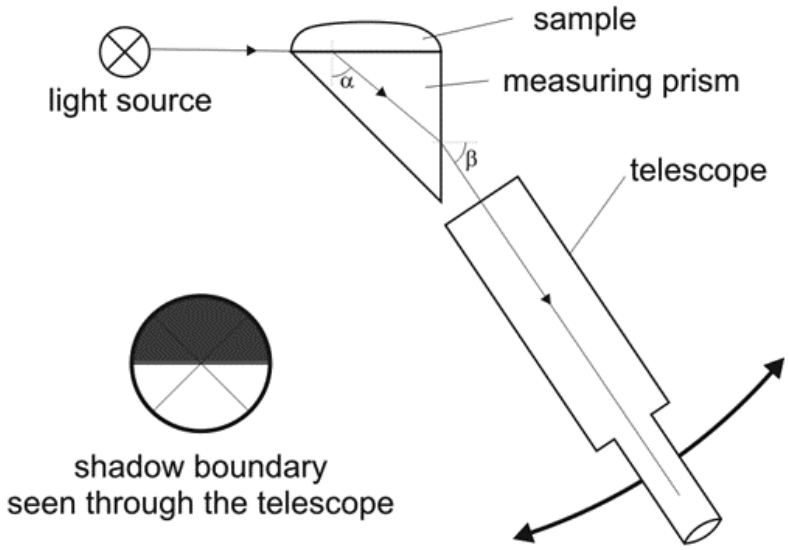

Figure 10: Illustration of a Pulfrich refractometer [76].

A third refractometer to draw inspiration from this the V block refractometer, designed by J.V. Hughes in 1941. The V-shaped block is ideal because it would be easy to allow the hyper saline water to flow into it.

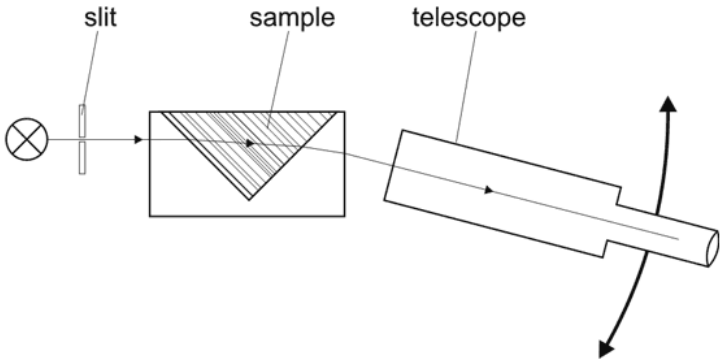

Figure 11: Illustration of A V-block refractometer [75].

The working principal of this refractometer is the change in angle of refraction based on the water that is in the sample spot. An adaptation of this design would involve a displacement sensing line detector instead of a telescope, to provide the necessary remote-control feature. Aquarium enthusiasts generally use a handheld refractometer that works off of the same principal of the abbe refractometer. It would be the ideal tool for this application if it weren't for the fact that it cannot be operated remotely and that it is slightly large for our purposes. Instead, an adaptation must be made that can be operated remotely.

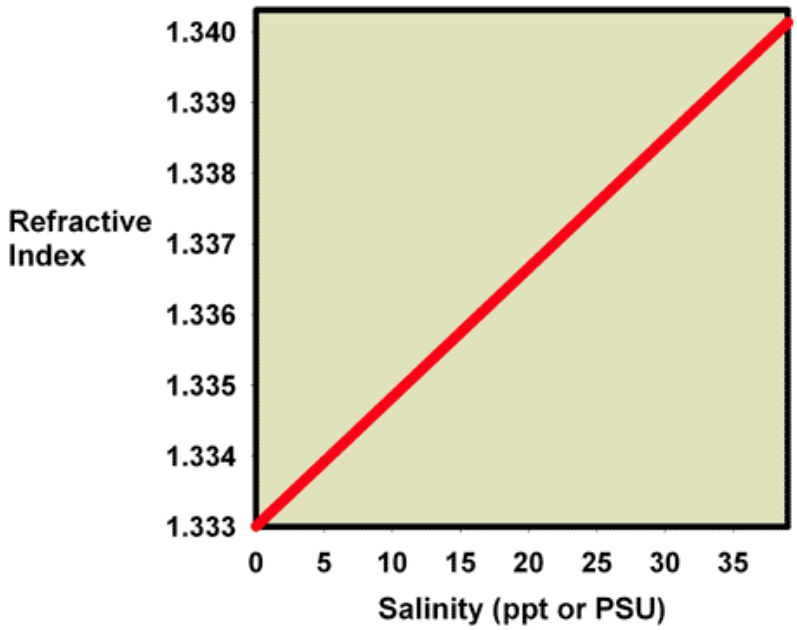

Figure 12: Graph showing linearity between salinity (in ppt) and refractive index.[19]

The refractive index of water also has other factors. For this application, the most predominate factor to account for is temperature. The temperature factor will be accounted for by the systems heating element, which will hold the water at a constant X degree. Another dominating factor is the particles in the water. They can easily destroy the beam quality and ruin a measurement that requires great precision. To account for this, a filter will be added in the water path to the external chamber containing the source, prism, and detector set up. The external chamber will also reduce water movement (and thus movement of whatever particles make it though the filter) which will also help the physical stability of the beam's placement.

3.6.2 Light Source

The refractometer needs a coherent light source to refract through the prism. An initial design decision must be made between a laser or LED based refractometer. An LED based refractometer would use a wide cone of light to shine through the prism which is in contact with a sample as shown in figure X. The difference in refractive index is indicative of what angle total internal reflection occurs. This angle is known as the critical angle the critical angle occurs. The transmitted light through the prism can be detected to tell where the light was dispersed onto a line array detector. The area of light on the line array detector is indicative of the angle of light that was transmitted from the prism. Using this measured angle, the refractive index can be measured via Snell's law.

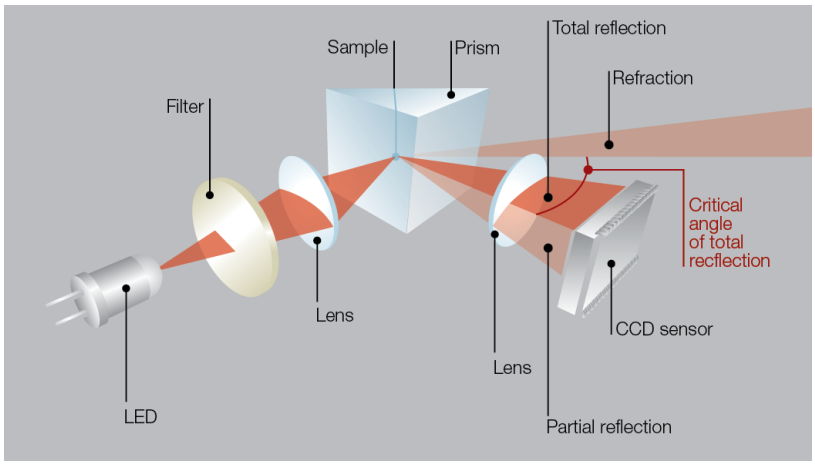

Figure 13: Illustration of a refractometer scheme using an LED as a source [91].

A similar concept involving a laser can be devised in which it is not total internal reflection that is used to take the measurement, but rather the displacement of a laser beam after passing through a refractive element containing the sample, or otherwise having an interface with the sample. The sample in our case is the hypersaline water [23]. By utilizing the fact that waters refractive index can change with salinity, we can alter the beam path by introducing water to the interfaces of the prism and then measure the displacement to use to back calculate the refractive index of the water. The wavelength of choice would be limited to the following options:

Wavelength (nm)
532
650
800
1064
1310
1550

Table 9: Laser Diode Wavelength Options

The size of the laser is of high priority, so we have chosen common diode laser wavelengths to choose from. The refractive index seen by the laser to the prism is dependent on wavelength, with the lower wavelengths experiencing a higher refractive index. This is preferred because it will result in a greater beam displacement and thus require less resolution from the detector. The laser wavelength should be mostly transparent with the chosen prism material. It's important to maintain some power though the prism to counteract absorption from the water and particles.

3.6.3 Prism

The prism material has its own refractive index and as well as the material in/around it (our environment water in this case). By Snell's law, $n_1 \sin\theta_1 = n_2 \sin\theta_{22}$, we know that the angle of refraction, θ_2, will change based off of these parameters. We also see from this relationship, that the angle of refraction will be greater with a greater distance between n_1 and n_2. The greater angle of refraction will be beneficial to our measurement which already requires a very high-resolution detector. The greater angle of refraction makes the displacement of the beam on the detector easier to see. For this reason, it is most optimal to pick a prism with the greatest refractive index. However, other important parameters of the prism are its size, if its hollow or not, and its transmission window. There will also have to be a cost benefit analysis of having one or two prisms. The three candidate materials of the prisms are BK7 (Schott, typical glass), zinc selenide, and zinc sulfide. The first thing to analyze is the refractive index of these materials. Like with most all optical materials, the refractive index is a function of wavelength. The plots of their refractive indices are shown below, please note that the y-axis scales are given differently.

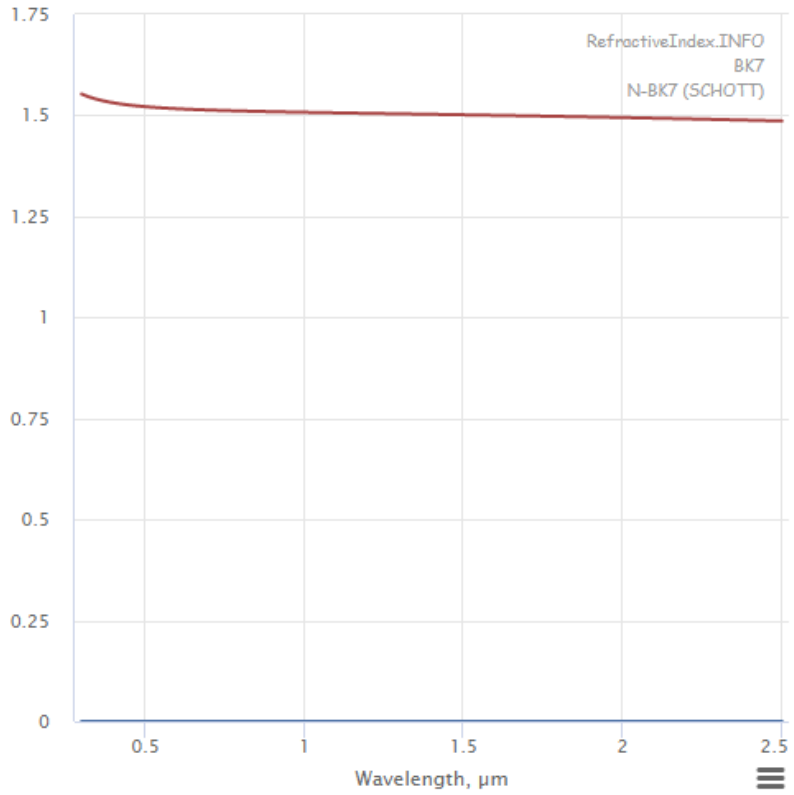

Figure 14: N-BK7 Refractive index vs wavelength.[25]

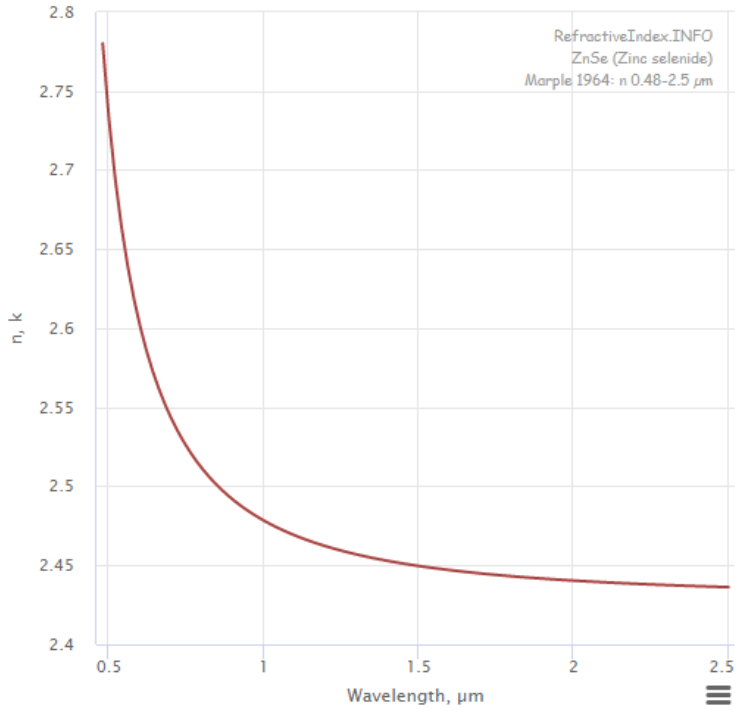

Figure 15: Zinc selenide Refractive index vs wavelength.[25]

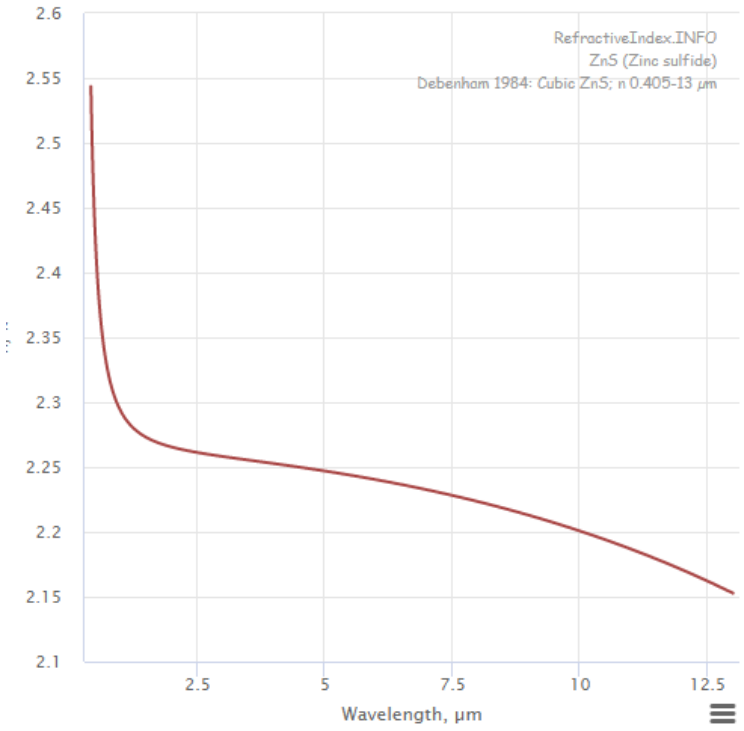

Figure 16: Zinc sulfide Refractive index vs wavelength. [25]

From these plots, we can see that the refractive indices decrease with increasing wavelength. We pull from these data sets the refractive indices at the wavelengths of interests, which are our options for source wavelengths.

Wavelength (nm)	**N-BK7 (SCHOTT)**	**ZnSe**	**ZnS**
532	1.5195	2.6763	2.3969
650	1.5151	2.5678	2.3504
800	1.5108	2.5115	2.3132
1064	1.5066	2.472	2.2883
1310	1.5036	2.4564	2.2776
1550	1.5007	2.4362	2.2717

Table 10: Laser Diode Wavelength (left column) vs. Refractive Index (remaining columns)

From the data set in Table 10 [25], we can see that Zinc Selenide has the highest refractive index of all the materials, making it he choice candidate for this parameter. Assuming a prism is equilateral, we calculate a few examples of beam angle deviation using different sources and prism materials, presented in figure 17.
From using these parameters (prism refractive index, and water refractive index) we can calculate a few examples of beam displacement. It is clear that proportionately, the refractive index of the ZnSe results in double the beam displacement as the traditional glass. A difference of 0.001 in refractive index provides only 0.103 degree of beam deviation. Another choice to analyze is whether the water/prism interface should be external or internal. As in, should the water surround the prism, or should the prism be hollowed out and the water should flood the inside of the prism.
Rewriting Snell's law, we obtain:

$$\theta_b = \sin^{-1}\left(\frac{n_a}{n_b}\sin\left(\theta_a\right)\right) \tag{2}$$

For the solid prism case, we solve for the exit angle in what we assume is an equilateral prism surrounded by water.

$$\theta_{exit} = \sin^{-1}\left(\frac{n_{prism}}{n_{water}}\sin\left(90 - \sin^{-1}\left(\frac{n_{prism}}{n_{water}}\sin\left(\theta_{entrance}\right)\right)\right)\right) \tag{3}$$

For the hollowed-out case (filled with sample), there are four interfaces. An interface between the outside medium and the glass, the glass and the inside medium, and then the two exit interfaces. We assume the following parameters: the prism is equilateral, its refractive index is 1.5, the side wall thickness is 1mm, air has a refractive index of 1, water has a refractive index of 1.333. By these assumptions, and applying the

rewritten Snell's law four times:

$$1 \sin^{-1}(\frac{1}{1.5} \sin(45°)) = 28.1255057° \tag{4}$$

$$\sin^{-1}(\frac{1.5}{1.333} \sin(28.1255057°)) = 32.03672304° \tag{5}$$

$$180° - 90° - 32.03672304° = 57.96327696° \tag{6}$$

$$\sin^{-1}(\frac{1.333}{1.5} \sin(57.96327696°)) = 48.87966975° \tag{7}$$

$$\sin^{-1}(\frac{1.5}{1} \sin(48.87966975°)) = undefined \tag{8}$$

We actually find that this surpasses the critical angle and the light is totally internally reflected at the exit glass/air interface. We can take the information derived from this example and derive for what input angle for these conditions do we reach the critical angle. By back tracing through the steps above and using general variables, we find that the critical angle can be determined as a function of the refractive index of the outer medium, inner medium, and prism for this case of an equilateral prism.

$$Deviation = \theta_{entrance} - A + \arcsin(n_{prism} \sin(A - \arcsin(\sin(\frac{\theta_{entrance}}{n_{prism}})))$$

(9)

Where deviation is defined as the angle in which the exit beam deviates from the original incident angle. A is the angle of the prism. Providing the experiment characteristics, solving this equation for will provide our metric for determining how the prism effects the beam path.
Based on the data in figure 17, a change in deviation that results from a change in 0.001 refractive index, will be hard to notice with any prism. A change of 5 PPT salinity will result in only approximately 0.075°deviation. This immediately calls for other prism configurations to be brought into consideration, preferably ones that will amplify this deviation. Additionally, this calculation will serve as an indication that a change of about 5 PPT salinity will be a reasonable limit for this measurement. Many limiting factors such as "noise" from particles in the water and movement will also disturb the beams placement on the detector.

Laser deviation with 532nm laser				
Material	Design type	Deviation @ 1.333	Deviation @ 1.334	Difference
N-BK7	Solid	6.726°	6.685°	0.042°
N-BK7	Hollow	x	x	x
ZnSe	Solid	55.407°	55.304°	0.103°
ZnSe	Hollow	x	x	x
ZnS	Solid	41.962°	41.880°	0.081°
ZnS	Hollow	x	x	x

Laser deviation with 650nm laser				
Material	Design type	Deviation @ 1.333	Deviation @ 1.334	Difference
N-BK7	Solid	6.566°	6.524°	0.041°
N-BK7	Hollow	x	x	x
ZnSe	Solid	49.983°	49.889°	0.094°
ZnSe	Hollow	x	x	x
ZnS	Solid	39.872°	39.793°	0.079°
ZnS	Hollow	x	x	x

Laser deviation with 800nm laser				
Material	Design type	Deviation @ 1.333	Deviation @ 1.334	Difference
N-BK7	Solid	6.409°	6.367°	0.041°
N-BK7	Hollow	x	x	x
ZnSe	Solid	47.276°	47.187°	0.089°
ZnSe	Hollow	x	x	x
ZnS	Solid	38.224°	38.148°	0.076°
ZnS	Hollow	x	x	x

Figure 17: Laser Deviation vs. Material

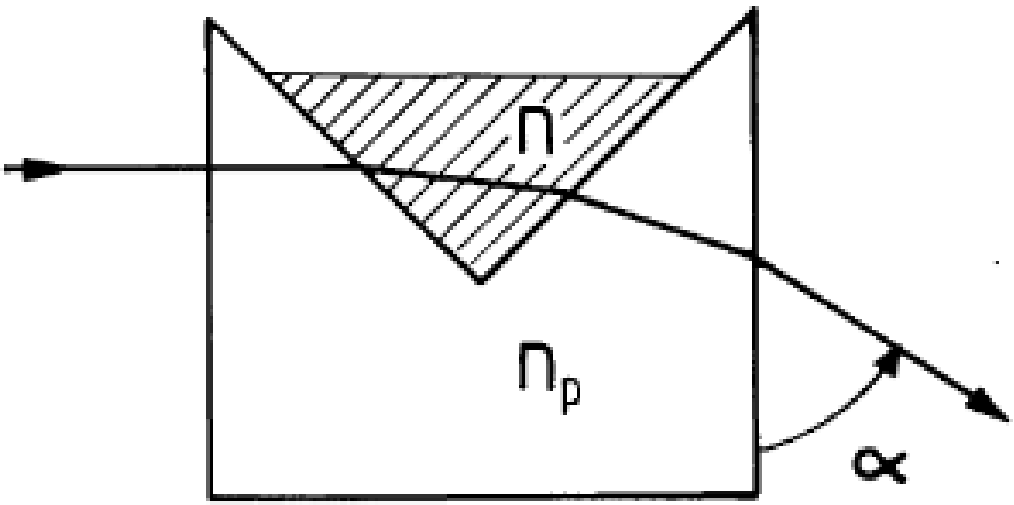

Figure 18: V-block refractometer showing a sample lodged between two prisms and how it results in a deviation angle [61]

The v-block style refractometer is the best bet for this measurement. It can be thought of as a double prism configuration, with the sample to measure being in between.

3.6.4 Detector

The refractometer needs detector that can detect the small laser displacements that will occur from changes in refractive index to at least the thousands place. A change in 1 PPT of salinity to water results in a change of refractive index of approximately 0.00018. From the figure in the previous section, we calculated that with optimal conditions, meaning a wavelength of 532nm (sees highest refractive index) and a prism made of ZnSe (highest refractive index of 2.6763 at 532nm), the best angle deviation we can observe is 0.103 degree. Over a generous distance of 75mm, that is a displacement of only 0.13483mm. This means that the lowest pixel resolution we can accept is about 50 µm. However, that is best case scenario. The distance allowed for the beam to displace may end up being smaller and the 532nm only has 50 percent transmission though ZnSe. We would want a detector to go as high resolution as possible for the right price.

3.6.5 Summary

We discuss in section 3.6.3 that the beam wavelength does not carry a heavy weight in determining the final displacement of the beam after passing through the refractive elements. We saw in section 3.6.3 that the prism material did carry a heavy weight in determining the beam displacement. Because we want to maximize beam displacement, we will choose a ZnSe prism for this experiment. Out of the available laser

sources, they are all transmissive but 532nm would be the least of all. Because the shorter wavelength lasers do slightly assist in beam displacement, we will choose the next longer wavelength diode, 650nm. These are cheap, small, and widely available. Through a 5mm thick ZnSe window (graph shown below), 532nm has 49.6 percent transparency while 650nm has a 67.1 percent transparency. The increase in power will be worth the extremely small sacrifice of beam displacement. Due to the precise nature of this measurement, the spot size of the 650nm laser will have to be rather small. The selected laser diode module would be the Mitsubishi ML101J25 658 nm 100 mW Red Laser Diode, which lases at 658nm and costs $18.70.

Symbol	Parameter	Conditions	Ratings	Unit
Po	Light output power	CW	**100**	mW
		Pulse(Note 2)	**250**	
VRL	Reverse voltage	-	**2**	V
Tc	Case temperature	-	**-10 ~ +75**	°C
Tstg	Storage temperature	-	**-40 ~ +100**	°C

Symbol	Parameter	Test conditions	Min.	Typ.	Max	Unit
Ith	Threshold current	CW	-	**65**	-	mA
Iop	Operating current	CW, Po=80mW	-	**150**	-	mA
Vop	Operating voltage	CW, Po=80mW	-	**2.4**	**3.0**	V
η	Slope efficiency	CW, Po=80mW	-	**0.95**	-	mW/mA
λp	Peak wavelength	CW, Po=80mW	**654**	**658**	**662**	nm
θ//	Beam divergence angle (parallel)	CW, Po=80mW	**7**	**9.5**	**12**	°
θ⊥	Beam divergence angle (perpendicular)	CW, Po=80mW	**14**	**17**	**20**	°

Figure 19: From Ref [1]

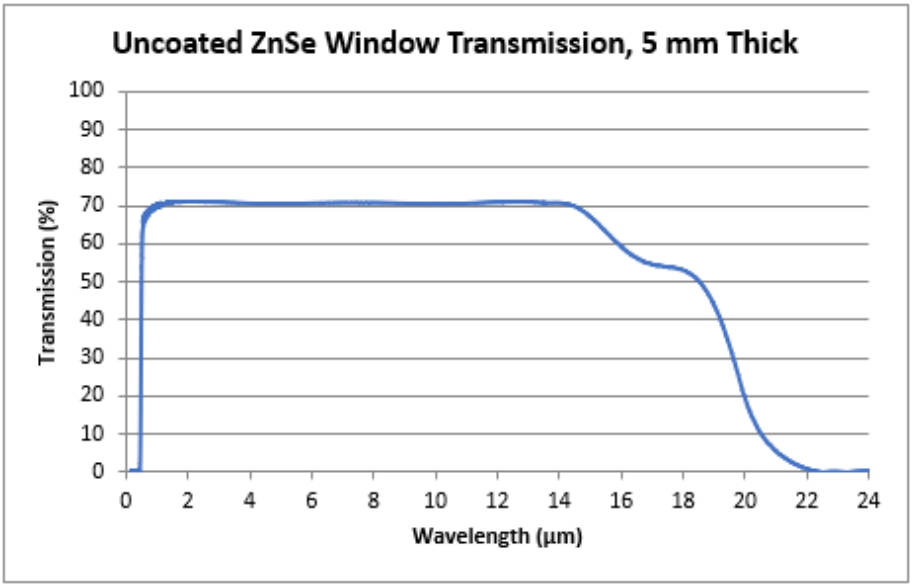

Figure 20: Plot of transmission as a function of wavelength for a 5mm thick sample of Zinc Selenide [33]

For the one-dimensional line array sensor, we determined that at minimum we would need 100µm resolution and preferably much lower. The Hamamatsu S3932 IR Photodiode has a position resolution of 0.3 µm which would satisfy our requirements and then some. The spectral response of 320 to 1100 is compatible with the decision to use a 650 µm laser diode module. The price of $63.27 is appropriate for its capabilities and is expected for in our budget.

Figure 21: Hamamatsu S3932 IR Photodiode [42].

3.7 Senior Design 2 Update

The design in the previous section was optimized for a Zinc Selenide prism refractometer. Unfortunately, due to the lack of availability and high prices of these prisms, a less optimal prism made of BK7 glass had to be chosen. The prisms were right angle 20mm side length BK7 prisms which are listed for $97, however these particular prisms were already owned by a team-member. Consequently, the laser wavelength was adjusted to 532 nm with a 5mW green laser diode to slightly increase the refraction angle over the previously selected 650 µm laser diode. The position detect remained as the Hamamatsu S3932 IR Photodiode.

3.7.1 Design & Assembly

Due to difficulties obtaining and the cost associated with ZnSe prisms, two BK7 prisms were chosen instead. The laser wavelength was correspondingly adjusted to 532 nm and the position sensor diode was kept as the high-resolution Hamamatsu S3931. The prisms have a refractive index of 1.5195 at 532 nm, which is a significant loss from the originally proposed 2.5115 refractive index of ZnSe at 800 nm. [25]

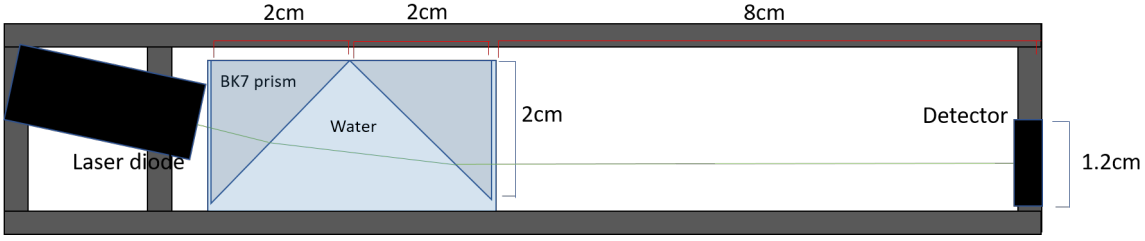

Figure 22: Modified v-block refractometer design.

The layout of the refractometer is shown in figure 22. The refractometer will be mounted externally and receive sample water from the main tank via a tube. The two prisms are arranged in v-block configuration and are surrounded in water contained by a plexiglass casing. A 532 nm laser diode is positioned such that it's beam is incident upon the prism housing at approximately 18 degrees from the surface normal, this is done because it allows for the exit beam to be approximately orthogonal to the exit plane of the prism housing when saltwater is in the sample housing. The data from the simulation and experiment section led to this design change. The Hamamatsu S3931 is mounted 8 cm away from the exit plane of the prism housing to allow adequate distance for the beam to displace enough to be reasonably resolvable, while also meeting size requirements. The Hamamatsu S3931 has a spectral response range of 320 to 1100 nm.

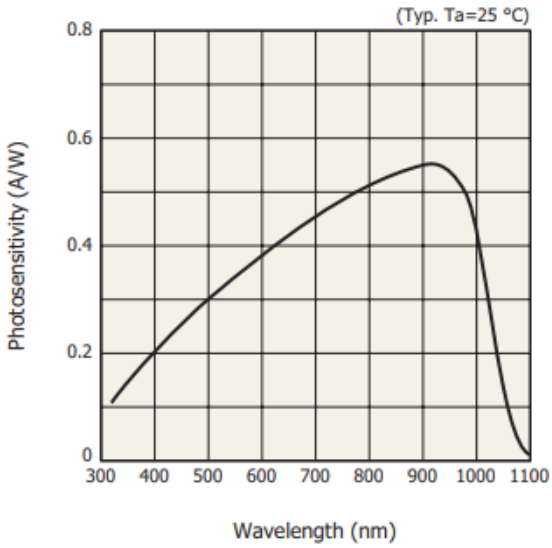

Figure 23: Spectral response of the Hamamatsu S3931. [43]

The spectral response of our position sensor diode is weaker at the updated laser wavelength of 532 nm, but testing proved the position sensor response was still adequate at 5 mW of 532 nm light. The positional resolution of the sensor is 0.3 μm, which when positioned at 8 cm away is equivalent to an angular resolution of 0.0000375 degrees. This is well beyond the expected noise due to particles in the water and will certainly not be a limiting factor in our system. The position detection sensor has two sets of an anode and cathode to probe the voltage off of. The voltage/current reading from each of these probes can be used in the following formula to back-calculate the position of the laser beam incident upon it:

$$(I_2 - I_1)/(I_1 + I_2) = 2x/L \tag{10}$$

where x is the position on the sensor, I1 and I2 are the currents obtained from the electrodes 1 and 2, and L is the length of the photosensitive area of the sensor (15mm). [43]

3.7.2 Simulation & Testing

An experiment was done to characterize and calibrate the refractometer system. This experiment was done with the laser normal to the prism housing surface, as shown in figure 24. Seven samples of water with different salinity's were prepared: 0 (freshwater), 10, 20, 30, 35 (approximately seawater), 40, 50, and 60 PPT. The laser diode was powered by 3.3V from an Arduino Mega. The analog inputs of the Arduino Mega were also used to read the voltage inputs from the PSD.

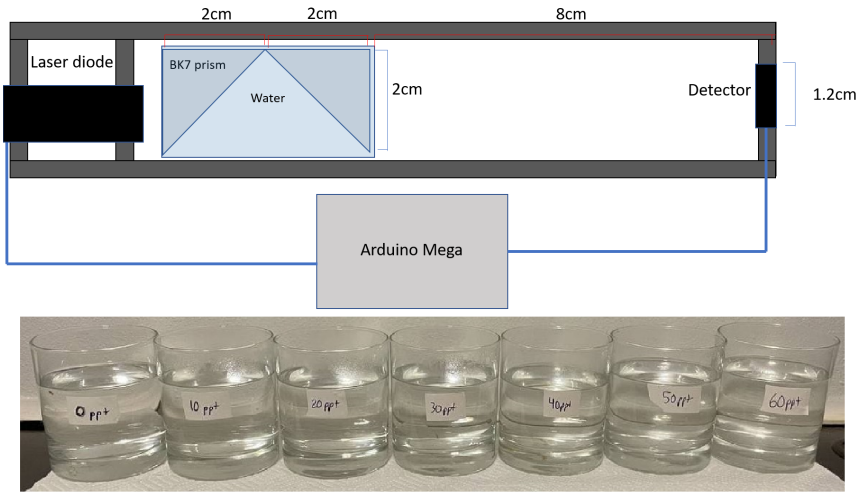

Figure 24: Layout of experiment to calibrate the refractometer. Pictured below are the water samples ranging from 0 to 60 PPT salt.

The following table details the results of the experiment, with the displacement being calculated via equation 2.

Salinity (PPT)	**V1**	**V2**	**Displacement from center (mm)**
0	0.384	0.461	0
10	0.380	0.476	0.63
20	0.377	0.482	0.94
30	0.378	0.497	1.35
35	0.377	0.501	1.51
40	0.376	0.515	1.96
50	0.376	0.529	2.35
60	0.374	0.540	2.73

Table 11: Table of experimental results from nearly complete refractometer configuration.

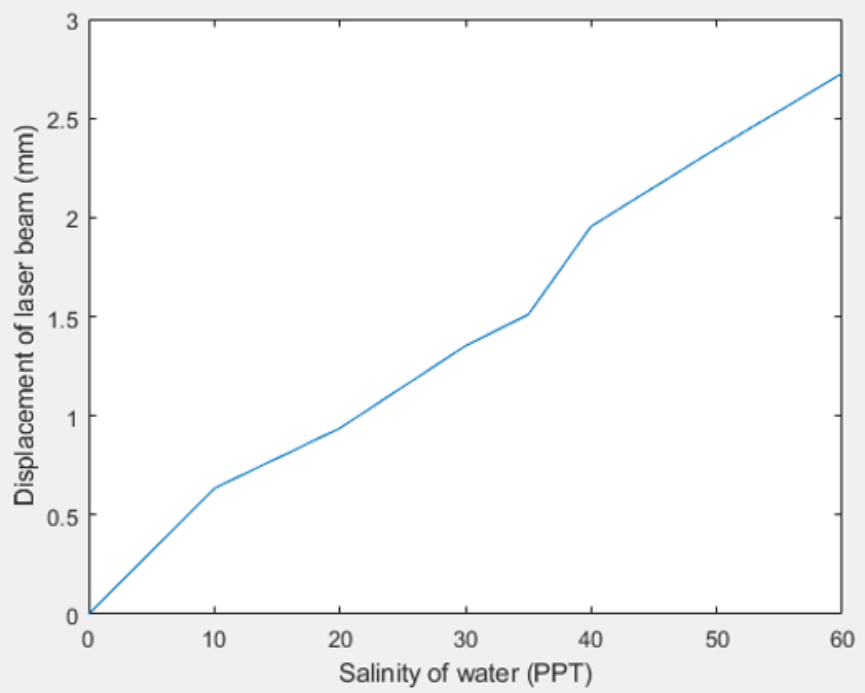

Figure 25: Simulation of displacement of laser beam over 8cm of travel.

This experiment was also simulated in MATLAB. The code accounts for 16 total interfaces and 4 different refractive indices (air, plexiglass, water, BK7). The simulation was used to plot the displacement of the laser beam from the center of the detector as a function of the refractive index (and thus salinity) of water in the sample housing. The plot from 1.33250 to 1.34335 in refractive index corresponds to water salinity's of 0 to 60 PPT as used in the experiment.

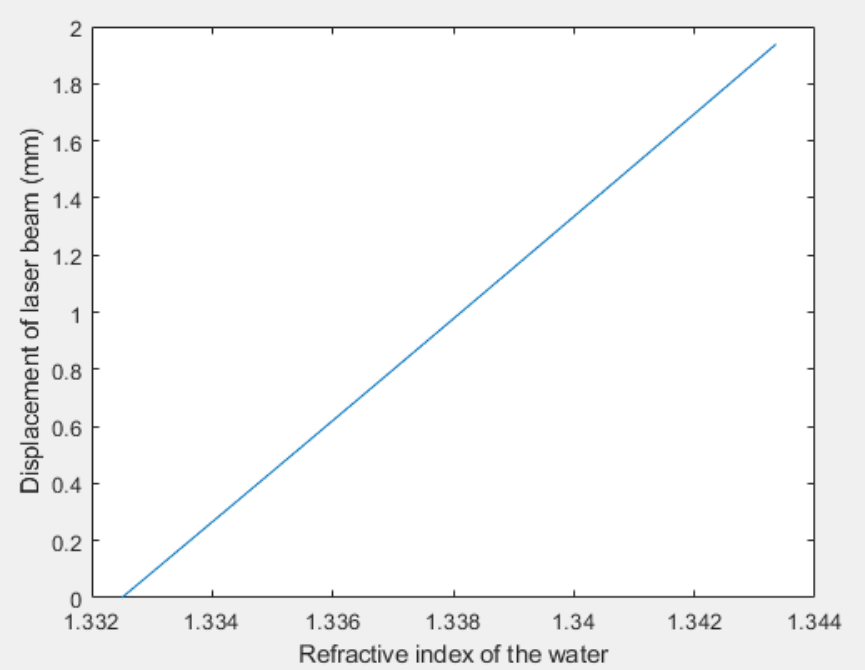

Figure 26: Simulation of displacement of laser beam over 8cm of travel.

We see that the device works quite nicely. The experimental and simulation results match, off slightly by some multiple factor, but share the most important aspect of being linear. A scale was be used to ensure accuracy of the salinity of the water samples, which revealed these nice results. Previously, in multiple experiements, results were off for this reason. The alignment of the system has been dramatically improved since the middle-term demonstration; no undesired vertical beam displacement is detected.The specifications of this system were surpassed by a factor of 7 as shown by testing. The original goal was to detect a 35 PPT change in salinity, but this system can easily detect 5 PPT changes.

3.8 Camera

We wish to take detailed images of the environment enclosed within the marine aquarium. We are limiting the image to 640 x 480 pixels due to our computing and data transmission capabilities, we must sacrifice a wide field-of-view for a narrower, ”close-up” image of the environment within the aquarium. Because there is no gravity in space, we expect an image of any section of the aquarium to serve as a representation of the aquarium as a whole, with minor differences in its corners. We wish to maximize our depth of field in order to be able to count all of the shrimp that exist within the camera’s view, from the front to the back of the miniature aquarium.

3.8.1 Preliminary Research

An imaging system that will satisfy our requirements constraints should be lightweight, feature a small footprint, and affordable for our extremely low budget. As such, we

will opt to use a compact camera module (CCM) as featured in modern cell-phone cameras, which is a CMOS sensor that is integrated with control electronics, as well as electronics to convert the analog signal into a digital signal, that is readable as a recognizable format that may later be recreated as an image on a display. We require a lens that will facilitate an imaging sensor placed very close to our marine aquarium, ultimately being very close to the object that it should form an image of. Our cubical aquarium will have a length of 100 mm, an image focused at the center of the aquarium will effectively have a path length that is a little more than 66.6 mm.

Commercially available camera lenses are not optimized to form images at this distance. With this being said, we must design our own compact plastic lens system that will form an image on our sensor.

Our CCM of choice, a CMOS OV5647 camera module, features a sensor with the dimensions $5.52mm \times 4.7mm$. Our lens must be capable of forming an image on this entire sensor, and in finding the radius of a spot that covers the entire sensor, we use Pythagorean's theorem:

$$r_{spot} = \sqrt{width_{image}^2 + height_{image}^2} = \sqrt{(5.52mm)^2 + (4.7mm)^2} = 7.2499mm \approx 7.25mm \tag{11}$$

If we aim to achieve a FOV of 10 degrees within the marine aquarium, and in considering that the image should be formed at the center of the aquarium, approximately 50 mm away from our lens system, we find that the image height is:

$$h = 50\ mm * \tan(10^\circ) = 8.816\ mm \tag{12}$$

It follows that we may find our transverse magnification,

$$M = \frac{h'}{h} = \frac{1.5\ mm}{8.816\ mm} = 0.17 \tag{13}$$

And while taking into account the optical path length in water, we find our image distance z'

$$z' = M * z = 0.17 * 50\ mm * 1.333 = 11.33\ mm \tag{14}$$

We may now use the gaussian equation to find the optical power of our lens system:

$$\frac{1}{z'} + \frac{1}{z} = \Phi \tag{15}$$

$$\rightarrow \Phi = \frac{1}{11.33mm} + \frac{1}{66.6mm} = 0.103\ mm^{-1} \tag{16}$$

Thus, we find a focal length of

$$f = \frac{1}{\Phi} = 9.683\ mm \tag{17}$$

Figure 27 is an illustration of our pre-design thus far, where blue represents water.

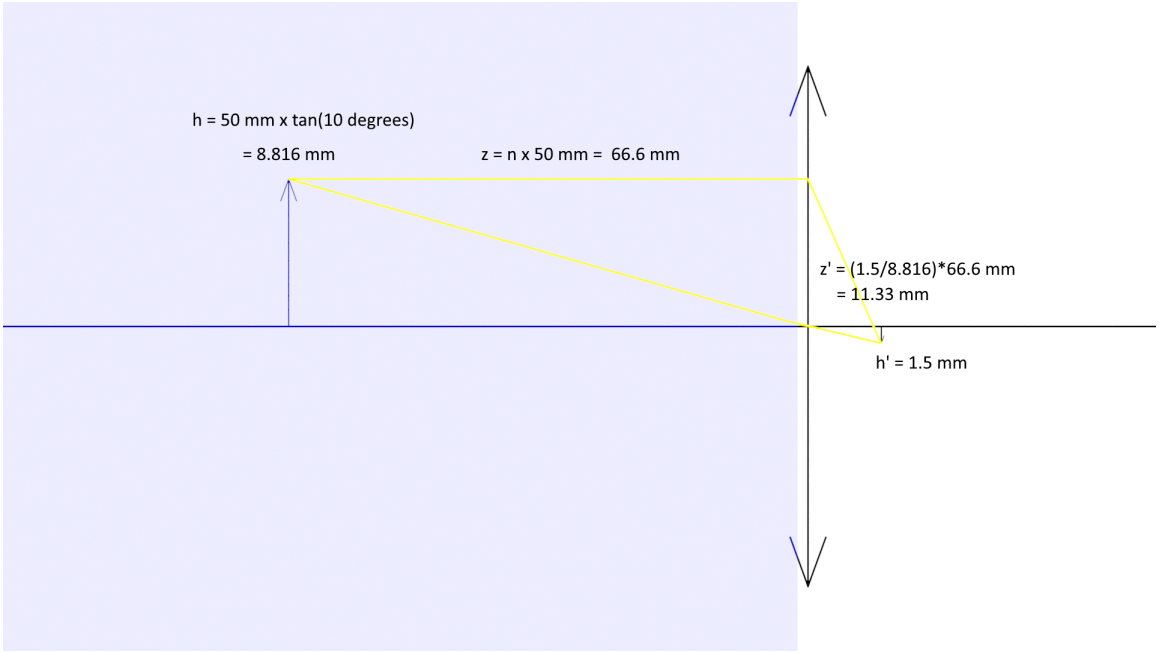

Figure 27: Simple Trace of Initial Pre-design

Unfortunately, the use of a single lens element will introduce chromatic and 3rd-order seidel aberrations. We also want to consider what factors contribute to the lens's ability to collect light to form a brighter image, and its depth of field. Depth of field can be described as the range in distance from the lens at which an object remains in focus [28]. It should not be mistaken with depth of focus, a term which is analogous to depth of field, which describes the amount of defocus on the image sensor that corresponds to being out of focus by one quarter wavelength of light [37]. Depth of focus follows the relation:

$$\Delta z' = \frac{2bz'}{D} = 2b(f/\#) \tag{18}$$

Where b is the spot size and D is the diameter of the exit pupil, and the F-number is defined as:

$$f/\# = \frac{z'}{D} \tag{19}$$

We may now define the depth of field, Δz as:

$$\Delta z = \frac{4\Delta z'(f^*)^2}{(\Delta z')^2 - 4(f^* - z')^2} \tag{20}$$

Where f^* is the back focal length of the lens system. In maximizing the size of our depth of field, it should be evident that we need to minimize our back focal length. However, in maintaining a sharp image, we wish to retain a small exit pupil

diameter and thus a relatively large F/# (In our design, we will be using an F/# of 2.8). Chromatic aberration can effectively be canceled out by using two lenses of high and low dispersion and refractive index respectively, s.t. the high-dispersion lens has a negative power and the low-dispersion lens exhibits a positive power. This is according to the following condition:

$$\frac{\delta n_1}{n_1 - 1} K_1 + \frac{\delta n_2}{n_2 - 1} K_2 = 0 \tag{21}$$

S.t. δn_1 and δn_2 represent the change in refractive index with wavelength for the positive and negative lenses respectively. Also, K_1 and K_2 indicate the optical powers of the positive and negative lens.

It is also critical to effectively cancel out third-order Seidel aberrations by using a sequence of lenses that have opposite effects on each given aberration as compared to the other lenses in the system, as the contribution that each lens has to each third-order Seidell aberration can be approximated as linear. These aberrations are:

- Spherical Aberration
- Coma
- Astigmatism
- Field Curvature
- Distortion

A number of compact lens systems have been designed which take advantage of six aspheric lenses of alternating powers to allow for resolving an image at a high quality. These aspheric lenses have aspheric coefficients up to the 14th order. The designed systems feature a focal length on the order of 3 mm and a F/# of about 2.5 [56]. Following this development, further efforts have been made to improve the performance of this aspheric lens system [21], s.t. the lenses alternate between cyclic olefin copolymer (n = 1.564 at the d line) and a material with a much higher refractive index, AL-6261 (OKP4) (n = 1.607 at the d line) in order to minimize chromatic aberration.
The geometry of an aspheric lens is defined by its sag:

$$sag(r) = \frac{Cr^2}{1 + \sqrt{1 - (K+1)C^2 r^2}} + A_1 r^2 + A_2 r^4 + ... + A_n r^{2n} \tag{22}$$

Where n is an even non-zero integer and defines higher order terms. Each of the coefficients A_n describe a certain deviation from the sag of a spherical lens. Such lenses may be designed to eliminate third-order seidel aberrations in highly compact schemes. However, aspheric lenses are typically very expensive to fabricate, due to their unique shape. These lenses become much more affordable when they are made of plastic, because plastic can be easily diamond-turned into aspheric lenses to create prototypes, and injection-molded when high volume is required.

3.8.2 Summary

Instead of purchasing a camera, we have decided to design and build an imaging system. This design is detailed in section 3.8.

3.9 Thermal Camera

It has been proposed to include a thermal camera to this module. In this section we will provide the necessary background to understand how thermal imaging works. This information will serve as an introduction to the selected candidate thermal imaging models to purchase from.

3.9.1 Background

Thermal cameras image infrared radiation (Near IR, mid-wave IR, long-wave IR) as opposed to regular cameras which image visible radiation (400-700nm). We analyze two distinct types of sensors that are used in thermal imaging, a microbolometer and photo-detectors. The working principal of the microbolometer is that a pixel changes it's electrical resistance as it absorbs heat. The photo-detector works like a regular camera, through absorption of photons which can be tuned by the pixel materials bandgap, but it images in the infrared. Infrared camera technology has developed rapidly over the last couple decades. The detectors can be separated into two categories, cool and uncooled, each with their own benefits and drawbacks. Artemia shrimp are small (insert size) and coldblooded, meaning that a sensor of high resolution and sensitivity is needed.

All objects emit what is called black-body radiation. Black-body radiation is thermal electromagnetic radiation that has a specific spectrum of wavelengths, inversely related to intensity that depend only on the body's temperature.[66] In simpler terms, an object's internal thermal energy is radiated as electromagnetic radiation, and the spectral components and intensity of the irradiation depends on the temperature of the body.

Notice that as the temperature of the object increases, as shown in figure 28, the energy density of the infrared components increases. At the same time, the peak of the irradiation also shifts. At higher temperatures the peak wavelength shifts to the lower wavelengths. This concept is why we know that predominately blue glowing stars in space are burning hotter than stars that appear predominately yellow or red. At room temperatures, things do not appear "glowing" hot like stars do. They typically appear black (as in they do not glow with signs of heat) and most of their thermal energy is released in the infrared, which is not visible to the human eye. Because of this release of energy, we can image objects in darkness (absence of visible light) and observe a spatial scene composed of an infrared signature. Each pixel's infrared signal can be calibrated to represent the temperature of a scene. For our particular application, we seek to monitor the scene for the temperature of individual

objects and shrimp. This would be more insightful than the temperature module that is being used to just measure the temperature of the water.

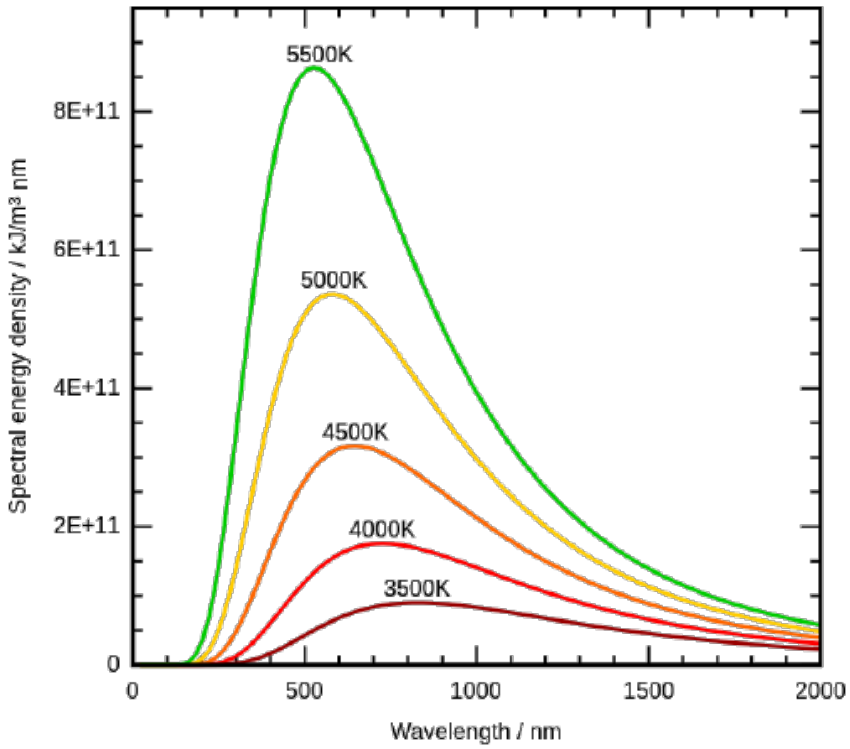

Figure 28: Black body emission at different temperatures.[66]

3.9.2 Infrared Optical Material Considerations

The thermal camera, which images in the infrared, has the same general working principal of a conventional camera: focusing light onto a sensor. However, the parts must be made out of different materials to image in the infrared. For the focusing optics, Zinc Selenide, Zinc Sulfide, Silicon (Fused Silica), and Germanium are most common.

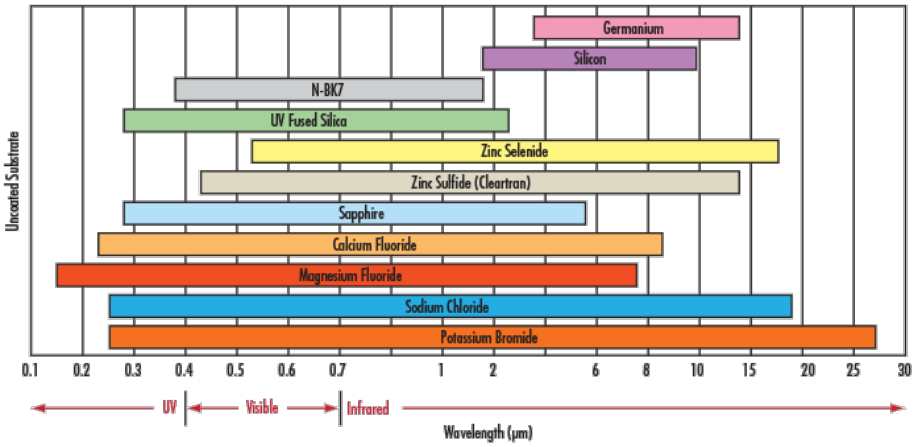

Figure 29: Common infrared material transmission windows [33]

Key attributes of the suggested common IR materials are shown below. Additionally, a very common visible glass, N-BK7, is shown as a baseline to compare to the IR materials. Index of refraction, as outlined before in this document, is the way in which the material slows the speed of the light that travels through it. The abbe number of a material is a measure of the material's dispersion (change of refractive index versus wavelength) to light. In simpler terms, it is how a material spread out light of different colors as they pass through it. CTE, coefficient of thermal expansion, is a measure of how the material expands or contracts as a function of temperature. A low CTE is almost always preferred, so that a change in temperature does not disturb any measurements. For our application, CTE is not vital because the temperature of the cube-sat will be regulated. dn/dT is coefficient that describes how the refractive index changes as a function of temperature. We would want this value to be low as well, so that any temperature changes does not disturb any measurements. Similarly to CTE, it is not that vital because the temperatures will be regulated.

Name	**Index of Refraction**	**Abbe number**	**Density** (g/cm^3)	**CTE** $(x10^{-6}/°C)$	**dn/dT** $(x10^{-6}/°C)$	**Knopp Hardness**
Fused Silica (FS)	1.458	67.80	2.2	0.55	11.9	500
Germanium (Ge)	4.003	N/A	5.33	6.1	396	780
Silicon (Si)	3.422	N/A	2.33	2.55	160	1150
Zinc Selenide (ZnSe)	2.403	N/A	5.27	7.1	61	120
Zinc Sulfide (ZnS)	2.631	N/A	5.27	7.6	38.7	120
N-BK7	1.517	64.2	2.46	7.1	2.4	610

Table 12: Comparison of key IR material attributes. [33]

The key takeaways from this graph are as follows:

- Germanium (Ge) has a high refractive index, high Knoop Hardness, excellent MWIR to LWIR transmission.
- Fused Silica (FS) has low CTE and excellent transmission in IR.
- Silicon is light weight.
- Zinc Selenide (ZnSe) has low absorption, high resistance to thermal shock.
- Zinc Sulfide (ZnS) has excellent transmission in both visible and IR, is harder and more chemically resistant than ZnSe.

Germanium typically sees uses in thermal imaging and rugged IR imaging. Fused Silica is used in interferometry, laser instrumentation, and spectroscopy. Silicon (Si) is low cost and is commonly used in Spectroscopy, MWIR laser systems, and THz imaging. Zinc Selenide is commonly used in CO2 laser systems and thermal imaging. Zinc Sulfide is commonly used in thermal imaging.[33]

Based on their respective common uses by professionals in industry and with their transparency windows, we favor the Zinc Selenide material for an infrared imaging optic. It's low absorption is ideal for powerful imaging all across the infrared spectrum.

3.9.3 Detector Considerations

The detector can be cooled or uncooled. A cooled detector is one that is typically housed in a dewar (or other similar housing. The cooling is done by a cryogenic, commonly by liquid nitrogen. This requires a lot of space and effort to be accomplished, and can be ruled out immediately from our design. Uncooled detectors are the choice by default. They work at ambient temperature and typically have a microbolometer based detector. The microbolometer typically works by absorbing heat and changing its electrical resistance with respect to this heat. This is in contrast to typical photo-detectors that absorb photons into a material with some bandgap which can be tuned to determine what wavelength is absorbed.

The most important parameters when selecting a detector are:

- Temperature cofficent of resistence (TCR) (we seek to maximize)
- $1/f$ noise (we seek to minimize)
- Resistance (we seek to minimize)

TCR is the coefficient that describes how the pixel's resistance changes with absorbed heat. $1/f$ noise, also called pink noise, is a signal or process with a frequency spectrum such that the power spectral density (power per frequency interval) is inversely proportional to the frequency of the signal. Resistance refers to electrical resistance, and we seek to have a detector with a low resistance at room temperaure and a high TCR to have high sensitivity to thermal changes.
Thermal imaging is usually done in a specific band of infrared, commonly divided into near infrared (0.9-1.7um), midwave infrared ($3 - 5\mu m$), and longwave infrared ($8 - 14\mu m$). For our application, detail is most important than exact temperature because of the small size of the shrimp.

IR Band	**Benefits**	**Drawbacks**
Near - IR	Highest detail	Misses many benefits of longer IR wavelengths
Midwave - IR	High detail	Less true to temperature
Longwave - IR	Truest to temperature	Lower detail

Table 13: Comparison of imaging in IR bands

3.9.4 Required Specifications

We seek then to find a camera that images in the NIR or MWIR, according to figure X, Zinc Selenide and Zinc Sulfide are the only materials that cover both of these bands. The detector needs to be an uncooled microbolometer with high resolution and high TCR. The following is a chart of suggested charactersitics for this camera. The budget immediately makes for sourcing a camera difficult, as these cameras are often expensive. The dynamic range must simply cover the temperature of the water, which the shrimp can survive at a relatively large range of temperatures, with 27°C

Budget	$150
Dynamic range	5-50°C
Accuracy	+/- 2.5°C
Frame Rate	10Hz
Sensitivity	0.1°C

Table 14: Requirement specifications for a thermal camera to be beneficial if it were to be included in our module.

being the most optimal. Therefore the camera should be able to cover from above freezing to decently warm. A range of 5-50°C would be sufficient. The accuracy is not that important of a parameter because the true temperature reading will come from our thermometer module. What is more important is the sensitivity, or the ability to distinguish a slight different in heat from one object to the next. This is critical as the shrimp are cold blooded, their temperature will vary from the water only slightly. For the camera to give any contrast between the shrimp, water, or algae we need a camera with great sensitivity/contrast.

3.9.5 Candidate thermal imaging systems

Adafruit AMG8833 8x8 Thermal Camera Sensor The Adafruit AMG8833 8x8 Thermal Camera Sensor is an example of a cheap thermal camera that actually operates as a true microbolometer. This module will actually be one of the very few that are within the $150 budget. The device would fit nicely as it is mounted onto a 1 x 0.8 inch chip.

Price	$44.95
Band imaged	LWIR
Dynamic range	-20-80°C
Accuracy	+/- 2.5°C
Resolution	8x8
Frame rate	10Hz
Sensitivity	0.25°C
Power use (during operation)	3.3 or 5V

Table 15: Adafruit AMG8833 8x8 Thermal Camera Sensor specifications.

This chip would be a strong contender if it weren't for the abysmal resolution. With an 8x8 array of pixels, this will not be any good for our application for which we seek to find contrast between small shrimp and their environment.

FLIR ONE Pro The FLIR ONE Pro is an interesting option that would require some modification to work for our application. The FLIR ONE Pro is designed to work over USB through a proprietary app, so this would be a major roadblock to using the device for our design. However, the option is still explored because this

device is one of the best performing true thermal cameras for under $500. With dimensions: 68 × 34 × 14 mm, the device is small compared to market competitors, but not as small as the adafruit sensor.

Price	$399.99
Band imaged	LWIR
Dynamic range	-20-400°C
Accuracy	+/- 3°C
Resolution	160x120
Frame rate	8.7Hz
Sensitivity	70mK
Power use (during operation)	Proprietary battery

Table 16: FLIR ONE Pro specifications.

This camera unfortunately requires a proprietary app. This would be a great deal of trouble to integrate into a system which needs to be fully automated. Designing our own app would be reasonable if the hardware was not locked down to only access this app. For the money, this device performs quite well when compared to it's $1000+ counterparts.

FLIR C5 The FLIR C5 is similar to the FLIR ONE Pro but is a standalone device that does not need a device to drive it over a USB cable.

Price	$599.99
Band imaged	LWIR
Dynamic range	-20-400°C
Accuracy	+/- 3°C
Resolution	160x120
Frame rate	8.7Hz
Sensitivity	70mK
Power use (during operation)	Proprietary battery

Table 17: FLIR C5 specifications.

This device is very similar to the FLIR ONE Pro. It's dimensions of 138 x 84 x 24 mm is slightly larger, but it shares all of the benefits of the smaller device. The device's resolution would be questionable for our application. It would depend where the shrimp were in the scene for how well they would be distinguishable. The 70 millikelvin is a good sensitivity for our application, but the price of $599.99 would be surpassing our budget by too much.
The cameras listed all image in the long wave infrared. The mid wave infrared cameras tend to be much larger and more expensive. Additionally, the near infrared cameras, which are much cheaper, simply do not do the job as they are less true to temperature and it would be more beneficial at that point to just use a camera that images in the visual wavelengths (which we already have).

3.9.6 Summary

The candidate choices do not fit the specified criteria while remaining anywhere near the budget. The temperature sensitivity of 70mK for the FLIR devices is impressive for a small thermal imaging device. It is enough to distinguish the cold-blooded shrimp from the water of which is closely takes the temperature on from, but the resolution of the cameras with the dimensions required to fit into our modules is not high enough to meaningfully distinguish shrimp from water. It's likely that the entire scene will be close to the same temperature, and this application would require a larger, more expensive MWIR camera. Even the most impressive cheap cameras on the market are out of our budget and do not meet our requirement specifications. For this reason, there is no suitable candidate for the thermal camera and it will be excluded from our project.

3.10 Computation

The computation component of this project is the core that ties the entire system together. Without it, there would be no way to send the raw data from the ecosphere to the ground where it would be able to be reviewed. The Micro Processing Unit, or MCU, that was chosen for this project needed to support enough I/O for the sensor array that was chosen, consume as little power as possible, and be able to effectively communicate with the image processing board. Our computation will have two subsegments in order to avoid some of the pitfalls of only having one processor.
The most intensive process that the computing system in our project will undertake is image processing. We likely could have chosen only one processor for our system, but that single processor would be at risk of becoming encumbered by the image processing task and be unable to accept interrupts from the other sensors. This would also cause the Power Management and Distribution (PMaD) system to freeze and would waste power, which is a precious commodity in a battery-powered system. In order to circumvent this issue, we will be using a smaller secondary MCU in addition to the primary image processing system. This secondary MCU will act as a device manager and will operate the PMaD system. This secondary MCU would accept inputs from the simpler sensors and feed the primary processor with each measurement. This will ensure that our computation system is able to handle all of the tasks required of it.

3.10.1 Processor Options

The first decision that had to be made when developing the computation for this project was the microprocessor unit (MCU) that would be used in its design. The options for the microprocessor to be used in this project were the ATmega328P, commonly used in the Arduino Uno, the ATmega2560, commonly used in the Arduino Mega, and the MSP430G2553, commonly used in the MSP430 TI Launchpad. These processors were selected for consideration due to the availability of community support, the open-source designs used in the parts, and their compatibility with the

project. A brief comparison of these microprocessors is shown in Table 18.

Microprocessor	MSP430G2553	ATmega328P	ATmega2560
Dimensions for SMT Package (mm)	6.5 x 4.4 x 1.2	8.5 x 8.5 x 1.0	16.25 x 16.25 x 1.05
Maximum Power Consumption (mW)	14	45	70
Mass (g)	0.191	2.2	0.58
Operating Temperature (°C)	-40 to 85	-40 to 85	-40 to 85
I/O Pin Count	20	23	84
Memory Capacity	16KB FRAM, 512B SRAM	32KB FRAM, 2KB SRAM	256KB FRAM, 8KB SRAM
Maximum Frequency (MHz)	16	1	16
Price (USD)	2.71	2.01	11.85

Table 18: Microcontroller Specifications Comparison [59, 7, 84]

Initially, we considered the ATmega2560 for the main MCU of this system due in no small part to its massive community support for issues we might encounter along the way. However, we realized that this MCU was not powerful enough for the main task we needed it for, which is image processing. Due to the large image size, we determined that the best course of action would be to select a Raspberry Pi Zero single-board computer to act as an image processor and a data transmitter. The MCU we decided on was the MSP430G2553.

3.10.2 Component Volume and Mass

One of the key considerations for these parts is the size of the component. In this project there is a severe limitation of space that we have to work with and design within. Because of this, every millimeter is precious in our design. The smallest MCU that we considered using is the MSP430 model. This MCU measures 6.5 x 4.4 x 1.2 mm and has a total volume of 34.32 mm^3 [84]. This MCU is an ideal candidate for our project given its small size. This MCU also has a mass of 0.191 g. This part is the smallest, most power efficient, and the least massive part.

Another key feature of the MCUs being considered is the mounting style. All of these components will need to be soldered in place, but the different mounting techniques also need to be taken into consideration when purchasing the parts. All of the components in question come in surface-mount varieties, but only the ATmega328p and MSP430G2553 come in a through-hole mounting package. Through-hole mounting for a component offers a number of advantages over surface mounting. The main benefit of through-hole mounting is the durability of the connections due to the increase in mechanical strength of the connectors. The main downside of through-hole mounting is the fact that it forces the components to be very large in comparison to fine-pitched surface-mount components.

3.10.3 Power Consumption and Clock Cycle Frequency

In all of these processors there is a trade-off between the frequency that the processor can operate at and the amount of power that the processor consumes. These MCUs require a higher voltage in order to operate at a higher frequency, and this often causes the current consumption to increase as well. The MSP430G2553 consumes about 14 mW when active at 16MHz, which is a power consumption more than 3 times lower than the ATmega328P, but with a clock speed 16 times as high[84, 59]. This is likely due to architectural and manufacturing process differences in the chips, as well as the difference in the number of instructions each can complete in one clock cycle. The fact that the MSP430G2553 can function at the same frequency as the ATmega2560 is very beneficial in this use case, especially considering the low power consumption.

3.10.4 Memory and I/O Pin Count

With all of these processors there is the issue of programming with the specifications of the MCU in mind. The MCU must also be chosen with the number of sensors that it will interact with in mind. We will have a small MCU to process the data from most of the sensors and have that MCU relay that data to the Raspberry Pi through a small number of I/O pins. This system will allow the Raspberry Pi to process the data from the image as well as the data from the other sensors and transmit that data through our antenna system. This process is necessary given our selection of parts since the MSP430G2553 only has 20 pins in total, with only 16 pins serving as I/O on the package we chose. This array of I/O pins will allow us to interface this MCU with the peripherals we need for this project to function as well as allowing for the control of the PMAD system. The PMAD system will only be delivering power to one sensor at a time to avoid interference between them, as well as to conserve power.

The other feature that sets these MCUs apart from one another is the memory and RAM size in each of these parts. From smallest to largest for both FRAM and SRAM there is the MSP430G2553, the ATmega328P, and the ATmega2560. The MSP430G2553 has only 512 bytes of SRAM memory to process its programs on, and 16KB of FRAM for persistent program storage. This likely contributes to the low power consumption of this unit. The ATmega2560 has 256KB FRAM and 8KB SRAM, which is much more than is needed in this application.

3.10.5 Integration of Processors

As stated previously, the MSP430G2553 will be the MCU in charge of the data intake from all of the sensors other than the camera. This MCU will also be in charge of the Power Management and Distribution system to ensure that the components don't interfere with each other's readings. The MSP430G2553 will be interfaced with the Raspberry Pi Zero with a UART connection. This will allow the MSP430G2553 to send the data that it collects and calculates from the sensor input to the Raspberry

Pi Zero. Once the Raspberry Pi Zero has the sensor data as well as the image, it will archive that batch of data and attempt to transmit it out. Given that the Raspberry Pi Zero has 512MB of RAM, there is plenty of space for the program, the image file, and the sensor data to be held before being transmitted.

3.10.6 Summary

There were several factors that were taken into consideration when deciding which MCU to use for our project. The critical factors were the memory capacity, I/O flexibility, and power consumption. Volume and mass also played a role in the decision, but a minor one. Taking these factors into consideration left us with only one clear choice for which MCU to design this project with. The MSP430G2553 is the lightest, smallest, and most power efficient MCU which also has the I/O flexibility and memory capacity needed in our selection. We will pair this MCU with a Raspberry Pi Zero in order to be able to process images from the SatCube as well as store and transmit the data effectively.

3.11 Batteries - Overview

There are many different types of batteries that can be used in a small satellite and the decision depends on the lifetime and the application of the project. If we were to have solar panels with the goal of recharging the battery when able, a secondary battery would be used. Secondary batteries are commonly used in phones and cars where they can be plugged in or recharged using an alternator, respectively. In our case, without solar panels and no desire for recharging, a primary battery could be used. A primary battery is essentially a one-time use power cell that would be discarded after it is drained and used.[20] Batteries consist of cells that can be combined to increase their potential. As our project's initial testing and development will be focused on the reading and implementing the sensors, the battery itself will come later in development. Once power requirements are better known, a more educated decision on the strength of the battery can be made.

3.11.1 Solar Cells

It is standard for a CubeSat system to have operating solar panels that are either built into the sides of the casing or expand in a wing set up after achieving orbit. Since CubeSats are extremely limited in available space and weight, solar cells are needed to complement the on-board battery. The typical lifespan of a CubeSat can measure in multiple weeks to a few months. This means that with the combination of limited space and limited weight, along with the desire for extended time of operations, solar cells are used to keep the battery going. The most common placement of the solar panels is simply adorning the sides of the CubeSat completely in panel covering. This takes up an enormous amount of space on the outside of the CubeSat since multiple panels are needed to increase the amount of time at least some of the

panels are facing the sun.

Without the ability to use thrusters and adjust a CubeSat to point towards the sun for maximum efficiency of the solar panels, a Fresnel lens can be used to redirect sunlight on to the solar panels. A Fresnel lens can be fitted around the corners of the CubeSat faces to increase collection of solar energy. As there is no way to control how often a solar panel will be facing the sun, this is a very efficient performance boost with minimal addition to weight or dimension. A Fresnel lens can be made extremely thin as small as a few thousandths of an inch. They can also be molded from light-weight plastic.

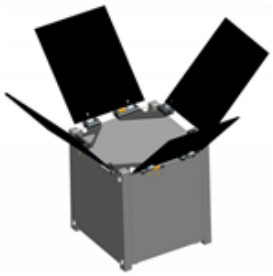

Figure 30: Example of Deployable Solar Panels

Another option for the solar panels is to make them deployable like wings where they lift up off from the faces of the CubeSat sides. This has the benefit of the satellite itself blocking less of the light as well as being a creative way to get around some of the dimensional requirements. The tradeoff is the need for extra mechanical hardware in order to deploy and hold the solar panels in this fashion. The example seen above was proposed for the PilsenCUBE picosatellite in a flower-like deployment by Ivo Vertat and Ales Vobornik. [87]

For our specific project we have decided that proper solar panels are not needed and beyond the scope of this project. CubeSat style solar panels fit for launching into space are well beyond our budget. Solar panels, as well as all hardware, are prone to radiation damage without proper shielding causing increased pricing. There is also no need for extending the lifespan of our battery outside of our proposed proof of concept demonstrations.

3.11.2 Battery Protection Circuit

The lithium-ion batteries that we have chosen to design with are unprotected, meaning that they have the ability to discharge at an uncontrolled rate. Because of this, we needed to either design or purchase a protection circuit for the batteries. Protection circuits serve three main functions for lithium-ion batteries, and these functions need to be kept in mind when designing the protection circuit.

The primary function of the protection circuit is to avoid overloading the batteries, which can cause catastrophic failures such as burning or exploding of the batteries. In order to avoid this, the protection controller can switch the battery out of the circuit in order to avoid damaging the cell. This is done using MOSFETs in most cases.

The second and third functions of the protection circuit are protecting the cells from over-discharging and from overcharging. This is done by ensuring that the battery voltage stays within the safe range of charging and discharging. This functions in the same way that the overcurrent protection circuit works and takes the cells out of the circuit if the voltage drops below the minimum value or raises above the maximum value.

Designing and manufacturing a custom battery protection circuit may be too time consuming and costly for a device that is often not necessary to be custom-made. The battery protection should be able to handle a 4S battery pack. Our batteries, Samsung 30Q 18650 3000mAh 15A, are 3.6 V and we have 4 of them in a pack. We need to analyze a few options for a 18650 battery and weigh the parameters of cost, maximum input voltage, maximum input amperage, and number of maximum cells in series allowed.

Battery Protection Circuit	**HiLetgo 18650 Li-ion Lithium Battery BMS PCB Integrated Circuits Protection Board Cell Balance**	**DEVMO BMS Protection PCB Cell Board Li-ion Lithium 18650 Balance**	**Comidox 18650 Lithium Battery Protection Board BMS Li-ion Charger Protection Module Anti-Overcharge/Over-Discharge/Over-Current/Short Circuit**
Price	$5.99	$9.50	$2.60
Maximum input voltage (V)	14.8	14.8	12
Maximum input amperage (A)	30	30	10
Maximum cells in series	4S	4S	3S

Table 19: Battery Protection Comparison.

This component was not factored into our initial budget, but it is cheap, so cost will not be the purchase-determining characteristic, unless they have the same perfor-

mance for different prices. Therefore, the slightly under-performing Comidox product will be discarded. Additionally, the Comidox model does not support the 4S configuration. Between the HiLetgo and the DEVMO models, they both meet the same specifications, which will be sufficient for our application. After analysis of these parameters for each of these circuits, we have decided to purchase the HiLetgo battery protection circuit because of it meets our needs and is half the price of the DEVMO equivalent model.

3.11.3 Power Management and Distribution – PMAD

Our project is built around operating many different sensors to take readings, processing this information with the onboard computer, and then transmitting this data. With the limitations of battery provided power, a system to manage and distribute this power will be required. This power management and distribution system is known as and will be referred to as PMAD. The goal of a PMAD is to increase efficiency and reliability of the flow of current and power to the different on-board devices as they are needed.

For our current project and prototype, the PMAD will be built in a way that can be simply controlled by the onboard computer to allow for the sensors, camera, heating element, and transmitter to be turned on and off as needed. Specifically which pieces of hardware, how many sensors can operate at a time, whether the heating element needs to operate alone, and the ability to cease RF transmission will be tested and developed as the project continues into its next stages.

The PMAD will be a simple construction compared to the typical case of a CubeSat. We do not need the additional input of solar panels which means we also will not face a need to discharge the battery or control its storage. When a launched CubeSat has a rechargeable battery with attached solar panels, it must be monitored and controlled to prevent overcharging while in direct sunlight for too long. The design of integrating any needed DC to AC or AC to DC conversions will be planned at a later stage of the project once final decisions and purchases of hardware have been completed.

3.11.4 Power Management and Distribution Design

Texas Instruments offers a web-based software tool called WEBENCH Power Designer. This software allows for the design of power supply circuits and will be the primary tool for our own project to design the PMAD. This product is free and allows easy creation of DC/DC and AC/DC converter circuits. With WEBENCH we can also run an electrical simulation and export it to a different CAD tool we will use to design our PCB.

3.11.5 Summary

As the entire project is dependent on being powered by battery, a power budget will be created. Once final decisions on hardware are made and data sheets are acquired a table will be created listing requirements for voltage, current, and peak power of the components. It is widely recommended for a CubeSat project to use a UL listed battery. UL, LLC is a company that tests and certifies batteries. Their certification is recognized to show the battery is reliable and meets industry standards. At that stage we will be able to decide on a battery. Since this is a project on a limited budget, we cannot afford to simply buy a battery that may be overkill, or even worse, under powered, at this time.

Batteries can come in many different voltages and ampere ratings. In order to fit our purpose, we can adjust the voltage and current to the different components of the system. All that is needed to accomplish that is additional circuitry or passive components built into the board. The main decision when it comes to a battery is how long it will last and how much power it will output in that time. While many batteries are advertised in mAh, or milliampere hours, that can be misleading. Without knowing the corresponding voltage of the battery, a mAh rating does not give the full picture. The best way to identify our battery comes in Wh, or Watt hours. All of our sensors and especially our heater may be operating at different voltage or current levels and so calculating the power required for each one is the best way to get a clear picture of the battery needed.

A typical battery in a CubeSat might be a 35Wh Lithium Ion battery. This allows an output of 35 Watts for one hour or one Watt for 35 hours. The Lithium Ion battery allows it to be recharged by the solar panels that are typically present on a CubeSat. Our project can be tested throughout development without the use of a battery if we need to save money by avoiding a rechargeable unit. An output of 35W would also likely be overkill. In order to demonstrate the sensors running through a cycle, transmitting our data, and heating the aquarium, we are much closer to needing power for only a handful of hours at most. The heater is going to be the biggest power draw and will likely run in the ballpark of around 4 Watts output. Since we will be surrounding our prototype with ice or some other method to test the heater and then recording a video, we do not plan on running the heater for hours on end. These limited duration demonstrations will allow us to save some on our budget compared to the heavy duty batteries usually used in a true, launched CubeSat.

For this project we will be using a series setup of 3.6 Volt batteries. With four of these batteries in series this allows us a top voltage of 14.8 volts. If there is an issue later on of space requirements we can attempt to run the system with three batteries in series with a top voltage of 11.1 volts. Using 18650 lithium ion batteries will provide more than enough amperage for every component. The design goal is to have more voltage and current than needed as it is more efficient and simpler to build a circuit design that will step down the voltage than attempting to use additional amplifiers for

Battery	**18650**	**20700**
Dimensions (mm)	18 x 65	20 x 70
Mass (g)	48	61
Capacity (mAh)	1500 to 3500	2800 to 4100
Price (USD)	4.50	9.50

Table 20: Battery Type Comparison

Battery Models	**Samsung 30Q**	**Samsung 25R**	**Murata VTC5A**
Dimensions (mm)	18.33 x 64.85	18.33 x 64.85	18.2 x 65
Nominal Voltage (V)	3.6	3.6	3.6
Weight (g)	48	45	47.8
Nominal Capacity mAh	3000	2500	2600
Max Voltage (V)	4.2	4.2	4.2
Cutoff Voltage (V)	2.5	2.5	2.0
Discharge Current (A)	15	20	25
Price (USD)	4.50	3.50	6.50

Table 21: Battery Model Comparison

particular power needy components. These batteries are very common and plentiful and are more than enough to suit our needs. The particular model is Samsung 30Q 18650 3000mAh 15A Battery.

3.12 Power Regulation

Electronic circuits and the components therein are designed to operate within certain voltage specifications, but the power source for these circuits may not provide a voltage that is stable enough for the circuits to work as intended. Fluctuations in voltages can damage circuits or cause them to perform differently than the design specifications require. In order to prevent this damage and out-of-spec performance, voltage and current regulators are used. In order to design these regulators we take into account the operating conditions for the power source and what voltage it will supply when operating as intended. If the power source supplies a voltage outside of these operating conditions then a protection circuit will be tripped and the supply of power will be cut off. This is done in order to protect both the circuitry and the device supplying the power. This protection circuitry is especially important given the device that we will be using for the storage and supply of power.

Power will be delivered from a battery pack with 4 series Samsung 30Q 18650 cells, which each have a peak charged voltage of 4.2V and a minimum voltage of 2.5V when discharged. These cells will therefore provide 16.8V when completely charged and 10.0V when completely discharged. These were selected due to their very high energy density and the ability for three of these cells to be placed in series in order to generate a voltage higher than the minimum voltage we need. We decided to go with a 4S cell design for the batteries so that we don't have to step up the voltage. Stepping up the voltage with a boost converter consumes far more power than stepping down the voltage with a buck converter. Since we will only be stepping down the current for the processor, we will be able to use much more efficient components for our power regulation devices.

3.12.1 Voltage Regulation - Buck Converters

Buck converters are used in order to lower the voltage and increase the current in a given circuit. This is done by switching the input to the circuit on and off at a specific frequency and duty cycle and then normalizing that output with a diode, an inductor, and a capacitor. Figure 31 shows a generic buck converter diagram with the components, currents, and voltages labeled. These labels are used in Figure 32 to demonstrate the normalization of the current at the output.

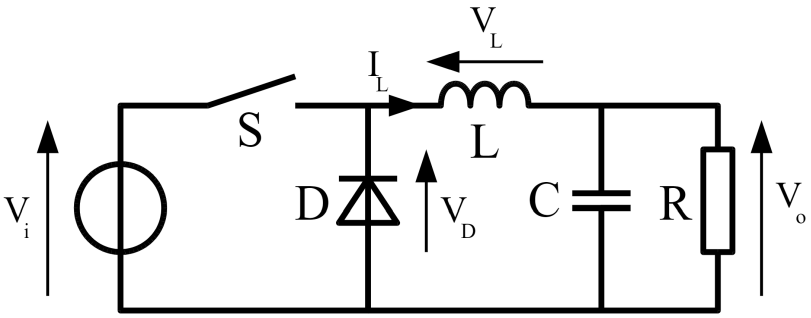

Figure 31: Generic Buck Converter Diagram [17]

The voltage normalization process with a buck converter occurs because of the resistance of the capacitor and inductor to change voltage and current instantaneously. Due to these effects, the current out does not drop to zero immediately after the input voltage it set to zero. Instead, the inductive current and capacitive voltage cause the diode to change from being reverse-biased to being forward-biased and allowing the stored current to continue to flow through the output. This continued flow of stored current is shown in the gradual decrease in current in Figure 32.

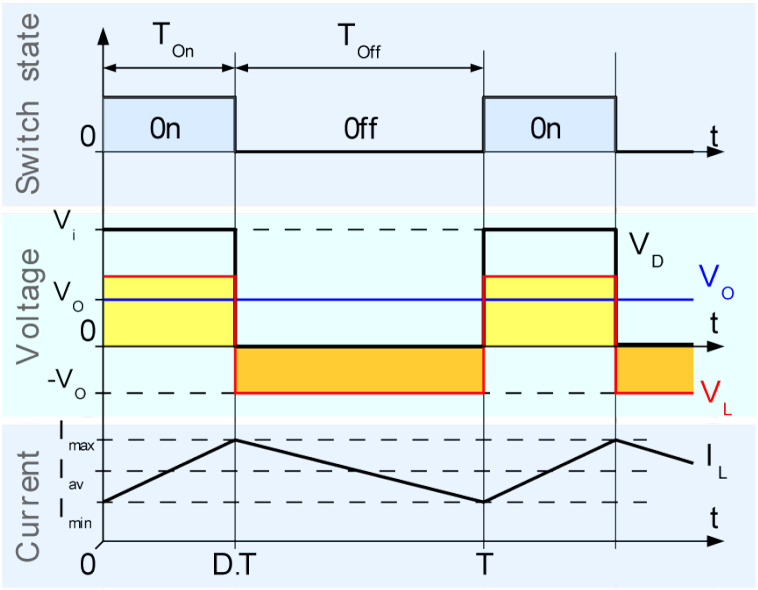

Figure 32: Voltages and Currents of a Buck Converter in Continuous Mode [16]

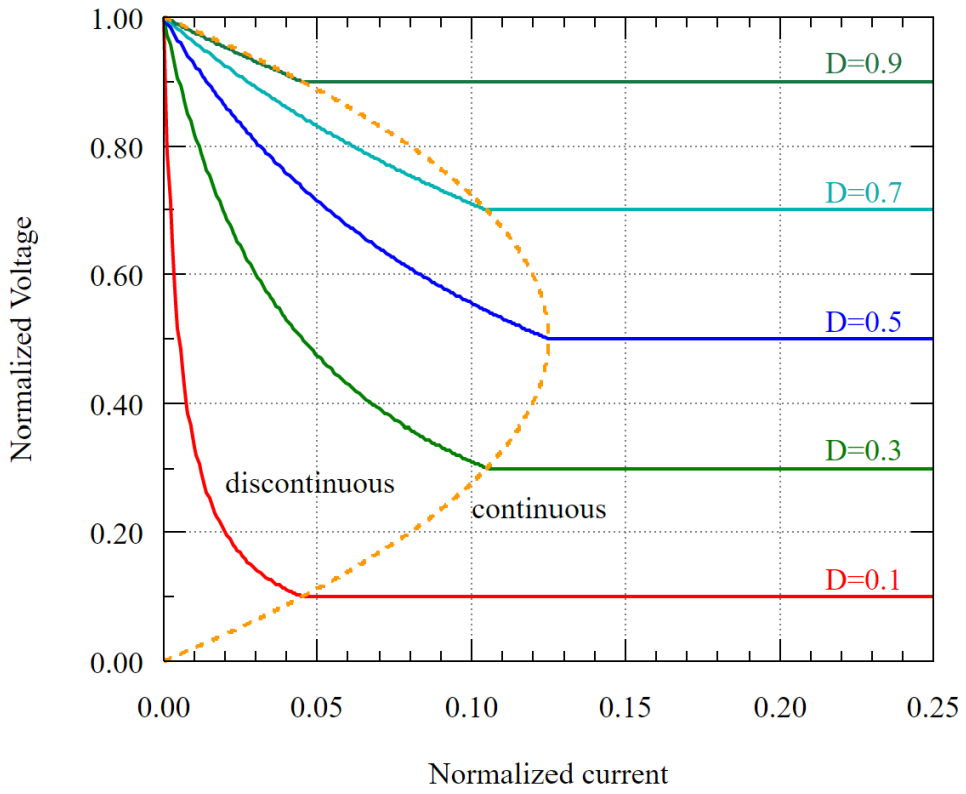

Figure 33: Output Voltage as a function of Duty Cycle in a Buck Converter [18]

The output voltage for a buck converter is typically tuned to a very tight ripple that isn't shown in Figure 32. For example, when in a steady-state situation, the voltage regulator that we have decided to use has a peak-to-peak voltage of 6.66 mV at 627.14 KHz. This ripple is situated around the 3.6 V that this regulator is designed to output, so the ripple is small enough that it doesn't effect any of the components receiving the power from this regulator. This output voltage is also a function of the duty cycle of the switching occurring with the input voltage in continuous mode. This is demonstrated with Figure 33, where the output voltage is half of what the input voltage is when the duty cycle of the input switch is 50%.

3.13 Thermal Considerations and Heating

This section will cover our options for keeping our components within operation temperature as well as our biological specimens in a survivable environment. We will cover the common methods for surviving the extremes of space as well as what we are able to apply to our own project. This section will also define the following: the goal of our heater, what will be done to demonstrate the effectiveness of the heater, our options of different types of heaters, and ultimately our choice of the type of heater to use in the system.

3.13.1 Thermal Control for Small Satellites

Once launched, a small satellite has to not only avoid the additional radiation of space but the extreme heat and the extreme cold that can come depending on where it is in relation to the sun. While NASA has extensive experience in dealing with the temperature difficulties for larger spacecraft, the development of these same techniques on a miniaturized scale for CubeSats is not as advanced. The size and weight limits add additional difficulties for all operations and the highest quality passive materials present financial pitfalls for any amateur CubeSat projects.

Passive systems for dealing with these thermal challenges range from paint, deployable radiators, heat pipes, thermal straps, and even sun shields as seen in Figure 19 below. These passive systems function through conduction which is the transfer of heat between two different materials without the need for any action by these materials. The inside of the CubeSat functions primarily using this method of conductive heat transfer. Using these materials to move the heat away from the sensitive components inside the cube allows for heat to dissipate through radiation outside of the satellite.

One way to prevent overheating can be seen in the sunshield in Figure 34 below. Stopping the radiation from the sun before it gets to the satellite can be more effective than going through the process of removing it afterwards. Other methods for preventing radiation come in thermal coatings, paints, and strips that focus on using materials that "have certain specific radiative properties, commonly referred to as solar absorptivity (implying wavelengths in the range of approximately 0.3 to 3 µm), and IR emissivity (approximately 3 to 50 µm)." [64]

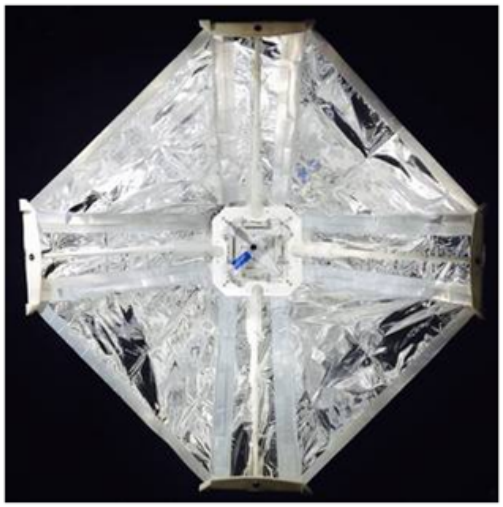

End view of Sunshield on CryoCube-1 developed at Sierra Lobo.
Credits: Sierra Lobo (2014).

Figure 34: Sunshield from Sierra Lobo

There are also active systems which is what we will be using for our project. Active systems, of course, require power to operate and so are generally harder to implement on a CubeSat that is limited in its dimensions and battery storage. The benefit of an active system and the main reason that we will be using one is that it can be more precise. In order to demonstrate that our heating element works in conjunction with the rest of our components, an active system is also needed. It will allow us to demonstrate reading and controlling the temperature on command as we do not have the budget to undergo a thermal vacuum test that many satellite projects use. A thermal vacuum test would be beneficial to expose our prototype to the extremes of space but is not necessary for our purposes.

As we will not be dealing with the extremes of space, we will not be focusing on any passive thermal regulation or any radiation-based dissipation. Our thermal testing will be done by inserting our prototype into a freezer or refrigerator in order to reduce the systems temperature. Once this drop in temperature is read, we will power on our heater until a suitable temperature is measured. Once the system has returned to an acceptable level, the computer will be programmed to turn the heater off. If we are able to achieve this in our testing, we will consider it a successful use and demonstration of our heating element.

3.13.2 Heat Cable

The life within our ecosphere is very resilient, because of this our main goal of the heater is just preventing freezing. An extremely common occurrence, outside of Florida at least, is the need to protect water pipes from bursting during the winter. This is done by using heating cables. These are essentially just resistor wires

at heart but have been developed and customized to be self-regulating and made of more efficient materials over time. It is also known as trace heating, electric heat tape, or surface heating. By running this component along pipes in a home, they can adjust to the ambient temperature and maintain temperature above freezing. They are designed to run along the length of the pipe and are usually wrapped in insulation along with the pipe in order to prevent heat from escaping.

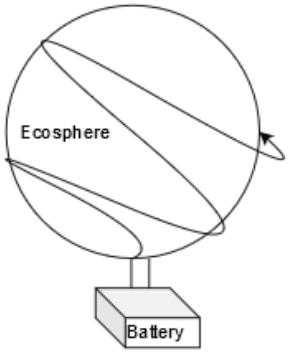

Figure 35: How Heat Cable Wraps Around Our Ecosphere

For our purposes, the main benefit of using heat cable would be the ability to customize the length and shape of the heating element. As space is our number one limiting factor in any decision, the type of wrapping as seen in Figure 35 would allow us to wrap the heater around the surface areas reserved for the sensors to view inside the ecosphere.This type of heat cable is designed to constantly be plugged in and on during the winter months which is not what we would want for our battery powered system. Another potential issue is that the self-regulated heat cables operate by expanding and contracting to increase or decrease the temperature along the cable. The expansion disrupts the electrical current throughout the cable leading to less heat transfer. When the cable contracts, the opposite occurs, where the electrical paths are reconnected, allowing more heat to flow. This is a great and useful technology, but not ideal for an experiment that we do not plan on running for days at a time.

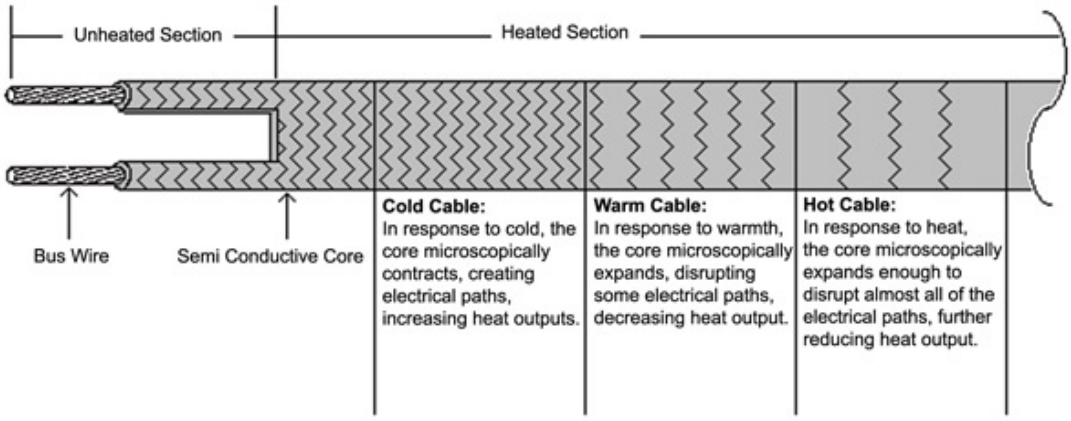

Figure 36: How Self Regulating Heat Cable Works. Courtesy of BriskHeat.com

One worry about using a heat cable is that they are designed to be on for months at a time. Our purpose of turning the heater on by command when an unacceptable temperature is measured might require a faster rise in temperature than this component is designed for. There are powerful heating cables that are designed to operate in -40 degrees Celsius level temperatures but they are typically plugged in to a home power outlet which is well beyond the voltage of our battery system.

3.13.3 Electrical Resistance Heater

For our purposes we will be using an electrical resistance heater. This is a very simple and efficient method of adding heat to a system. It operates just by sending a current through a resistance in the form of a wire. This is the same concept as the heat cable in the previous section with a more specialized overall layout. There is no self-regulation and instead of the entire component designed for heating, there are power cables that lead away from where the heating wire is concentrated and wrapped into a pad for localized heating. In our case it will be sending current through a resistant wire that we attach to a heat plate or insulator. This heat plate will then be attached to the base of the ecosphere. Since the ecosphere is so small and intended to be enclosed, we did not want any heating element running into or through the water itself.

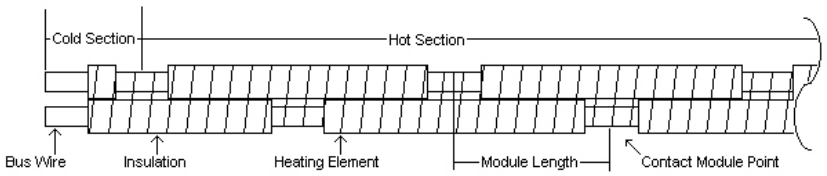

Figure 37: How Constant Wattage Heat Cable Works. Courtesy of BriskHeat.com

In Firgure 37 we can see how a constant wattage heating cable works. We have the option of designing our own cable wrapped around the ecosphere as previously discussed. This may be a better option than the self-regulating cable since we will be turning the power to the heater on and off on our own and do not require the extra regulation. Wrapping the heat cable around the ecosphere will require some additional components such as glue or tape. If there is nothing keeping the cable in place then it adds to the complexity of our system once the prototype is enclosed. For this reason a pre-shaped pad like heater is a better choice. An example of the heating element we will be using is seen below in Figure 38. This is an identical design to what we will be using once we determine the proper current that will be needed for our system.

Figure 38: PTI Pelonis Ultra-Thin Flexible Heater

Once we enter our testing phase, we will be able to find out if simply attaching such a heater is enough or if a modification will be needed. Possible modifications include wrapping the heating element around the aquarium in order to spread the heat out. If there is too much direct contact with the heat and it starts to cause problems with the material of the aquarium, we have the option of adding additional covering or molding it to a heat plate to further disperse the direct heat around the container.

This heater will need to be controlled by the computer as it reads the temperature of the system. As it is likely to be the largest single current draw, the computer will be designed to shut down the other sensors and transmitter as needed in order to meet the current requirements for sufficient heating.

3.13.4 Silicone Rubber Heater

An extreme option to consider for our purposes would be a silicone rubber heater. These types of heaters have widespread uses in the food industry and even in the air travel industry. A common use of such a heater with etched foil elements are used in restaurants and in steamers to keep food warm. They can heat and keep water at 60 degrees Celsius which is beyond any of our requirements. Because of this extra heating power, it could be considered an option if there is a need to heat the system at a faster rate than a weaker heater. Since our primary goal is demonstrating cohesiveness of all of our components, it has been decided that the electrical resistance heater is better suited for our purposes.

A benefit of using such a heater is that they are easily obtained, readily available, and simple to operate. This would definitely be more than enough to prevent our eco-sphere from freezing. Even though this type of heater would essentially be plug and play, it would not fit our constraints. They require more power than we can accommodate with our battery operation. A typical silicone rubber heater would also be too big to fit within our required dimensions. For these reasons, we will not be using a silicone rubber heater.

3.13.5 Summary

After looking at our choices for heaters it comes down to two main constraints, size and power. Although the heat cables offer the benefit of shaping the heater around the aquarium to fit as needed, the PTI Pelonis heater has the benefit of very low power required as well as being almost as small. The specific model is the TSA0100010bR35.4 from PTI Pelonis. As development of our aquarium went on, we made the decision to increase its size by a large margin. This meant that the model of heater we chose at the beginning of our project would not be able to deliver enough heating power for us. We ended up still going with the same type of technology, just at a higher wattage. We ended up going with 3 Icstation 12V 7W heaters. We found that it would take approximately 10,000 Joules in order to increase the temperature of our aquarium by 1 degree Celsius, though, so even though we have 21W of heating we were not able to develop a realistic solution with this method. Since we would have to run our heaters for an extended period of time, this solution would require solar panels to recharge our batteries. Solar panels are a common occurrence on a CubeSat, just not a part of this project.

Heater	**TSA0100010bR35.4**	**Freezstop 12FLV Heat Cable**
Dimensions (mm)	10 x 10	8.5 x 3.9
Voltage (V)	3	12
Power	0.25 W/cm^2	12 W/m

Table 22: Heater Comparison

3.14 Transmitter, Receiver, and Antenna

This section will cover our options and designs for our telecommunication systems of the project. We will explain our goals, constraints, options, and choices of hardware. Our goal for a successful demonstration will be to transmit from our prototype to a receiver approximately 500 meters away. The second goal of this part of our project is to be able to send a termination signal to the prototype. This termination signal will need to be able to cease all RF transmissions just as if a situation occurred where we were requested to do so by the FCC.

3.14.1 Transmitter and Receiver

As previously stated in the regulation guidelines, our chosen operating frequency is 433 MHz in the 70cm wavelength band. As seen in the below chart, the original choice of 433MHz was based on the allowed amateur operating frequency bands. The regulation changed to 435 MHz after the start of the project and an attempt to adhere to it will be made if it is within the budget to do so.

Wavelength band	ITU Region 1	ITU Region 2	ITU Region 3	Sharing requirements *see* § 97.303 (paragraph)
VHF	MHz	MHz	MHz	
6 m		50–54	50–54	(a).
2 m	144–146	144–148	144–148	(a), (k).
1.25 m		219–220		(l).
Do		222–225		(a).
UHF	MHz	MHz	MHz	
70 cm	430–440	420–450	430–440	(a), (b), (m).
33 cm		902–928		(a), (b), (e), (n).
23 cm	1240–1300	1240–1300	1240–1300	(b), (d), (o).
13 cm	2300–2310	2300–2310	2300–2310	(d), (p).
Do	2390–2450	2390–2450	2390–2450	(d), (e), (p).

Figure 39: Amateur Operating Bands for Technician, General, Advanced, or Amateur Extra Class License

Once the amount of data that needs to be transferred is decided, we will be able to select a proper data rate to be transmitted. As we will be both sending and receiving data from our satellite, we are going to need two of everything. A laptop will be used to act as our Earth Station. At a range of 500 meters we will set the lap top up with the Earth Station transmitter, receiver, and antenna.

A typical CubeSat mission can include three different points of transmission and receiving. There is a location on Earth that initiates the contact or gives a command to the satellite in orbit. The transmitter on Earth or within 50km of the Earth's surface would be called the transmitting Earth Station. The satellite receiving the communication, which could be a command to take a measurement, cease operations, initiate a procedure, or send back a reading, would be considered the Space Station. Finally, since a CubeSat is not going to be in geostationary orbit, there is a third location that would receive the transmission back from the satellite called the receiving Earth Station.

For our project, since we will be stationary in the same lab or just 500 meters away, we will only have two locations. A laptop or computer with a connected receiver on a bread board circuit will count as both our transmitting and receiving Earth Stations. This Earth Station will be responsible for receiving the data read outs from the satellite and verifying the operation of the project on the laptop that it is connected to. The transmitting part of this mock Earth Station will be responsible for sending out the cease transmissions signal in order to demonstrate compliance with the FCC regulation that requires this ability. The Space Station in this experiment is the prototype CubeSat itself. It will be responsible for receiving the cease transmissions signal during that part of the experiment. The transmission part of the Space Station will be sending the sensor readings log back to the mock Earth Station laptop.

3.14.2 Cease Transmissions Signal

For demonstration purposes of our project the goal is to have a receiver on board the device that can shut down RF transmissions. As the only requirement for this particular component is essentially a yes or a no logic read by the computer, a powerful transmitter/receiver combination is not needed. We only need to demonstrate the range.

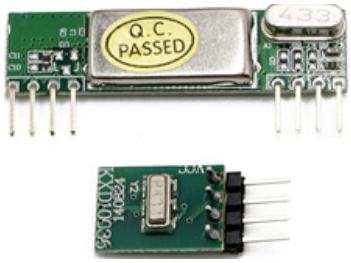

Figure 40: RioRand 433MHz Superheterodyne RF Link Transmitter Receiver

The combination in Figure 65 above has been purchased and chosen for this "kill switch" type of operation during testing as it meets our needs to operate in a lab space type of environment. It would need additional power and an attached antenna in order to meet our 500 meter requirement. This component has been chosen for testing since our LoRa SX1278 components will take longer to arrive through shipping and also requires some soldering to put together. Using a separate component during the testing phase adds extra programming work but is deemed necessary for a project that is on a tight time budget.

3.14.3 LoRa - Long Range Spread Spectrum Modulation Technique

LoRa stands for Long Range and is a Low Power Wide Area Network, LPWAN, protocol. This protocol was originally developed by Cycleo SAS with its primary use in connected devices to the Internet of Things, IoT. Cycleo was a privately held company in France that develops IP for wireless semiconductor products. Semtech Corporation acquired Cycleo SAS and all of its assets back in 2012 in order to incorporate their technology for future RF platforms. The primary benefits of using LoRa are that it has low cost, low power consumption, and is easy to position since the components can be very small, battery powered, and integrated into or with many different devices. This modulation technique was developed using the Chirp Spread Spectrum.[69] The Chirp Spread Spectrum (CSS) was originally developed to use in radar applications back in the 1940's.[80]

LoRa devices use sub-gigahertz RF bands like the 433MHz that we will be using. LoRa itself describes the lower physical layer (PHY) which is the actual chip itself. These chips can use different protocols for the upper layers of the network. One

common networking protocal is the LoRaWAN, or Long Range Wide Area Network, which acts as a network layer protocol. The LoRa Alliance is a nonprofit, 501(c) organization, of which Semtech is a part of. This alliance is a network of over 100 LoRaWAN operators across the globe. This network allows the connection and communication of devices that help in natural disastor prediction, fire alarms, animal tracking, water monitoring, and irrigation networks. We will not be using a network of connected devices for this project, but we will be using it in a similar fashion as a smart home, where we will be monitoring the wireless sensors on board the CubeSat.

3.14.4 Shannon-Hartley Theorem

Much of the LoRa technology is under protected patent and so cannot be directly analyzed and evaluated in all aspects. Much of the science and documentation is based on predictions and derived approximations based on computer modeling and numerical results.[31] Since we must work within those constraints we can start on the basics such as the Shannon-Hartley Therorem. This theorem states that "the maximum rate at which information can be transmitted over a communications channel of a specified bandwidth in the presence of noise." [80] This theorem is represented by the following equation:

$$C = B * log_2(1 + \frac{S}{N}) \tag{23}$$

Where C is our channel capacity represented in bits per second. B is our channel bandwidth represented in Hertz. S is our average received signal power measured in Watts. N is the average noise or interference power measured in Watts. S/N is the signal to noise ratio, commonly referred to as SNR, which is represented as a linear power ratio. For spread spectrum applications such as our own, the signal power is lower than the noise power, resulting is a small SNR which is usually much less than one. With a little bit of algebra and making that assumption that S/N is much much less than one, we can rewrite the equation to get the following approximate equivalency:

$$\frac{N}{S} = \frac{B}{C} \tag{24}$$

With this equation it can be seen that in order to transmit error free, only the transmitted signal bandwidth needs to be increased if we have a channel of fixed Noise to Signal Ratio. This means that in order to compensate for an SNR that is degrading, we can increase the bandwidth of the signal. To give an idea of what is accepted as good or great quality for transmissions we can look at what satellite are commonly used for, TV transmissions.

- 55dB, Studio Quality Signal Transmission.
- 45dB, Good Quality, Small Amount of Noise.

- 35dB, Poor Quality, Absolute Minimum, Mostly Unwatchable.

In our project since we are not trying to transmit a television signal, which includes many frames per second of high quality pictures as well as a high quality audio signal, we can accept a SNR lower than a poor quality television transmission and do not have to aim for something even as high as 35dB. Since we are only transmitting data, even with a simple picture, we are aiming for SNR of around 18dB which should be enough for us to transmit error free.

3.14.5 Spread Spectrum

Armed with the knowledge that we can improve the SNR by increasing the channel bandwidth of the signal we move on to the principle of Spread Spectrum. This method uses a modulation technique of using a chip sequence. This chip sequence is of a much faster rate than the original data signal. When the chip sequence is multiplied with the data signal, the signal bandwidth is expanded far beyond the original signal bandwidth as seen in Figure 41. The most common form of this spread spectrum is known as Direct Sequence Spread Spectrum, DSSS.

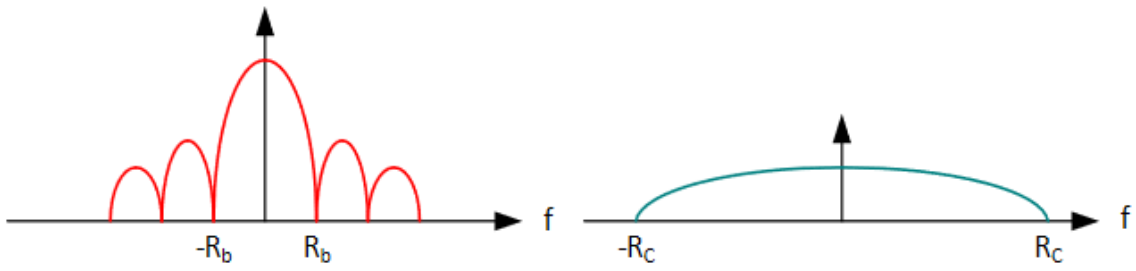

Figure 41: Increased Bandwidth of Spread Spectrum Modulation

On the receiver side of the transmission we are able to demodulate this signal to obtain the original data signal. This demodulation is done by multiplying the incoming signal with a replica of the spreading sequence. The same chip code must be used in the receiver as in the transmitter in order for the demodulation process to work correctly.

This spreading technique is able to give us a processing gain, or Gp. This processing gain is based on the ratio of the chips per bit of the coded sequence. Chip is a term that is used to distinguish between the shorter coded bits of the signal to the longer un-coded bits that are present in the signal. Since this gain is expressed in a decibel ratio we can determine the benefit from the following equation:

$$Gp = 10 * log_{10}(\frac{Rc}{Rb}) \tag{25}$$

Another benefit of using this spread spectrum process is that interfering signals are also spread by the modulation. This means that any interference or noise that is spread beyond the desired bandwidth is easily removed on the receiving end by using the desired band-pass filter. Even though this spread spectrum modulation is widely used, it does have a down side. Since the signal is being spread out, it takes a longer time to perform a correlation over the entire code sequence. For a battery operated device like our project, the longer something takes to perform its action, the more power is consumed.

3.14.6 LoRa Spread Spectrum

With the ultimate goal being as little power consumed as possible, we move on to the selected modulation technique of our device, which is the LoRa Spread Spectrum. Originally developed around World War II, the Chirp Spread Spectrum was made with radar technology in mind. Besides the benefit of requiring low power transmissions, it is also robust against the Doppler effect and interference. This robustness against the Doppler effect is of great benefit for a satellite system which typically is moving at great speeds and distances. On an Earth system this can also be a benefit when used in cars or other mobile situations. For us, since our project is going to be stationary at 500 meters, it is not as big of a benefit as the low power consumption is.

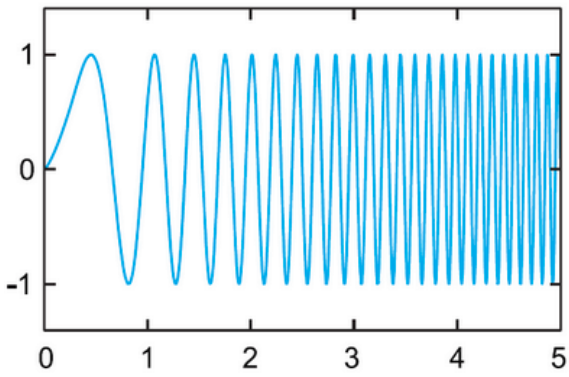

Figure 42: LoRa Chirp Signal - Up-Chirp

LoRa modulation has adopted the use of this Chirp signal. In this case, the Chirp signal continuously varies in frequency. These frequency offsets are equivalent on both the transmitter and the receiver which reduces the complexity required on the receiver design. For this chirp, the frequency bandwidth is equivalent to the spectral bandwidth of the signal.[80] As with the previous system of spread spectrum, LoRa modulation also uses a chipping multiplication of the data signal. The difference here is that the the signal is chipped at a higher data rate and then it is also modulated onto the chirp signal. An example of a chirp signal can be seen in Figure 42. We can

see how in a chirp the frequency either increases or decreases with time. These are known as either up-chirps, when the frequency increases with time like our example, or down-chirps, when the frequency decreases with time.

With LoRa modulation we can define the data bit rate, symbol rate, and the chosen chip rate as in the following equations:

$$Rb = SF * \frac{1}{\frac{2^{SF}}{BW}}, bits/sec \tag{26}$$

Where BW is the modulation bandwidth measured in Hertz. SF is the spreading factor which for LoRa modulation is an integer value between 7 and 12. The symbol rate, Rs, is the reciprocal of Ts, the symbol period and defined as:

$$Rs = \frac{1}{Ts} = \frac{BW}{2^{SF}}, symbols/sec \tag{27}$$

The chip rate, Rc, which is defined on the data sheet as "one chip is sent per second per Hz of bandwidth,"[80] is a combination of the symbol rate and spreading factor. We can see below that a little bit of algebra involving the definition of the symbol rate can prove the data sheet definition.

$$Rc = Rs * 2^{SF} \tag{28}$$

$$Rc = \frac{BW}{2^{SF}} * 2^{SF} \tag{29}$$

$$Rc = BW, chips/sec \tag{30}$$

As with any kind of signal transmission, no matter what the data transfer rate is, it is worthless if we are just transmitting error filled data. LoRa modulation has a built in variable error correction scheme used. Just like with a forward error correction scheme that is common in satellite signal transmissions, this error correction scheme is accomplished by using redundancy. Just like the Spreading Factor which is an integer value, the code rate, or CR, is an integer value between 1 and 4. This code rate is integrated into the data rate by use of a Rate Code as defined below. After multiplying the data rate with this Rate code, we can finally obtain the nominal bit rate.

$$RateCode = \frac{4}{4 + CR} \tag{31}$$

$$Rb = SF * \frac{RateCode}{\frac{2^{SF}}{BW}}, bits/sec \tag{32}$$

The combination of the built in variable error correction along with the ability to change the spreading factor, rate code, and bandwidth of the channel is why the

LoRa chirp modulation is so fitting for our use. It allows great customization to fit each specific purpose. The low data rate and increased bandwidth improves the sensitivity of the receiver. This increased sensitivity increases the link budget and allows such a low power transmitter like the 100mW transceiver that we will be using. We will only be transmitting small bits of text and singular pictures where the speed of transmission is not needed to be extremely high. Since the goal is just a successful transmission of the data, clarity is more important than continuous transmission and the benefits listed here far outweigh any negatives from a low data rate.

3.14.7 Summary - LoRa SX1278 433MHz

Transceiver Models	**ACROBOTIC Ra-02**	**ALLPARTZ SX1268 LoRa HAT**	**DIYmall LoRa32u4**
Range (km)	8	5	1
Sensitivity (dBm)	-139	-147	-148
Peak Current (mA)	120	120	120
Price (USD)	10	30	37

Table 23: Transceiver Comparison

The importance of the -73dBW calculation in the previous section comes in to play when choosing the transmitter. This calculation was done using a transmitter power of one Watt. Using a LoRa SX1278 433MHz Transceiver will give us a transmitter power of 100mW. This means that in terms of dB calculations we would need to drop the power another 10dB. This gives us a new received power calculation of -83dBW. Many such low power transmitters and receivers do not use dBW, or decibel Watts, but instead use dBm which is decibel milliwatts. There is a factor of 1000 change with the conversion which equates to a 30dB change. This means that with a transmitter power of 100mW, we want a receiver with a sensitivity of at least -83dBW or -53dBm. This would of course give us absolutely no leeway which would be a terrible idea.

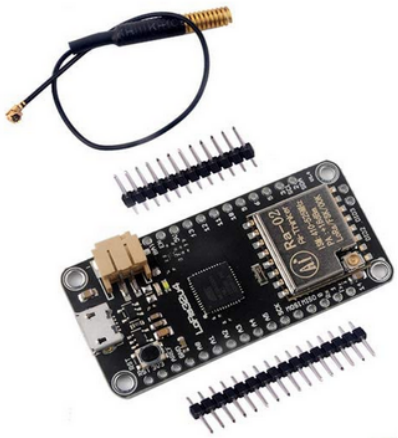

Figure 43: DIYmall LoRa32u4 LoRa RA-02 Module and Spring Antenna

A link margin is used in satellite transmission calculations to determine the margin for error before the performance of a transmitter and receiver connection experiences problems beyond what is determined acceptable. In the real world these margins are built in to the systems to account for losses that come from rain or other bad weather. In our case since our primary focus is not in getting perfect performance out of the transmission of data, which would include precise temperature, distance, resistance, interference, or other noise and losses in the system. For this reason even though we need a minimum sensitivity of -53dBm for acceptable performance, that is, before we even begin to account for any bit error rates that can affect the reading of the data itself, we will account for a large margin of error. A LoRa SX1278 module has a receiver sensitivity down to -148dBm. This gives us a link margin of nearly 100dBm. We can expect our cheaper, low budget components to not work as perfectly as a data sheet may say. We can also expect that with our inexperience we will need this extra room for error. Using a LoRa SX1278 transceiver should give us more than enough power to send our data the 500 meters required to be considered a successful demonstration.

The LoRa SX1278 can also function as a receiver. For our purposes we can use a similar set up of having the transmitter and the receiver being made from the same components. This will allow us the simplicity of being able to work on the coding and programming of both systems at the same time. There is a downside of this component which is that it requires some assembly and soldering before it can work. That would normally not be a big deal except for our present climate of having to work on everything remotely and away from our team members. For this reason an additional testing component was introduced in the RioRand RF Link Transmitter Receiver discussed in the section below.

The LoRa SX1278 Transceiver has the following power requirements for its operating range:

- 1.8 - 3.7 Supply Voltage

- -40 - +85 °C Operational Temperature Range
- 120mA Supply Current in Maximum Transmit Mode
- 12mA Supply Current in Maximum Receive Mode
- Bandwidth of 500kHz to 7.8kHz with Spreading Factor between 6 and 12, respectively
- 37.5kbps Bit Rate in LoRa Mode
- 300kbps Bit Rate in FSK Mode
- RF Sensitivity in LoRa Mode between -111dBm and -148dBm Depending on SF and BW

After initially using the Acrobotic Ra-02 transceivers and even soldering them to our PCB break out boards, the decision was made to switch hardware. In order to demonstrate our ability to transmit the goal of 500 meters, a python program was written to test the transmissions at different LoRa and power settings. The Acrobotic transceivers were extremely inconsistent when constantly altering the settings and so we switched to Adafruit RFM9X Radio Bonnets. These are based on the SX1276 chip which is nearly identical to the SX1278 in every way that is relevant to this project besides operating at some frequencies we were not going to be using anyway. This transceiver had the benefit of built in buttons and an OLED that allowed simpler demonstration without the need to be typing on a keyboard or interacting with a mouse. Since our testing was done on top of parking garages where there was extreme glare, this proved to be extremely useful.

3.15 PCB

In order to create the PCBs that will be designed for this project we will need to order them from a custom PCB fabrication company. The fabrication process is complex and includes more steps the more layers the design being fabricated has. In general, the traces are made by plating the non-conductive substrate with layers of copper, applying a stencil to that copper-plated board in accordance with the given design, and etching away the copper that is not covered by that stencil. This is mostly done by computer-automated systems and can now be done at such a scale that custom multi-layer boards are now able to be created for the general public by various companies for hobbyist uses at very affordable prices.

3.15.1 Manufacturers

Although PCB manufacturing is affordable from some vendors, that does not mean that those vendors are as reliable as is necessary for this project. Due to the tight time constraints of this project, it was necessary to select a PCB manufacturer with a record of high quality and fast turnaround on parts. Selecting for these qualities in a

custom PCB fabricator can and will increase the cost of the boards in question. However, this increase in cost is worth it to cut down on the PCB prototyping turnaround time and the increase in reliability of the boards we will be designing.

The PCB fabrication company we decided to purchase our custom boards from is OSH Park. We chose this fabrication company because they have a track record of good quality control in their manufacturing and use high quality base parts for their fabrications. Some of the other custom fabricators we considered were AISLER and BasicPCB.com. However, OSH Park appeared to be the better choice due to their reputation for defect-free boards and the quality of the substrate that they use. Although this manufacturer will not be able to provide PCBs that would be space-worthy, their quality will be more than enough for prototyping purposes.

The cost of boards from OSH Park depend on a number of different characteristics that the boards are required to have. The first question when determining the cost is the number of layers that the board will have, as mentioned earlier in the MCU voltage regulator section. The pricing for a basic prototype board with 2 layers is $5 per square inch, but if there are 4 layers then the price goes up to $10 per square inch. The table below lays out the pricing for the different service options that we will be considering for this project.

	Cost	**Time to Ship**
2-Layer Prototype	$5 per square inch	12 calendar days
2-Layer Super Swift	$10 per square inch	5 business days
4-Layer Prototype	$10 per square inch	9-12 calendar days

Table 24: OSH Park Service Costs as Advertised

The main service option that we will be considering is the 2-layer prototype service option, but if there needs to be a more complex circuit for the main board then we will, of course, select the 4-layer circuit board. This option is likely given that the MCU that we have selected has 144 pins on it that all need to be routed to the proper components as well as I/O pins. Because a number of these pins will need to go in conflicting directions, the use of vias and multiple layers for the routing will be a useful consideration when designing the main board.

4 Standards, Regulations & Design Constraints

4.1 Standards & Regulations

It is imperative to abide by standards that are set both for the final product and the development of the final product. Regulations will require that the final product perform a certain way and certain parameters of it fall within some given thresholds. Regulations will also require that the processes by which the product is developed follow certain requirements, mainly as a requirement by Environmental Health and Safety. These regulations are in place for ensure that chemical processing and other work is done correctly so that it does not pose a risk to those who are building the product.

4.1.1 Lab Safety

Fundamental in the fabrication procedure of our optode is the safe execution the procedure. Many chemicals used in the laboratory will cause great harm if they are misused. It is imperative to follow safety precautions because they will drastically reduce the probability that an accident occurs [24]. Safety precautions should not be taken to un-achievable standards. Their own contribution with respect to the overall safety and underlying potential to allow normally separated events to be coupled, may give rise to catastrophe [68]. This is why safety must be approached with great attentiveness, and it is not as simple as saying "oh of course I won't do anything stupid." Such a saying is too often spoken amongst lab workers who do not understand the importance of keeping a safe laboratory. Safety procedures must not be unreasonable, or they will not be followed. Environmental health and safety (EHS) creates regulations that are critical to make the laboratory a safe workplace, and they keep in mind that the goal is prudence, rather than 100% immunity from anything going wrong. With that being said, every regulation required by EHS must be followed, as they are not unreasonably difficult to follow, and the challenges of following such regulations present significantly less trouble than the potential for consequences that may result regulations are not followed. In general when working in a laboratory that specializes in fabrication of photonics components, the following may occur as a result of chemical misuse: development of chronic injuries, exposure to carcinogens, death, or even catastrophe when highly reactive materials are misused. Safety measures around chemicals in a laboratory focus primarily on: thoughtful storage of the material, prudent (and proper) use of the material, and responsible removal of the material after it becomes chemical waste.

The materials that we will be using for fabrication of our optode which may be defined as hazardous to some extent, are the PtTFPP (our fluorophore of choice) and the toluene (our solvent of choice). The PtTFPP is a solid and its MSDS (Ref [71]) provides the following hazard statements, with the signal word "warning":

`H315: Causes skin irritation`

H319: Causes serious eye irritation

H335: May cause respiratory irritation

The PtTFPP has the following requirements for handling and storage:

Precaution for safe handling:Avoid contact and inhalation.
Do not get in eyes, on skin, on clothing.
Avoid formation of dust and aerosols.

Conditions for safe storage: Keep container tightly closed
in a dry and well-ventilated place. Store in cool place.

The PtTFPP is not particularily hazardous. It is not highly reactive with common chemicals in the laboratory, it chemically stable so it will not degrade into a more reactive compound, and it is not known to have any chronic toxicity.
The toluene MSDS from Fisher Scientific (Ref [38]) lists the following hazard statements:

Appearance: colorless liquid. Flash Point: 4 deg C.
Warning! Flammable liquid and vapor. Causes eye, skin,
and respiratory tract irritation.
Breathing vapors may cause drowsiness and dizziness.
May be absorbed through intact skin.
Aspiration hazard if swallowed.
Can enter lungs and cause damage.
Possible risk of harm to the unborn child.
May cause central nervous system depression.
May cause liver and kidney damage.
Target Organs: Kidneys, central nervous system,
liver, respiratory system, eyes, skin.

Potential Health Effects
Eye: Causes eye irritation.
Vapors may cause eye irritation.
Skin: Causes skin irritation.
May be absorbed through the skin.
Repeated or prolonged exposure may cause drying and cracking of the skin.
Not expected to cause an allergic skin reaction.
Ingestion: May cause effects similar to those for inhalation exposure.
Aspiration of material into the lungs may cause chemical pneumonitis,
which may be fatal.
May cause central nervous system depression.
Inhalation: Causes respiratory tract irritation.

Inhalation of high concentrations (>200 ppm) of toluene are clearly associated with CNS encephalopathy, headache, depression, lassitude (weakness, exhaustion), impaired coordination, transient memory loss, and impaired reaction time.
Chronic: Prolonged or repeated skin contact may cause defatting and dermatitis.
Repeated exposure in combination with constant, loud noise can produce hearing loss and dizziness.
Chronic hydrocarbon abuse (for example, sniffing glue or light hydrocarbons such as contained in this material) has been associated with irregular heart rhythms and potential cardiac arrest.
Toluene abuse has been linked with kidney disease, as evidenced by blood, protein, & pus in the urine, accompanied by elevated serum creatinine, decreased urinary output, & metabolic & renal tubular acidosis.
Although kidney toxicity has not been common in cases of occupational toluene exposure, there has been at least one report of renal toxicity following a 40-year occupational toluene exposure.
Toluene does not cause the severe injury to the bone marrow that is characteristic of benzene poisoning.
Intentional abuse of toluene vapors has been linked to damage of the brain, liver, kidney and to death.
Repeated inhalation exposure of toluene to animals causes histological changes in the brain, degeneration of the heart tissue, and possible immune

This hazard statement indicates chronic effects that will result from overexposure of the material, as well as immediate health effects that could be fatal, both of which pose danger if the material is misused. With this being said, a fumehood or proper respiratory equipment *must* be employed, and done so correctly, when this chemical is being used.

The fabrication procedure for the optode sensing material will take place entirely inside a fumehood for the duration of toluene being used. The sensor will remain in the fumehood after coating for a duration of 5 hours to guarantee that the thin coating of PtTFPP dissolved in toluene has time for the toluene to completely evaporate.

The following is the handling and storage requirements as stated by the MSDS provided by Fisher Scientific:

Handling: Wash thoroughly after handling.
Remove contaminated clothing and wash before reuse.
Ground and bond containers when transferring material.
Avoid contact with eyes, skin, and clothing.
Empty containers retain product residue, (liquid and/or vapor), and can be dangerous.

```
Keep container tightly closed.
Do not pressurize, cut, weld, braze, solder, drill, grind,
or expose empty containers
to heat, sparks or open flames.
Use only with adequate ventilation.
Keep away from heat, sparks and flame.
Avoid breathing vapor or mist.
Storage: Keep away from sources of ignition.
Store in a tightly closed container.
Store in a cool, dry, well-ventilated area
away from incompatible substances.
Separate from oxidizing materials.
```

4.1.2 Laser Saftey

LASER is an acronym which stands for Light Amplification by Stimulated Emission of Radiation. The laser produces an intense, highly directional beam of light. Lasers can cause damage to the human body, especially the eye. Lasers are divided into safety classes based on their potential for causing injury or harm.[34]

The classification of lasers is set by the International Electrotechnical Commission (IEC) 60825-1 standard.[45] The classes are as follows: 1, 1M, 2, 2M, 3R, 3B, 4. Classes 1, 2, 2M, and 3R are relatively safe for eye exposure; classes 3B and 4 are considered hazardous. For class 1 lasers, no extraordinary precaution is necessary. For class 1M, 2, 2M, and 3R, avoid looking into the beam or using any focusing optics without safety goggles. For classes 3B and 4, the correct laser safety goggles are required. Typically, the glasses will have an OD+ (optical density) rating at a certain wavelength. This is defined more specifically in figure44. It is critical to select a pair of glasses that have the appropriate OD+ rated saftey goggles at the wavelength of the laser in operation.

Class 1		Class 2		Class 3		Class 4
Class 1	Class 1M	Class 2	Class 2M	Class 3R	Class 3B	Class 4
Class I	No special FDA class	Class II	No special FDA class	Class IIIa (definition is different but results are similar)	Class IIIb	Class IV
For visible light, emits beam less than 0.39 milliwatts, or beam of any power is inside device and is not accessible during operation.		Emits visible beam of less than 1 milliwatt.		For visible light, emits beam between 1 and 4.99 milliwatts.	For visible light, emits beam between Class 3R limit (e.g. 5 milliwatts) and 499.9 milliwatts	For visible light, emits beam of 500 milliwatts (1/2 Watt) or more
No special caution/ warning indication		No special caution/ warning indication		CAUTION	WARNING	DANGER
	DO NOT VIEW DIRECTLY WITH OPTICAL INSTRUMENTS	DO NOT STARE INTO BEAM	DO NOT STARE INTO BEAM OR EXPOSE USERS OF TELESCOPIC OPTICS	AVOID DIRECT EYE EXPOSURE	AVOID EXPOSURE TO BEAM	AVOID EYE OR SKIN EXPOSURE TO DIRECT OR SCATTERED RADIATION

Figure 44: Description and hazards of laser classes.[34]

It is of critical importance to follow the guidelines set by OSHA standards and the International Stands Organization (ISO) when working with lasers of any kind.

OSHA Standard 910.132(a):
Application. Protective equipment, including personal protective equipment for eyes, face, head, and extremities, protective clothing, respiratory devices, and protective shields and barriers, shall be provided, used, and maintained in a sanitary and reliable condition wherever it is necessary by reason of hazards of processes or environment, chemical hazards, radiological hazards, or mechanical irritants encountered in a manner capable of causing injury or impairment in the function of any part of the body through absorption, inhalation or physical contact. [2]

More specifically to lasers, OSHA Standard 1910.133(a) guarantees eye protection: The employer shall ensure that each affected employee uses appropriate eye or face protection when exposed to eye or face hazards from flying particles, molten metal, liquid chemicals, acids or caustic liquids, chemical gases or vapors, or potentially injurious light radiation.[3]

While these standards apply to the workforce, we can implement them into our research to ensure laser eye safety.

For this particular project, a class 3B laser delivering 100mW will be utilized. It will be best practice to select a pair of safety goggles that has an OD+ of at least 5 at a wavelength of 650nm and adhere to the (IEC) 60825-1 and OSHA 1910.133(a) standards.

4.1.3 Related Regulations, Licenses, and Realistic Prototype Constraints

This section covers the related regulations that would apply to our final project as well as the chosen constraints that we will apply to our prototype in order to fit our

time frame, budget, and proof of concept scenario. We will also define who is the operator of the project, what the function of the project is, and how the prototype would be defined for the purpose of these licenses.

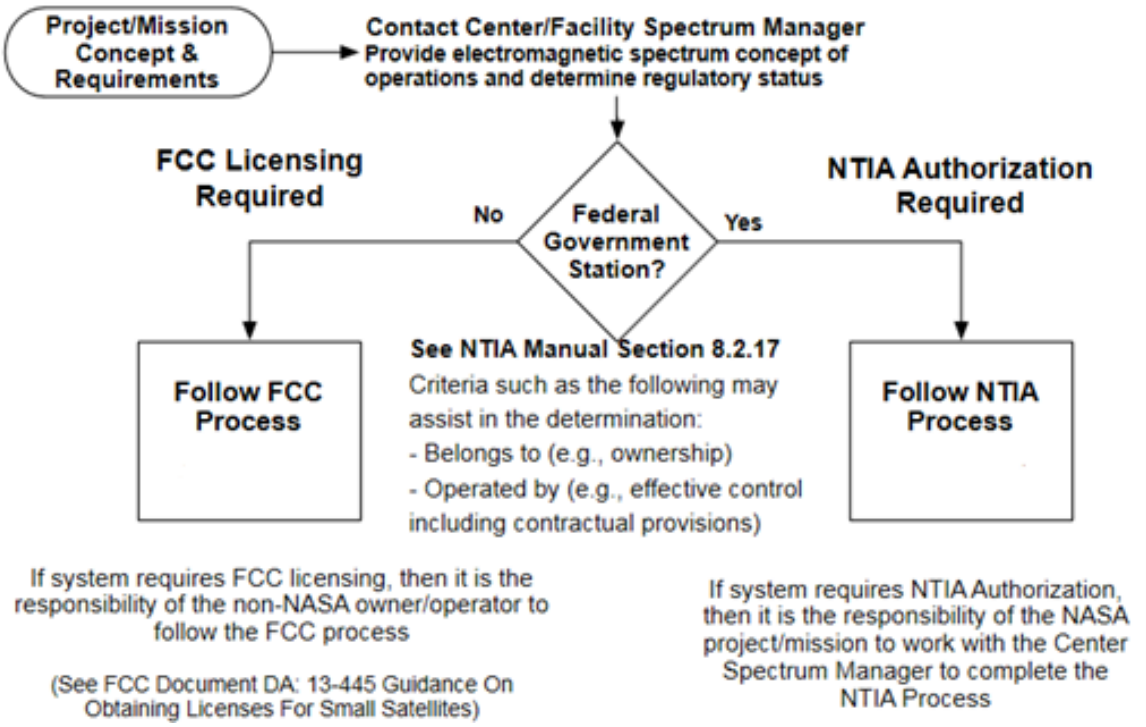

Figure 45: Project/Mission Determination of Spectrum Regulatory Status & Process from NASA

4.1.4 Related Licenses - FCC

With the real-world goal of our project eventually being a launched CubeSat, there are several regulations that we would need to follow to communicate with the CubeSat. There are many different regulatory constraints[46] that would be involved to transmit signals to and from the launched CubeSat on a radio frequency (RF). There are two organizations that cover these licenses, the National Telecommunications and Information Administration (NTIA) and the Federal Communications Commission (FCC). The NTIA handles licenses for dealing with U.S. Government operated satellites while the FCC handles the non-Federal Government operated satellites.

Proper licensing is required when a CubeSat is capable of transmitting RF signals or taking images. In our case, the goal is to do both functions and so research into obtaining such a license is being done. The type of license classification is based on both who will be operating the CubeSat and how it is going to be used. The end goal of our project is to be operated for and by our customer, NASA, but for the purposes of our prototype and proof of concept demonstration, licensing will be researched as if operated as an amateur, for educational and experimental purposes.

As our operation is now defined as amateur, educational, and experimental, we must then recognize it as a "space station." According to the ITU Radio Regulations, which the FCC also uses to define the term, a "space station" refers to "one or more transmitters or receivers or combination of transmitters and receivers necessary for carrying on a radiocommunication service, and located on an object which is beyond, is intended to go beyond, or has been beyond, the major portion of the Earth's atmosphere." [22] This definition is used by the FCC but is from the ITU Radio Regulations S 1.61 and S 1.64. Even though our prototype is not intended to be launched into space and so would not fit this definition, for our proof of concept purposes we are planning accordingly to operate as if it were.

By the above definition, our space station would require that the amateur satellite control operator apply for a license from the FCC. According to the FCC, "this operator should have the ability to remove the satellite from a launch manifest and disable space station operations." [22] Even though we are not launching the prototype, we want to adhere to this last part of the FCC rules regarding being able to disable the space station operations. This is something that is realistically possible to demonstrate with our prototype and prove that we would be able to meet this guideline. If there were an emergency or for any particular security or interference purposes, the FCC may at any time request that we cease transmission of our RF signal. To meet this requirement, we will design the prototype to be able to receive a signal to end transmissions.

There are multiple guidelines related to the actual launching of the CubeSat that have been researched, but do not apply to our prototype. These other regulations relate to the need for coordination of another satellite being present in orbit, especially if there is a possibility of affecting spectrum that are being used by other entities. Outside of spectrum interference there are also regulations related to potential debris if any part of the spacecraft is expected to survive re-entry of "surviving materials presenting a casualty risk other than zero." [22] Since our customer NASA has extensive background launching satellites and it does not apply to anything that can be feasibly demonstrated with our prototype, these additional regulations will be left out for the purposes of this project.

4.1.5 Related Licenses – NTIA

For the purposes of a NASA satellite mission, our project would be an orbiting system under 180 kilograms. Even though the project is not directly developed by NASA or supported through a contract, we would be defined as supported through "other financial agreements," and so must adhere to NASA Policy Directive (NPD) 2570.5E which states "any small satellite mission ... that require[s] the use of the electromagnetic spectrum shall follow the United States spectrum regulatory rule and processes as referenced in the documents listed in "Authority Documents" as well as all appli-

cable international spectrum regulations." [62] As our project is being developed with NASA as our customer, we will abide to all demonstrable rules that fit our budget and prototype.

As our project is an amateur one for the purpose of this prototype and project, once it enters operations under guidance by NASA, the rules of the NTIA apply for Federal Government systems. These guidelines would apply "a variety of technical rules ... to small satellites regarding launches, orbital debris, frequency selection, and other matters." [62] While we have chosen to operate in the amateur frequency bands as defined in Section 7.4 of this report below, there exists the NASA Spectrum Management Program that would handle the "overall planning, policy, coordination and implementation necessary to ensure adequate access to and protection of electromagnetic (EM) spectrum in support of NASA's present and future programmatic goals."

4.1.6 Chosen License – FCC Technician Class Operator License

We can see from Figure 45 that our project would need to follow the FCC licensing process in its current iteration. The goal of our proof of concept would be to eventually be owned and operated, with the additional funding and research, by NASA. If that goal were achieved, we would then need to follow the NTIA licensing process to abide by NPD 2570.5E stated previously.

Under the FCC license regulations our chosen space station operator would be required to obtain a Technician Class operator license. [ham] The requirements to obtain such a license include answering 26 questions from a 35-question written examination. These examinations are typically offered by local and licensed amateur radio enthusiasts operating as volunteer examiners (VEs). There is a sub-goal of the project for one of our members to obtain such a license and act as the licensed station operator. Unfortunately, during the current pandemic, these examinations are extremely limited, and the organizing body is currently looking into the possibility of remote, online examinations. The FCC began allowing online testing in order to obtain licenses and so we were able to successfully obtain the call sign KO4MSG.

4.1.7 Batteries – Regulations

For launch of a CubeSat, a battery can take up a large part of the available weight. Its placement has a large impact on the center of gravity and possibly the largest single element of any inertia changes. As there will be no launch, these regulations will not be a focus for our project. What will be included and adhered to are the requirements for specific battery information that is usually found in the Missile System Prelaunch Safety Package (MSPSP). This includes the following that will be made into a table once the battery has been purchased. Battery dimensions, Battery UL number, Manufacturer specification sheet, Manufacturer part number, Mass, Battery model

number, Battery manufacturer, Number of cells and their configuration, Discharge characteristics, Charge characteristics, Lithium battery short circuit test, Safety circuit diagram, Technical datasheet, and any modification documentation. [46]

Our prototype will be required to operate for what NASA considers a short mission duration which is usually around one day and up to one week. This opens us up to the possibility of using either a primary or secondary type battery. Since we do not need extensive battery life, our main focus will be on fitting the weight and dimension constraints while delivering enough power for operation. A key metric for this is energy per unit mass and would be important for efficiently getting more power without adding too much weight. Typical types of batteries that meet these criteria are silver-zinc, lithium sulphur dioxide, lithium carbon monofluoride, and lithium thionyl chloride. [63] The more modern, secondary batteries that can be recharged using solar panels will not be considered as they are beyond our needs and budget.

4.1.8 Heat Tracing Standards

As the heater is likely the most dangerous component of our design, it is important to be aware of the related industry standards and regulations. There are laws out there that require warning labels every 10 feet if there is an insulated heating element hidden from view but that will not apply to our project where the heater will be measured in inches. Such a law is not designed to prevent people from touching the wires, but more so for firefighters or other emergency personal so they are aware of potential hazards if they are on the scene.

Specific to heat tracing, which is the technology we will be using, is IEEE 515-1997 which is the IEEE Standard for the Testing, Design, In-stallation, and Maintenance of Electrical Resistance Heat Tracing for Industrial Applications.[78] This standard has three different functionally related definitions that focus on the fluid temperature tolerance of what is being thermally maintained inside the pipe or container that the heat tracing is being used on, seen below.

- Type I, where the temperature should be maintained above a minimum point.
- Type II, where the temperature should be controlled within a moderate band.
- Type III, where the temperature should be controlled within a narrow band.

Our case is Type I, which is essentially just freeze protection. Further classification of our purposes comes down to either No Control Constant Wattage Heaters 10-70 °C or No Control Self Regulation Heaters 10-50 °C. The plan is no control as we are limiting our control to either power the heater on or off. This lack of control benefits in that less components are needed to regulate or change the temperature of the heater which helps reduce the space required inside of our prototype. According to the IEEE standard, "monitoring should be an independent and parallel system,"[78]

which is true in our case. We have a separate temperature sensor which will be read by the computer and then either power on or off the heater. A constant wattage heater is likely to re-heat our system faster but a self regulating heater would be better suited for a longer experiment. They can both be obtained for a similar price and operated using low voltages, so even though a constant wattage heater has the benefit of a faster heat up, they usually come in a circular or rectangular pad which might require a small modification to fit our limited space.

4.1.9 Amateur Frequency Band for Transmission

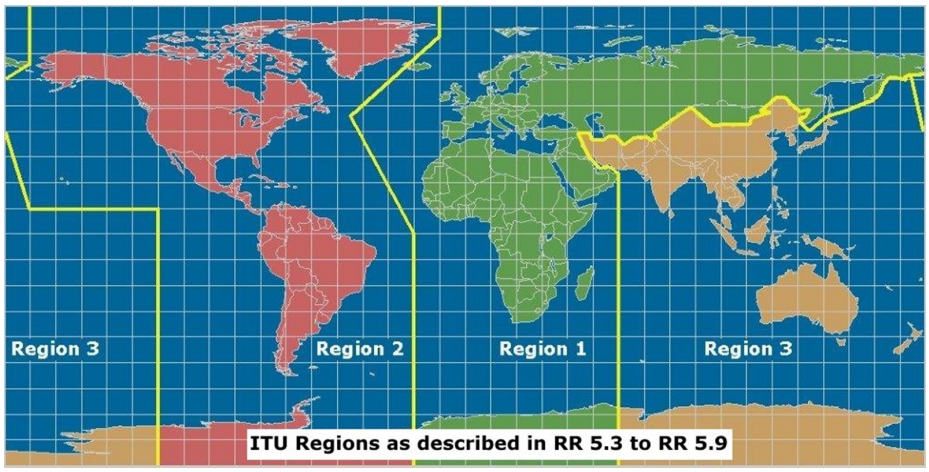

Figure 46: ITU Regions to Identify Operating Frequencies

As seen above in Figure 46, we are located in ITU Region 2. In order to abide by FCC regulations of what frequency someone with a Technician Class operator license can operate in, we have chosen 433 MHz as our transmission frequency. That frequency is approved for amateur use and found on the 70 cm band listed in the tables found in 47 CFR § 97.207 - Space station of the FCC Regulations. [35]

This operating frequency is commonly found in widely available parts and circuitry that can be bought as an amateur and a hobbyist. Unfortunately, in the middle of this project and after the initial planning stages, an amendment was released by the FCC. This amendment dated October 9, 2020 and found under 85 FR 64068 [36], has changed the available frequencies to be slightly higher beginning at 435 MHz. Due to limited time and budget, at this current stage of development we are continuing to operate as if 433 MHz will be used. If there is available budget and time to obtain a new transmitter, we are willing to make the switch to update the hardware to the new regulations. As NASA's customer requirements for our project are mainly focused elsewhere outside of the transmission of data, it is not a high priority in our time and budget to make this switch to a new frequency. Our main priority to demonstrate our ability to follow FCC requirements remains to be 47 CFR § 97.207 - Space station. (b) which states, "A space station must be capable of effecting a cessation

of transmissions by telecommand whenever such cessation is ordered by the FCC." [35]

4.1.10 Programming Languages - C

The programming language being used in this project is C. More specifically, the revision being used is C17, which was solidified as a standard as ISO/IEC 9899:2017. The international standard lays out the syntax, interpretation rules, representation of input and output data, and the limits of the programming language [47]. The scope of this standard covers all of the software that will be written for this project and is being used due to its compatibility with the hardware that has been selected for this application. Because of this broad scope, this standard will influence several of the key functionality implementations that will be used for this project.

This standard determines the input and output data of C programs, so it will also determine the way the file systems that are used for this project are developed [47]. The header files and the output buffer files are included in this file system, so this standard will influence the way our program manages, calculates, stores, and finally transmits data that our sensors will be sending to the primary MCU. Our system will also have secondary MCUs which will run calculations for Analog to Digital conversions for the sensors that they are attached to and send that data to the main MCU for transmission. The portions of this standard that cover the way that the programming deals with input and output data will also influence this portion of the project and the inter-connectivity of these devices.

4.1.11 Institute of Printed Circuits

IPC-2221A and IPC-2222 are standards created by the Institute of Printed Circuits, the global trade organization which creates many of the standards used in the electronics industry as a whole. These standards are meant to be used together as guidance when creating designs for rigid printed circuit boards. This standard was created in order to avoid confusion between manufacturers when sharing designs or ordering parts to be fabricated. Both of these standards complement each other in that IPC-2221A gives more general guidance on all types of printed boards, whereas IPC-2222 lends more specificity to the aspects relevant to printed boards where the substrate is a rigid organic material like FR-4. The broad nature of IPC-2221 allows for the standard to cover printed boards more broadly and have secondary standards, like IPC-2222, bring more specificity when there is the need for it.

Both of these standards use "shall" statements in order to show which aspects of the standard must be adhered to in order to claim compliance with the standard. Unfortunately, the details of these standards cost over $150 per standard in order to purchase a PDF from the IPC. Unfortunately, we were not able to find any publicly available materials on these standards. Due to this paywall in order to gain access to the more up-to-date standards from this organization, we will not be able to ensure

compliance with every aspect of these standards, but we will attempt to use best practices as we've been taught.

4.2 Constraints

4.2.1 Design Constraints Related to Regulations

The following constraints are related to meeting typical NASA, NTIA, FCC, and/or ITU regulations. While these are not all the constraints that would be required, we have deemed them practical to demonstrate with our proof of concept prototype. The typical constraints related to launch, orbit, post-launch debris, or the like will not apply to this project. The requirements that are achievable on and within the CubeSat itself were our primary goal to meet.

The first design constraint is the ability to inhibit any radio-frequency emissions within certain time frames around launch or when requested by, in our case, the FCC. This is the previously mentioned 97.207 (b) regulation. The separate time frame portion around launch and through 45 minutes after deployment does not apply, but the ability to remotely cease transmission does. For our project we will be implementing a receiver to accept a command that will shut off our transmitter. There are other common methods to meet this requirement, such as limited battery life, transmitting only when an uplink is active, or various timing and scheduling methods that we will not be using.

The second design constraint is related to the power of the transmission itself. This is a complement to the previous constraint and further adds to limit interference of other systems. From NASA, this operational consideration states, "Transmission Power Limit: The small satellite will have on RF inhibit and have a RF power output of no greater than 1.5W at the transmitting antenna's RF input." [62] The one RF inhibit mentioned is achieved by the previously mentioned receiver that can accept our shut off command. The 1.5W power limit is a suitable and realistic constraint for our project. Since we are setting a goal of transmission up to 500 meters, this 1.5W power limit will not be a problem to remain under.

There are many technical design constraints that are not being considered to maintain our budget and focus. We will not be broadcasting to a stationary Earth Station and so the power limits, power flux density limits, and bandwidth constraints that would apply are not being considered for this project.

4.2.2 Economic Constraints

The CELSS is well funded by a NASA sponsorship. The sponsorship provides $2000 in funding, which is an estimated surplus of $400 based off of our budgetary analysis. This funding by NASA alleviates a majority of economic and budgetary constraints

that otherwise would have been imposed on our project. This does not mean, however, that it is not a constraint at all. The budget was carefully planned to maintain below $2000 dollars. For example, one particular component effected by even what we deem as a large budget, was the thermal camera. The thermal camera's were found to generally run in the thousands of dollars range, so this economic constraint forced us to do a cost-benefit analysis for the thermal camera considerations. ultimately, the thermal camera was scrapped because the cost could not be justified. The marketability of this product was not a concern, because it was not meant to be commercialized. This is an engineering product with a contracted customer that gave an appropriate budget, therefore we were able to design much of the initial considerations without having to surrender ideas due to cost.

4.2.3 Environmental Constraints

The CELSS is not expected to negatively impact the environment in any way. The device will be battery powered and will remain on earth as a prototype. If this device was more than just an educational proof-of-concept and was going into space, we would have a major challenge for ethically protecting the environment from carbon emissions from a space launch. The benefits of the research being done would have to outweigh the damage done from the launch, additionally, we would hope to see that the cubesat this device would be shipped on would be accompanied by many more to make this more economically feasible and to adhere to any environmental standards that the EPA or the government has set. Because we will not actually be using living species, just be developing a system that could facilitate that for a government entity, we did not seek to challenge any EPA standards or regulations, only adhere to NASA's specifications.

4.2.4 Ethical Constraints

This CELSS platform was designed with the fact that a government entity may use it to conduct research on living organisms. For us, this imposes the restrictions that we must develop, to the best of our ability, an environment that serves as a basis for a safe environment for any possible life-form research to be conducted in the future. The system shall feature a few safeguards for the potential Artemia that may inhabit it, and everything is designed to be as noninvasive as possible. Ultimately, it will be up to NASA, with a much larger budget and much more capable engineering resources, to bring the environment up to their standards if they wish to actually host a living organism in space with it. We fully expect any government organization that experiments with living organisms to adhere to EPA standards and also to understand that any potential risk to a living organism is far outweighed by the benefits it brings to science.

4.2.5 Health and Safety Constraints

The CELSS platform should not inherently put anyone into any danger. However, during the manufacturing process, we will ultimately have to deal with a class 3B laser.

This will only affect us in that we will adhere to saftey standards and obtain saftey goggles and operatre in the correct laboratory environments. During any testing or any use of this technology, we will use the the correct laser safety goggles that are required. Typically, the glasses will have an OD+ (optical density) rating of at least 5 at a wavelength range that covers the 650nm used, as indicated by the International Electrotechnical Commission (IEC) 60825-1 standard and the OSHA Standard 1910.133(a).[45] [3]

4.2.6 Size Constraints

The design will be limited to a 6U cubesat configuration, with a 60cm x 10cm x 10cm dimension. The design processes considers this constraint by buying parts with efficient sizes and laying out components in the most optimal configuration in senior design II. The modular design of this platform will allow for a reconfiguration later that will mitigate any unforeseen size constraint related issues.

4.2.7 Time Constraints

Time constraints will be a major driving factors in the design process and the prototyping process of the CELSS. The ultimate goal is to have the system fully functional by the end of senior design II. Unforeseen delays, such as parts arriving late or design challenges will have to be be mitigated by being proactive. When possible, parts will be sourced from vendors that ship the fastest. We took steps early in the semester, beginning on 9/2/2020 to familiarize ourselves with the project, assign roles, and identify system components.

Additional time will be used, that wasn't originally planned for, over this winter break to meet time constraints. The PCB and system inter-connectivity are going to be the most time consuming parts of this project, and some expectations were not met. To keep progress satisfactory, the extra time over the winter break will be spent designing and then soon testing any designs. Additionally, some place holder parts were ordered to begin preliminary testing of components. For example, a regular glass prism and a different, faster shipping laser diode was ordered to do preliminary testing of the refractometer before the real parts arrive. Time constraints are going to be a dominant factor in the rest of senior design II, so these extra steps are being taking now to mitigate that.

4.2.8 Testing Constraints

Our project is relatively limited in how it can be tested and show cased. For one, we cannot put it in its intended environment, which is space, so the design considerations for making it vacuum proof are never even considered. We require a few additional steps to simulate or facilitate some of our testing. For one, we must simulate a cold, space environment. As stated, we cannot go to space, so instead we will use a large deep freezer to place our CELSS in and do our thermometer and heater testing in. For refractometer testing, it will be difficult to calibrate the accuracy of the test, because

another system is required to confirm the salinity of the water. Alternatively, the test for the refractometer to measure salinity will involve two controlled samples of water with known salinity to mitigate this obstacle. For the optode and camera, we will have to simulate expected aquatic environments with known samples. Much of the environments and situations the CELSS is intended to be adapted for and measured, will have to be simulated or found alternatives for due to testing constraints.

5 Design

5.1 Overall Device

Here we discuss every element of our CELSS in further detail, in order to get a better idea of how every component contributes in satisfying the overall purpose of the sensor suite. Our device can be thought of as many independent sensor modules being tied into one research platform. This subsection will outline the device proposed for each measurement described in the previous section, and how they will be integrated into an all-in-one, remote-controlled, research platform. This suite will use electronic and optical sensors to observe dissolved oxygen, specific gravity, ammonia (NH_3), average temperature, turbidity, and algae color to characterize the self-sustaining, hypersaline, Closed Ecological Life Support System (CELSS) of brine shrimp, algae, and possibly other microorganisms.

Measurement	**Sensor**
Dissolved oxygen	Optode
Salinity	Refractometer
Ammonia	Ammonia Alert Strip/-Camera
Temperature	Thermometer module
Algae color	Camera

Table 25: Table of each measurement desired and its respective sensor.

Dissolved oxygen will be measured with an optode device that will be manufactured. Salinity will be measured with a device that will be configured. The other measurements largely rely on visual indicators coming from sensors that are transmitted via imagery. Visual indicators have been considered in a number of experiments involving closed ecosystems containing Artemia [92] [60] [77]. These indicators include "color of the culture, the fluid volume, and the size and number of brine shrimp; overall culture transparency, and, when mostly free of algae or at low algal density, and the degree of cloudiness" (turbidity)[77]. A phone camera will be utilized with a wide-angle lens system that offers a depth of field that covers most or all of the depth into the tank,

that will be placed immediately next to the camera. This will require the focus to be a very short distance from the lens system. Our requirements are such that the F, d and C lines will have a focal shift that is within 12 μm. We will achieve a RMS spot size that is within two times the size of our pixels (7.2μm) for on-axis and 6° incident rays onto the system from object space. The lens system will have a focal length of 4 mm and a semi-field angle of 24 degrees, with these specifications subject to change with its placement in the tank and overall geometry of the tank (should a better or simpler solution be found than what is currently being designed for). Our lens system is going to be plastic, to save on weight and cost. This will be designed in Zemax.

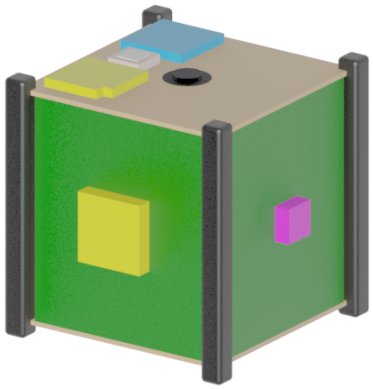

Figure 47: 3d Illustration of Cubesat with Each sensor on its own face of the CubeSat
Purple: optode, yellow: refractometer (camera is not visible)

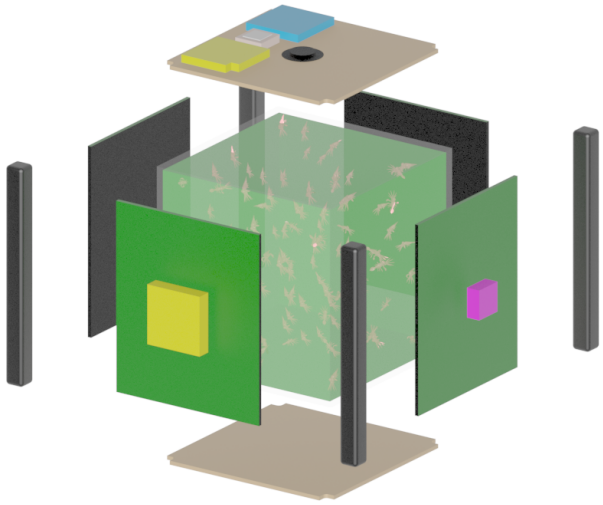

Figure 48: Exploded View of Cubesat Illustrating Cubic Aquarium in Center

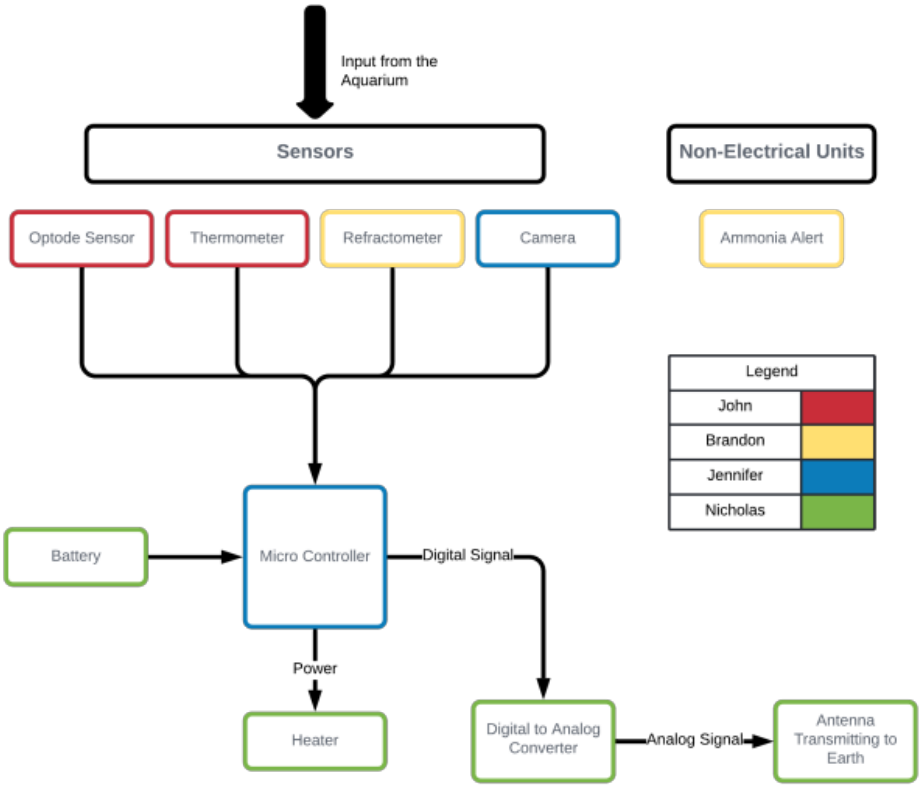

Figure 49: Hardware flowchart

5.2 Printed Circuit Board Design

This project requires the development and fabrication of custom PCBs in order to ensure that the circuitry and electronics involved are as compact, lightweight, and durable as possible. Since the application we're using these PCBs for is a satellite, size and weight are extremely important criteria to consider when choosing components and when designing the boards. In addition to being compact and lightweight, the boards that we design need to have components that can withstand at least reasonably harsh conditions. Due to budget and scope constraints of this project, the long-term durability of the PCBs will not be tested, but the durability will still be a consideration for component selection.

5.2.1 Design Technology

When designing a PCB, the technology that is used has a great impact on the final outcome of the design. Before computer-aided design (CAD) software was used to design PCBs, they had to be laid out by hand on clear film with pens, tape, and pads. Fortunately, this is no longer necessary thanks to the aforementioned CAD software. Now that we're able to route the traces needed for the PCBs virtually rather than by hand on film we're able to design circuits that used to take weeks to plan the traces on in a matter of hours.

Most of the PCB CAD software used today works in two steps. The first step is to lay out the components in their symbolic form on an abstract schematic. This is done so that the electrical characteristics of the circuit design don't yet have to be bound by the physical layout of the wiring and components and can instead ensure that everything works as it should and is connected properly. The second step of the design is taking that abstract schematic and creating it on a virtual representation of a physical PCB. This process is made much easier by both the fact that the nature of the prototyping is virtual and by the fact that PCB CAD software comes with additional tools that aid in the process.

Some of the additional tools at our disposal thanks to CAD software include the snap grid with adjustable grid spacing, netlists in the abstract schematics, "rats nest" overlays on the components, forward and backward annotation between the board and the schematic, and finally the auto routing tool. The snap grid with adjustable spacing allows for the placement of components on a course grid and the subsequent adjustment of the spacing to allow for more fine-tuning when it comes to the smaller components on the board. Netlists allow for the symbol-based schematic's connections to be translated directly onto the components in the board design portion of the PCB CAD program. This communication between the abstract schematic and the PCB representation allows for forward and back annotation and synchronization of changes made to either the schematic or the board design.

One additional tool that Texas Instruments has released is WEBENCH, an online

voltage regulation design tool that allows us to input specifications for the input, output, operating temperature, and other specifications that would be relevant to the design of power regulators. This tool outputs different design schematics and associated PCB layouts that we are able to sort through based on efficiency, Bill of Materials (BOM) cost, footprint size, and several other specifications that are pertinent to the designs in question. This greatly cuts down on the design time and parts selection time for the power regulation components and allows for more work to be put on other aspects of the overall design of the system as a whole. The schematics and parts lists for these designs are also able to be downloaded in a number of different popular PCB CAD software formats, allowing for easy customization of the design in question. Figure 50 shows an example of one of the boards that were designed for this project.

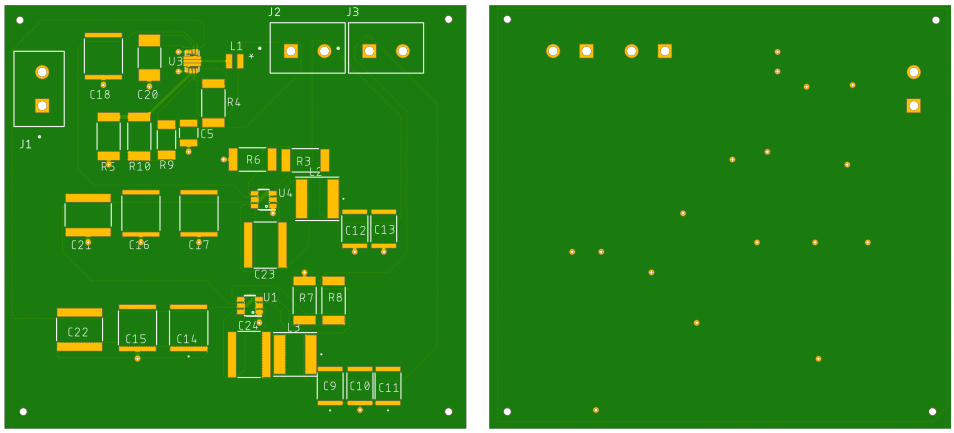

Figure 50: DC to DC converters designed with the aid of WEBENCH

5.2.2 CAD Software

The PCB CAD program that we are using for this project is Autodesk's Eagle application. This application was chosen primarily due to the previous experience that we've gained in classes using this program. Additionally, Autodesk offers an educational license for this program and allows for the cross-communication of this software with their regular CAD software, Fusion 360. This cross-communication allows for the PCB being prototyped in Eagle to be imported into Fusion 360 and have the work sync between them. With this feature, any changes that are made on the Eagle or Fusion 360 files are synced with the other program. For example, if in Eagle the designer changes the size of the PCB on their board then the size of the board would change in the Fusion 360 model as well.

5.3 Power Supply

With our prototype being battery powered there is no need for an AC to DC converter but we do have the need for multiple different voltages since we have so many different

electric components. In this set up we have three main voltage drops using buck boost converters. The main converters being used are the TPS565208DDCR for the 3.3V and 5.0V rails, and the TPS62147RGXR for the 12.0V rail.

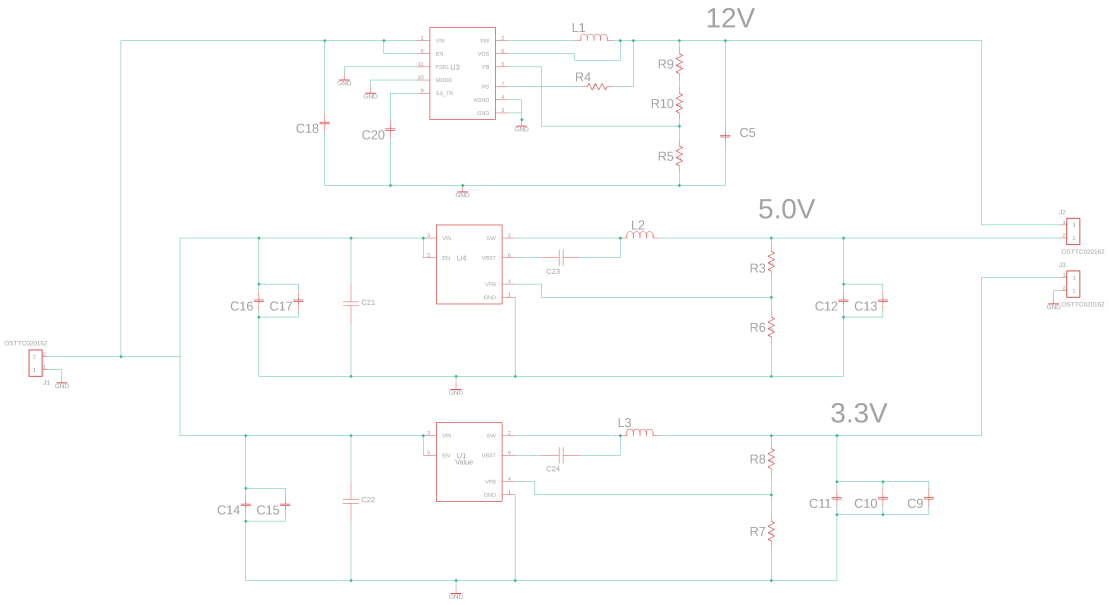

Figure 51: 16.8V DC to 3.3V, 5.0V, and 12.0V DC

5.4 Optode

An oxygen optode is designed in order to measure the dissolved oxygen in the aquatic system. Both the dye-coated substrate and the housing need to be prepared in order to develop this device.

5.4.1 Optode Fabrication & Design

We are going to develop our prototype optode sensor based off of the design of optode as presented by Tengberg et al. [81] and as seen in figure 52. The sensor simply consists of a blue LED, a red reference LED, silicon photodiode, a glass substrate, a gas-permeable silicon black layer [81], blue and red filters, and PtTFPP or PdTFPP. The PtTFPP is an oxygen-quenchable luminophore with emission maximums at 647 and 710 nm, and absorption maximums at 390 nm, 504 nm and 538 nm [73]. PdTFPP features similar characteristics, however it finds is use in sensors that require a very high sensitivity for detecting trace oxygen. Our choice to use PtTFPP over alternative luminophores also resulted after detailed analysis that has been overviewed in the previous section on dye selection, favoring it for the same reasons that reference [73] favors this luminophore over alternatives. PtTFPP is commercially available [55], and 100 mg of it may be obtained from Advanced BioChemicals ($650), Ambeed ($332.8), BLD pharm ($331.6) and PorphyChem ($202.44) amongst other distributors.

We however have chosen to modify the design slightly in order to accommodate the resources we have available to fabricate the sensor on our own, and to reduce its cost: we have chosen to use a single long-pass filter in our optode design instead of a combination of long and short-pass filters, as a long-pass filter at 570 nm will sufficiently block any unwanted light from our UV source from being incident upon the photodiode. We have also chosen to eliminate the use of an oxygen-permeable black silicon layer on top the device, in order to simplify device fabrication. Finally, we decided to use a 830 nm LED in the near-ir as a reference LED, as its output will still be picked up by our photodiode, however it is cheaper, and owing to its external quantum efficiency and shorter wavelength, it is more power efficient to drive.
PorphyChem sells PtTFPP at a far more affordable price than the other distributors of the material. Additionally, shipping was only an additional $30 when purchasing from PorphyChem despite shipping from France, and they newly synthesized the material for us upon our request. Suffice to say, we are very impressed by PorphyChem and their service in selling us this material.

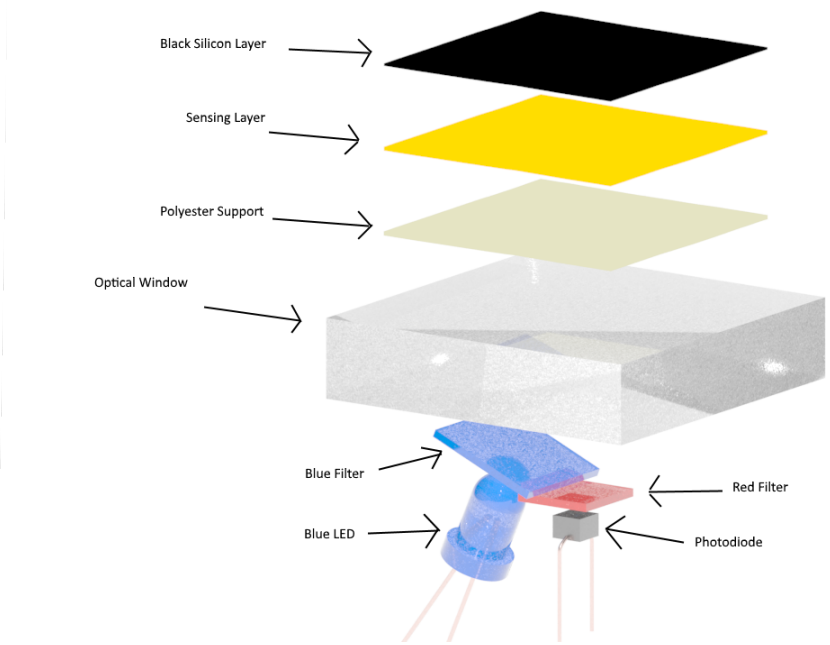

Figure 52: Illustration of the Optode Design that is Discussed in Reference [81] .

5.4.2 Optode Housing

Presented in Figures 53 and 54 is the oxygen optode housing that will include the LEDs, photodiode, and filter. This housing is simply fabricated out of PLA filament by 3d-printing. The components in this housing make up the bulk of the optode, and the resulting device is simply glued onto the side of the outside of the aquatic system, so that a glass slide coated in the PtTFPP and PS may be illuminated by the LEDs

within the optode housing. The fluorescence of the glass slide is then picked up by the oxygen optode, to indicate the concentration of dissolved oxygen present in the water.

Figure 53: 3d-printed optode housing, containing LEDs, photodiode and filter

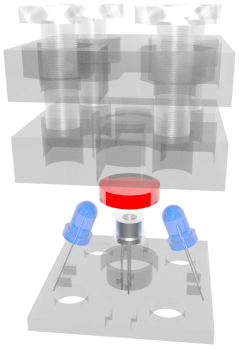

Figure 54: 3d-render of optode housing

5.4.3 Optode Demonstration

In a test with a water sample containing 2 parts per million(ppm) or mg/L of dissolved oxygen, and a water sample that is found to contain 6 ppm or mg/L of dissolved oxygen, we report a range of 0.7 volts after amplifying the signal from the photodiode to report 1 V when in air. This resulted in a report of 1.5 Volts in the 2 ppm water, and 0.8 Volts in water with 6 ppm of oxygen. Noise is present on the order of 10 mv, this provides that our measurement is accurate up to 0.36 ppm(mg/L). Verification of the dissolved oxygen concentration in our water was completed via the Winkler method.

5.5 Refractometer

It was discussed in section 3.6.3 that the best course of action was to use a double prism configuration in some way, with a v-block refractometer being best. Due to the constraint of a v-block prism being hard to source, it was best to decide to simply use two equilateral prism and configure them equivalently to a v-block design. The dimensions are shown in the diagram below, however through the manufacturing process we will seek to minimize each of these elements size.

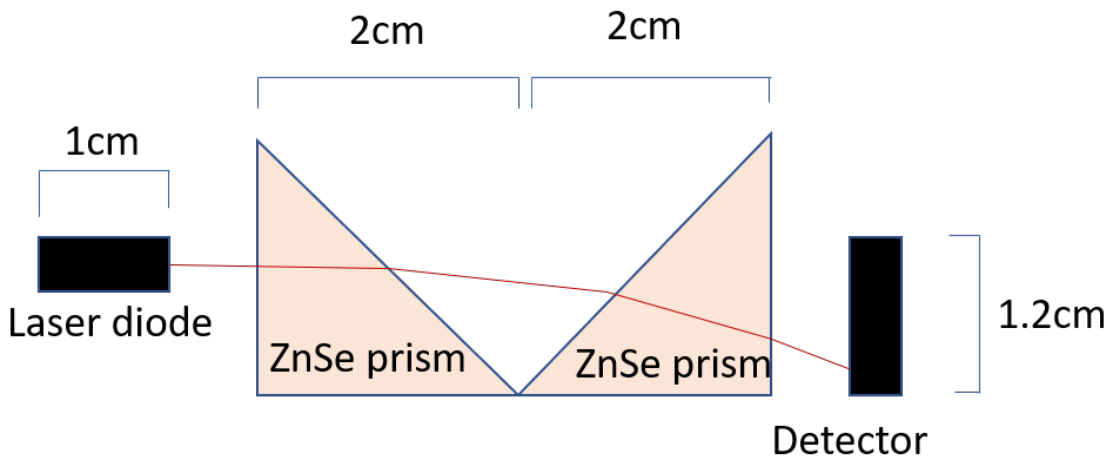

Figure 55: Refractometer design.

The laser is a Mitsubishi ML101J25 and the detector is a Hamamatsu S3932 IR Photodiode.

5.6 Camera

The camera was used in order to measure both turbidity and ammonia in the tank. It is connected to the Raspberry Pi Zero, and the Raspberry Pi is using image processing to extract data from the images.

5.6.1 Initial Design

We began by duplicating the design found in [21] which was adapted from the solution presented in [56]. This was designed for imaging an object at infinity. It is required that this is adapted to imaging an object that is placed about 50 mm away in water. It should be noted that because this is in water, the optical path length translates to 66.6 mm. The whole of the setup, featuring the object space being in water, is presented in figure 56. The lens system in particular is shown in figure 57. Figures 58 and 58 show the initial design lens data and higher-order aspheric coefficients accordingly. Figure 60 shows the spot diagram, and it can be seen that the RMS radius is already in the single digits in microns for the 0° and 7.45° rays. This adaptation of a lens design is already performing well, despite being given the different parameters of a finite (and relatively small) object distance, and the presence of a spherical boundary that to a small degree functions as a meniscus lens.

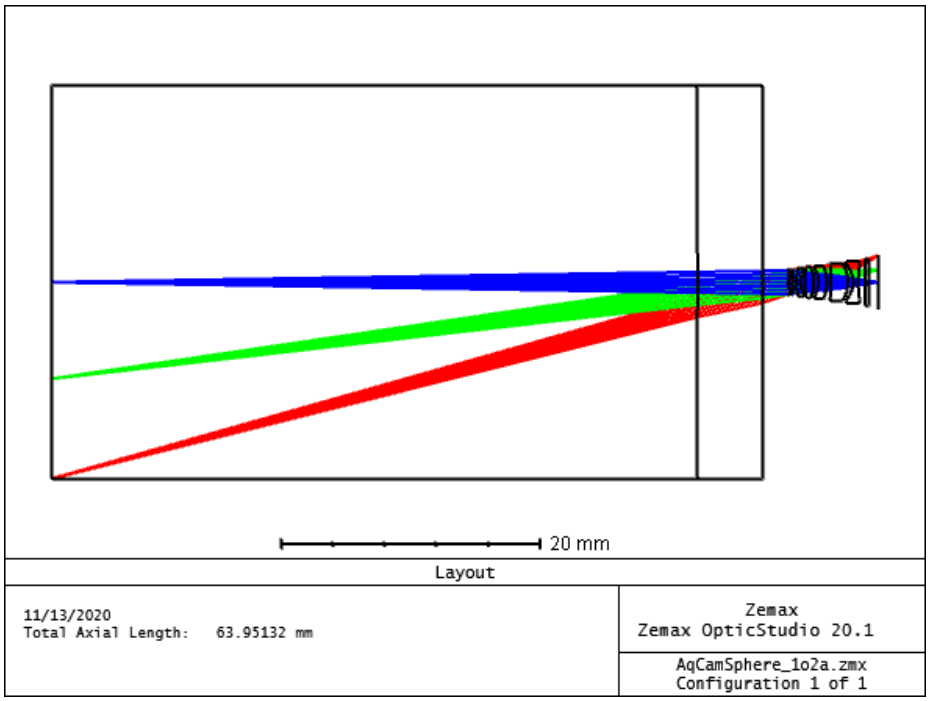

Figure 56: Perspective with respect to object space

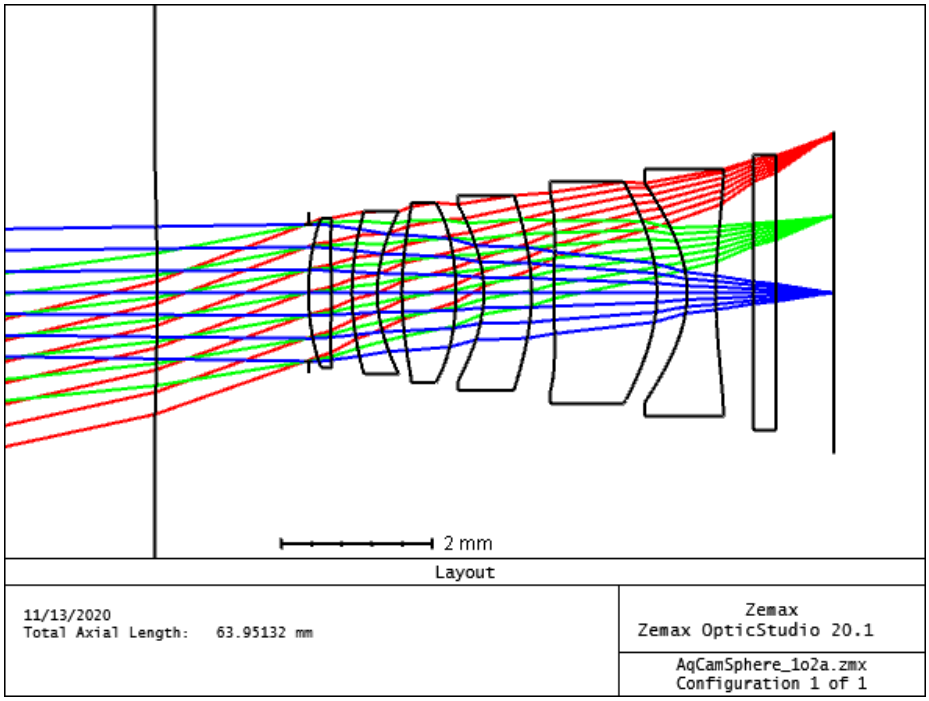

Figure 57: Layout of Initial Design

	Surface Type	Comment	Radius	Thickness	Material	Coating	Clear Semi-Dia	Chip Zone	Mech Semi-Dia	Conic	TCE x 1E-6
0	OB Standard		Infinity	50.000	WAT...		15.184	0.000	15.184	0.000	-
1	Standard		-49.237	5.000	ACR...		2.692	0.000	15.184	0.000	-
2	Standard		-49.237	2.000			1.605	0.000	15.184	0.000	0.000
3	STO Standard		Infinity	0.000			0.903 U	0.000	0.903	0.000	0.000
4	Even Asphere		3.019	0.300	COC		0.977	0.000	0.987	-6.239	-
5	Even Asphere		-47.962	0.277			0.987	0.000	0.987	-1.715	0.000
6	Even Asphere		3.125	0.331	OKP4		1.069	0.000	1.073	-9.926	-
7	Even Asphere		1.737	0.330			1.073	0.000	1.073	-3.404	0.000
8	Even Asphere		4.541	0.713	COC		1.135	0.000	1.187	-9.049	-
9	Even Asphere		-3.234	0.369			1.187	0.000	1.187	0.000	0.000
10	Even Asphere		-1.725	0.630	OKP4		1.166	0.000	1.283	-1.895	-
11	Even Asphere		-3.062	0.297			1.283	0.000	1.283	-9.815	0.000
12	Even Asphere		14.440	1.361	COC		1.320	0.000	1.462	50.588	-
13	Even Asphere		-2.164	0.400			1.462	0.000	1.462	-1.926	0.000
14	Even Asphere		-1.568	0.378	COC		1.445	0.000	1.633	-1.715	-
15	Even Asphere		6.319	0.500			1.633	0.000	1.633	-44.660	0.000
16	Standard		Infinity	0.300	N-BK7		1.755	0.000	1.814	0.000	-
17	Standard		Infinity	0.765 M			1.814	0.000	1.814	0.000	0.000
18	IMA Standard		Infinity	-			2.129	0.000	2.129	0.000	0.000

Figure 58: Initial Design Lens Data

	Surface Type	2nd Order Term	4th Order Term	6th Order Term	8th Order Term	10th Order Term	12th Order Term	14th Order Term	16th Order Term
0	OB Standard								
1	Standard								
2	Standard								
3	STO Standard								
4	Even Asphere	0.000	0.022	-9.405E-03	0.014	7.058E-04	-7.048E-03	1.164E-03	6.441E-03
5	Even Asphere	0.000	3.429E-04	0.012	0.017	-0.013	4.047E-04	-2.870E-03	8.921E-03
6	Even Asphere	0.000	-0.023	0.041	-6.779E-03	-8.959E-03	-6.313E-04	1.704E-03	4.778E-04
7	Even Asphere	0.000	-0.021	0.040	-0.011	-2.142E-03	-3.683E-04	-3.342E-04	5.551E-04
8	Even Asphere	0.000	-2.259E-03	-7.890E-04	4.534E-04	2.067E-05	-4.402E-05	5.170E-05	-1.387E-05
9	Even Asphere	0.000	-8.769E-03	-4.238E-03	-2.968E-03	-5.103E-04	4.703E-05	3.470E-05	5.760E-06
10	Even Asphere	0.000	0.018	-6.087E-03	7.402E-05	-4.218E-04	1.295E-05	7.414E-06	3.996E-06
11	Even Asphere	0.000	-0.018	5.734E-03	1.809E-04	-8.269E-05	-2.591E-06	-5.495E-07	6.846E-08
12	Even Asphere	0.000	-0.036	-2.187E-03	1.701E-04	-1.645E-04	3.182E-07	-8.248E-08	-4.158E-08
13	Even Asphere	0.000	4.789E-03	-9.143E-04	3.299E-05	2.807E-06	-2.026E-08	-5.465E-09	-7.650E-10
14	Even Asphere	0.000	6.645E-03	-4.548E-05	4.189E-06	-2.611E-07	1.038E-08	3.407E-10	-2.292E-10
15	Even Asphere	0.000	-4.813E-03	-1.291E-04	-2.870E-06	4.729E-08	5.041E-09	3.247E-10	1.771E-11
16	Standard								
17	Standard								
18	IMA Standard								

Figure 59: Initial Design Higher-Order Aspheric Coefficients

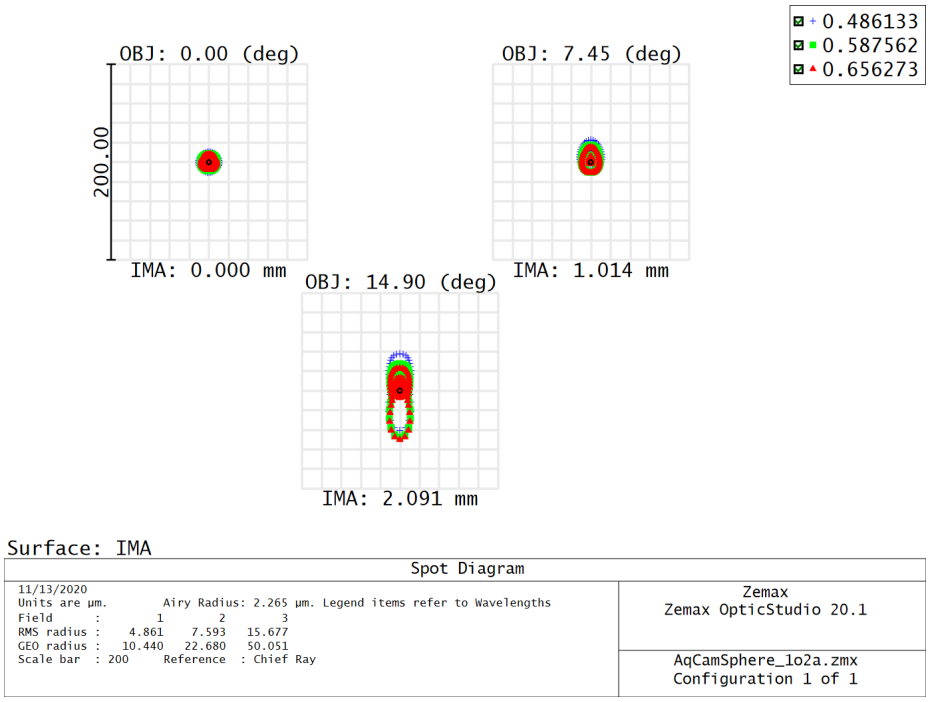

Figure 60: Spot Diagram of Initial Design

5.6.2 Optimized Design

The lens's performance is impressive despite its new requirements to image our rather small aquarium. However, in order to optimize the performance of the lens system for our application, Zemax OpticStudio is utilized to perform lens-bending with the merit function tool. We have used the optimization wizard to optimize based off of the wavefront through the system, of type RMS and gaussian quadrature pupil integration with 6 rings and 6 arms. We have also added a merit function to minimize chromatic aberration on the F and C lines. The results are as follows in figures 61, 62, 63, 64, 65 and 66. The resulting field of view is satisfying, and small focal length of $4.837mm$ that the system features will allow for a large depth of field, while maintaining a sharp image with the F/# of 2.8.

5.6.3 Implementation Failure

Unfortunately, due to the cost of diamond-turning this lens system having been quoted to cost $5,300, and the difficulty of fabricating the optomechanics required to hold the lens system, we have opted not to pursue the implementation of this lens for our final design. This design is maintained as a viable solution in the event that this product is taken to the next phase, such that it is integrated into a production that justifies injection-molding aspheric plastic lenses. Such a production would reduce the cost of each individual injection-molded lens to the order of a dollar, thus allowing this approach to be viable. With that being said, it has been decided not to include this lens system in the final demonstration.

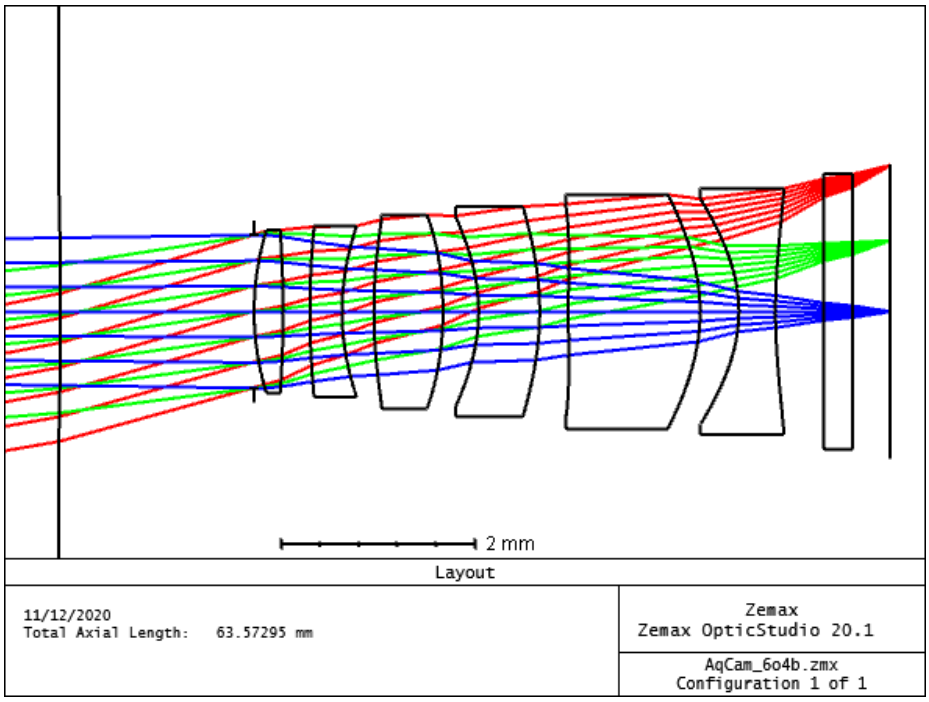

Figure 61: Layout of Final Design

	Surface Type	Comment	Radius	Thickness	Material	Coating	Clear Semi-Dia	Chip Zone	Mech Semi-Dia	Conic	TCE x 1E-6
0	OB Standard		Infinity	50.000	WAT...		12.130	0.000	12.130	0.000	-
1	Standard		-49.237	5.000	ACR...		2.205	0.000	12.130	0.000	-
2	Standard		-49.237	2.000			1.342	0.000	12.130	0.000	0.000
3	STC Standard		Infinity	0.000			0.795	0.000	0.795	0.000	0.000
4	Even Asphere		2.743	0.300	COC		0.832	0.000	0.843	-6.239	-
5	Even Asphere		-10.321	0.277			0.843	0.000	0.843	-1.715	0.000
6	Even Asphere		8.707	0.331	OKP4		0.877	0.000	0.885	-9.926	-
7	Even Asphere		2.416	0.330			0.885	0.000	0.885	-3.404	0.000
8	Even Asphere		5.366	0.713	COC		0.950	0.000	1.000	-9.049	-
9	Even Asphere		-3.381	0.369			1.000	0.000	1.000	0.000	0.000
10	Even Asphere		-1.815	0.630	OKP4		0.987	0.000	1.086	-1.895	-
11	Even Asphere		-3.027	0.297			1.086	0.000	1.086	-9.815	0.000
12	Even Asphere		21.507	1.361	COC		1.110	0.000	1.209	50.588	-
13	Even Asphere		-1.980	0.400			1.209	0.000	1.209	-1.926	0.000
14	Even Asphere		-1.514	0.378	COC		1.164	0.000	1.273	-1.715	-
15	Even Asphere		5.768	0.500			1.273	0.000	1.273	-44.660	0.000
16	Standard		Infinity	0.300	N-BK7		1.374	0.000	1.422	0.000	-
17	Standard		Infinity	0.387	M		1.422	0.000	1.422	0.000	0.000
18	IM/ Standard		Infinity	-			1.517	0.000	1.517	0.000	0.000

Figure 62: Final Design Lens Layout

	Surface Type	2nd Order Term	4th Order Term	6th Order Term	8th Order Term	10th Order Term	12th Order Term	14th Order Term	16th Order Term
0	OB Standard								
1	Standard								
2	Standard								
3	STO Standard								
4	Even Asphere	0.000	0.022	-9.405E-03	0.014	7.058E-04	-7.048E-03	1.164E-03	6.441E-03
5	Even Asphere	0.000	3.429E-04	0.012	0.017	-0.013	4.047E-04	-2.870E-03	8.921E-03
6	Even Asphere	0.000	-0.023	0.041	-6.779E-03	-8.959E-03	-6.313E-04	1.704E-03	4.778E-04
7	Even Asphere	0.000	-0.021	0.040	-0.011	-2.142E-03	-3.683E-04	-3.342E-04	5.551E-04
8	Even Asphere	0.000	-2.259E-03	-7.890E-04	4.534E-04	2.067E-05	-4.402E-05	5.170E-05	-1.387E-05
9	Even Asphere	0.000	-8.769E-03	-4.238E-03	-2.968E-03	-5.103E-04	4.703E-05	3.470E-05	5.760E-06
10	Even Asphere	0.000	0.018	-6.087E-03	7.402E-05	-4.218E-04	1.295E-05	7.414E-06	3.996E-06
11	Even Asphere	0.000	-0.018	5.734E-03	1.809E-04	-8.269E-05	-2.591E-06	-5.495E-07	6.846E-08
12	Even Asphere	0.000	-0.036	-2.187E-03	1.701E-04	-1.645E-04	3.182E-07	-8.248E-08	-4.158E-08
13	Even Asphere	0.000	4.789E-03	-9.143E-04	3.299E-05	2.807E-06	-2.026E-08	-5.465E-09	-7.650E-10
14	Even Asphere	0.000	6.645E-03	-4.548E-05	4.189E-06	-2.611E-07	1.038E-08	3.407E-10	-2.292E-10
15	Even Asphere	0.000	-4.813E-03	-1.291E-04	-2.870E-06	4.729E-08	5.041E-09	3.247E-10	1.771E-11
16	Standard								
17	Standard								
18	IMA Standard								

Figure 63: Final Design Higher-Order Aspheric Coefficients

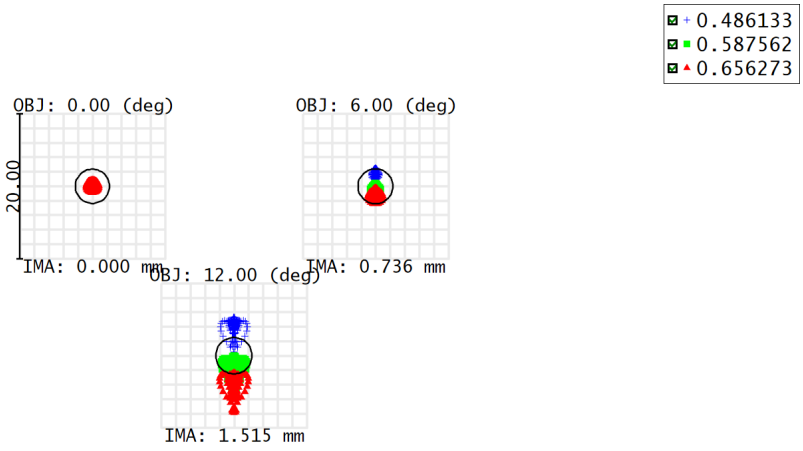

Surface: IMA

Spot Diagram

11/12/2020
Units are μm. Airy Radius: 2.367 μm. Legend items refer to Wavelengths
Field : 1 2 3
RMS radius : 0.384 1.375 3.565
GEO radius : 0.876 2.513 7.892
Scale bar : 20 Reference : Chief Ray

Zemax
Zemax OpticStudio 20.1

AqCam_6o4b.zmx
Configuration 1 of 1

Figure 64: Spot Diagram of Final Design

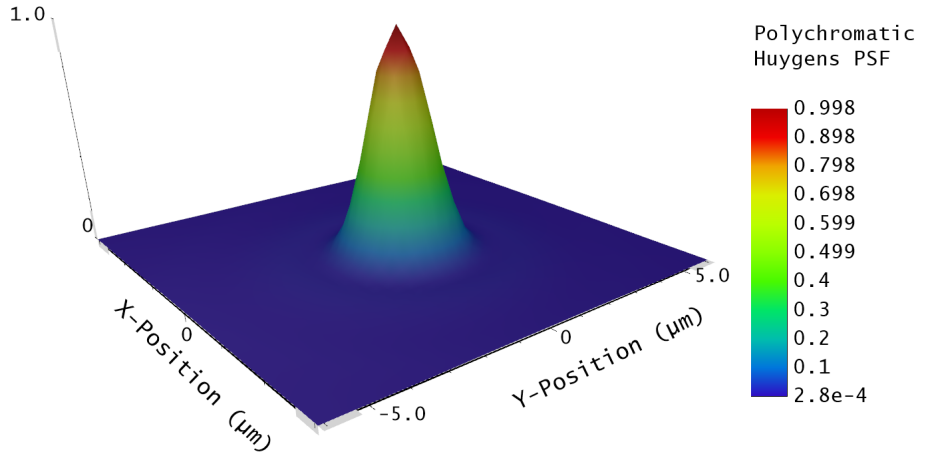

Polychromatic Huygens PSF	
11/12/2020 0.4861 to 0.6563 µm at 0.00 (deg). Image size is 12.26 µm square. Strehl ratio: 0.998 Center coordinates : 0.00000000E+00, 0.00000000E+00 Millimeters	Zemax Zemax OpticStudio 20.1 AqCam_6o4b.zmx Configuration 1 of 1

Figure 65: Huygens PSF of final design

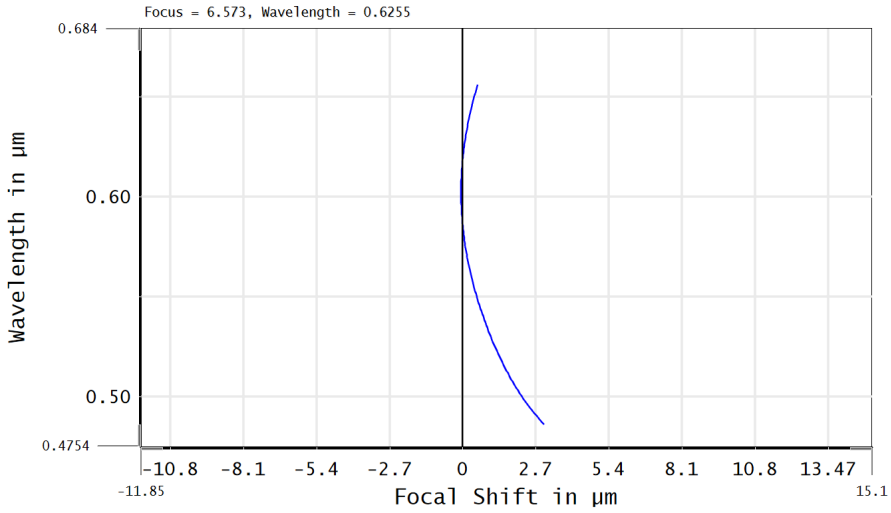

Chromatic Focal Shift	
11/12/2020 Maximum Focal Shift Range: 3.0681 µm Diffraction Limited Range: 25.634 µm Pupil Zone: 0.0000	Zemax Zemax OpticStudio 20.1 AqCam_6o4b.zmx Configuration 1 of 1

Figure 66: Focal shift of final design

6 Overall Integration

The main processor will be on its own board with connectivity to the periphery boards that are home to the sensors. The main concept for this sensor array is going to one in which the main microprocessor is connected closely with the camera and the antenna. These two components will likely be on the same board as the main microprocessor so that they will have a more durable connection and be able to communicate much more easily between them. This close connection for these components is because of the amount of data that will be traveling from the camera to the processor. We've had issues in preliminary testing with the picture from the camera becoming distorted due to noise in the environment. In order to limit this noise, the design is to connect these three pieces of hardware as close together as possible to minimize the exposure to external interference.

Additionally, this board would serve as the hub where all of the data from the other sensors is sent out through the antenna. The data that would be sent to the main board would be processed by the sensors as part of their design so that the sensors output a digital signal to the main board. The reason for this pre-processing of the data is that the main board accepts a digital signal on 54 of its pins, but only accepts analog inputs on 16 of its pins. Saving the analog pins for devices like the antenna makes it much simpler for the data to be processed and sent out in an efficient way.

6.1 Software Design

Deciding which microprocessor met our specifications and designing the circuits that supplied it with power and data was only one part of the problem when it came to designing the computational aspect of this project. The other part of the work to do with the microprocessor is the software programming and logic design that takes the data from our array of sensors and turns it into something useful and transmit/store the resulting data.

We are attempting to minimize the possibility of our sensors interfering with each other. In order to achieve this, only one sensor in our array will be taking measurements at one time. This is partially due to the fact that things like the Camera, Optode, and Refractometer all rely on photovoltaic systems in order to function and all of these systems have their own source of light in order to collect their measurements. In order to prevent the light source from one of these sensors from interfering with the measurements being taken by the other sensors involved, the sensors will only be powered on by the power management and distribution (PMAD) system. This will also allow us to conserve power and only use the power we need for the specific measurements.

The PMAD system will be controlled by the main MCU through commands which will switch the power delivery from one subsystem to another while taking measurements from the subsystems in sequence. A subsystem in this context is one sensor in the

array since it consists of multiple components which each need power and are treated as discrete systems that make up the sensor array as a whole. The MCU will also be putting itself in sleep mode in order to conserve power while it is not taking these measurements or transmitting them via the on-board antenna. This will also have the benefit of not consuming power when the subsystems are not in use and conserve as much power as possible.

6.1.1 Algorithm Design

The programming logic for the code will have multiple functions that each serve different purposes and are able to be customized for the different roles they play. Figure 67 gives a breakdown of the main algorithm logic and data flow.

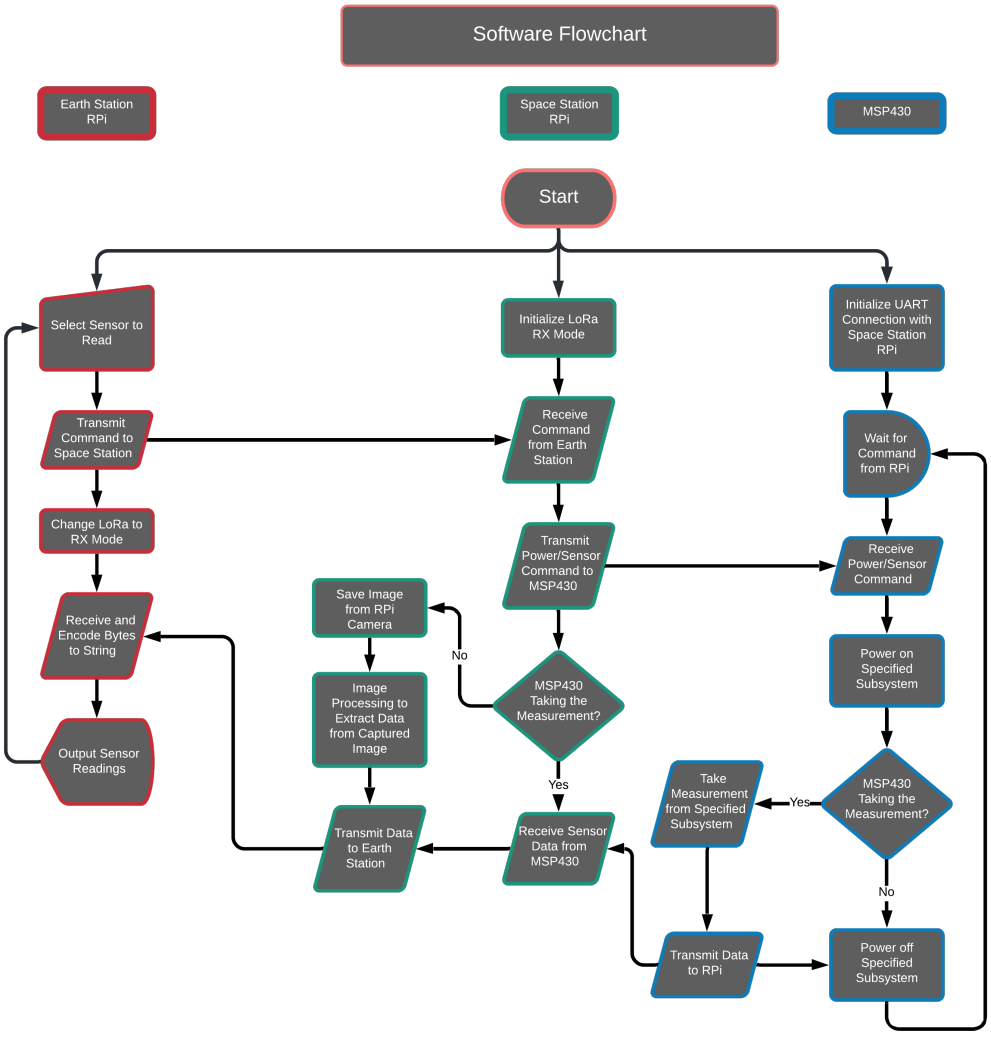

Figure 67: Main Logic Flowchart

6.2 Software Testing

Creating software for systems isn't something that is able to be done without also properly checking if the software in question functions as intended. In order to properly test a program there are certain steps that must be taken. Due to the small-scale nature of the project that we're working on, the main tests that we will be running will be those of functionality and flaws. The end goal of this project is to create a functional prototype that would be able to be improved upon in order to create a finished product, but one that is simply functional at the moment of demonstration. For this reason, we will be testing the software along with the hardware in order to ensure functionality, but not perfection.

The main purpose of this project is to create a functional prototype. Due to the nature of the project that we have chosen there is no user input apart from a cease transmission signal built into the programming, there is little input to program for apart from the actual data that the system will be collecting. As such the programming logic that dictates the behavior of the system will be fairly simple, even if the programming implementation is slightly more complex.

6.3 Hardware Programming and Memory Flashing

The MSP430G2553 will be programmed using TI's Spy-Bi-Wire (SBW) technology. This technology allows us to program the flash memory on the chip using a 2-wire JTAG interface, and to write programs to the microprocessor much easier. The Raspberry Pi Zero will be running the Raspbian operating system from an SD card. This SD card will be flashed using a secondary computer. The only programming that will need to be done on the Raspberry Pi is in software.

6.4 Space Station

The Space Station for our project is the prototype itself. A typical CubeSat may include multiple strip antennas or an array of deployable antennas in order to account for the losses that can come from poor line of sight or bad angles between the transmitting and receiving stations. Antennas are designed to operate even when they receive very little power but when you start to account for the massive distance, or slant range, that can come from a satellite in orbit, any little change in angle can add to the power loss. These changes in angles are included in antenna boresight calculations and mis-pointing losses. A high level and expensive CubeSat may have built in thrusters in order to keep the mis-pointing losses to a minimum, but even then they are not going to be in geostationary orbit. That means that these CubeSats will typically be transmitting to a relay of receiving Earth Stations. There are even orbiting satellites to help with communication like the European Data Relay Satellite System (EDRS) that remain in geostationary orbit and can transmit information from non geostationary satellites. An orbiting geostationary network like that allows for faster, on-demand access to information without the need to wait for a satellite

to come within view of a particular ground station.

One of the main issues for a transmission from space is the noise that is encountered when beaming down to Earth. Distance and power limitations can be big sources of loss, but this noise is something that must always be overcome. Rain and other weather is one big factor present on Earth that is not encountered as big of a problem when the receiving station is in space. This weather loss affects the temperature noise and rain attenuation of an antenna. One of the ways this is overcome is with the use of large satellite dishes and powerful amplifiers. This will not be the case for our project as NASA has extensive experience in radio communications and the main priority of our experiment is the sensors, not the transmission itself. Another issue that is present in the real world is called atmospheric loss. This will obviously not be present in our system of transmitting across a field and not through Earth's atmosphere. Since we are not going to be building to account for extra noise from weather, temperature, or atmospheric losses, our main hurdle to overcome that we can demonstrate is going to be distance.

Distance can be present in several calculations but the first one we must account for is the Incident Flux Density. Most satellites use directional antenna dishes which allow them to benefit from a transmission gain. On the receiving side, a typical satellite array uses parabolic reflector dishes to accumulate the signal and bounce it back to a concentrated receiving point to amplify the gain. In our case, we will be using an isotropic spring antenna. This antenna is not directional and so it does not get anywhere near the benefit of a directional antenna. In order to calculate the flux, we use the Friis transmission formula below:

$$F = \frac{P_t G_t}{4\pi R^2}, \frac{W}{m^2} \tag{33}$$

Where F is the measured flux, Pt is the transmitter power, Gt is the gain of the transmitter antenna, and R is the radius of the sphere that measures the distance between the transmitter and the antenna. As can be seen from the formula, the flux decreases according to the square of the distance. A typical Earth Station antenna can have a transmitting gain between 10,000 and 1,000,000 which seems like a massive spike in power. When a Space Station is usually out around 38,000 kilometers in space, which ends up being even larger when you square that distance in meters, or around 1.444E15 meters, that huge transmitting gain is needed.

Our transmitting power measures at 1 Watt. Our spring antenna has a transmitting gain of 3dB which is approximately two when measured in linear. An isotropic source usually does not have any kind of transmission gain that would be considered for a real satellite transmission, but for our purposes dealing with such low power we will acount for it. We must account for our distance to overcome which is 500 meters. This gives us the following calculation when done in linear:

$$F = \frac{1 * 2}{4 * \pi * 500^2} = 6.35 * 10^{-7}, \frac{W}{m^2} \tag{34}$$

$$10 * LOG_{10}(6.35 * 10^{-7}) = -62dB \tag{35}$$

This is a very small number when measured in Watts per square meter. Considering our antennas are tiny spring antennas that are not going to act like a typical parabolic receiving dish, we must make sure we obtain one that is sensitive enough to still pick up the signal. With the flux density calculated, our next step is to measure the received power. The received power is based on the effective capture area of the receiving antenna which is why you will usually see such large dish antennas in satellite arrays. With our use of a small spring antenna, we are not going to get a gain to raise the received power. Since our receiving spring antenna is much less than a square meter, we are adding more losses to our system.

$$P_r = F * A_e, Watts \tag{36}$$

$$A_e = \frac{Gr * \lambda^2}{4 * \pi} \tag{37}$$

$$P_r = -62 + -11 = -73dBW \tag{38}$$

Our receiving spring antenna has an advertised gain of 3dB and our 433MHz transmission has a wavelength of approximately 70 centimeters. This would give us an effective capture area of close to eight square centimeters which equates to -11dB. For this calculation, since we are not accounting for any system losses, this would be the idealized received power. The true received power would require precise temperature measurements that are beyond the scope of the goal of this project. For this project we can approximate the received power to be -73 dbW.

Since the gains and transmitter power of our components are not flexible, these calculations can be organized in a way to isolate the variables that can be controlled. The transmitter power and the transmitter gain are both controlled by the set components in the CubeSat. This combined calculation is known as the effective isotropic radiated power or EIRP. The other electrical component involved is the receiver power. In professional systems there can be amplifiers placed but for our system our only gain comes from the receiving spring antenna which is in the calculation as Gr. This leaves two variables in our system that are the easiest to modify, the radius or distance between our two systems, and the wavelength which is based on the frequency of transmission. Once these variables are isolated into the separation described, we are left with path loss. This path loss is the focus of our demonstration as we set a goal of 500 meters to overcome as seen below.

$$P_r = P_t * G_t * G_r * [\frac{1}{4\pi(\frac{R}{\lambda})}]^2 \tag{39}$$

$$L_p(PathLoss) = [\frac{1}{4\pi(\frac{500}{0.70})}]^2 = -79dB \tag{40}$$

As we can see from the calculated path loss above, -79dB, the only gains in our system so far are coming from the attached spring antennas. Our transmitted power is too small to add any noticeable gain, which is not surprising considering we are aiming for a very low power, battery operated system. Since both of the spring antennas are built for 3dB gains, this extra 6dB of power combined with the path loss gives us our idealized received power, Pr or approximately -73dBW.

6.5 Earth Station

While an antenna is not necessarily required for our demonstration, we believe it is important to include in the project as it would be needed for an actual CubeSat. This will operate in conjunction with the transceiver and will be selected to fit our budget. Many CubeSats are set up with multiple antennas, usually spread out to all sides of the satellite to increase reliability. For our purposes we will be testing across an open field with a direct line of sight. This has been chosen as NASA has extensive knowledge and experience with data transmission through satellites and our goal is just as a proof of concept.

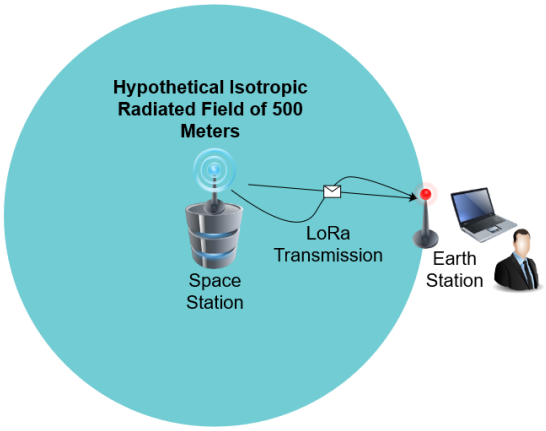

Figure 68: Projected Mock Space and Earth Station Set Up

A common method of signal strength is called carrier to noise ratio. As previously discussed, since we are not transmitting in bad weather or with the high space temperatures and atmosphere that can add to the noise, we must still account for path loss when we are calculating the received carrier power. Our system is only going to have one channel so all of the transmitted power is directed through the one channel. A normal space station can have hundreds or even thousands of channels that distribute the power throughout, but of course they have the benefit of much more power and directional, large gain antennas. The carrier to noise ratio is defined as the amount of power present in the signal itself over the amount of interference and noise that is present to distort or block the signal. Since we have the large link margin, we are

comfortable that there is not enough noise or interference to affect our demonstration.

The noise power on the downlink Earth Station comes from the equation below. Tsys is the overall system temperature which includes the noise figure power ratio, sky, antenna, and receiver temperatures. k is the Boltzmann's constant. Bn is the noise bandwidth which comes from the transponder bandwidth being used.

$$N = k * T_{sys} * B_n \tag{41}$$

$$N = -228.6 + 24.77 + 57 = -146.83dBW \tag{42}$$

$$C/N = -73 - -146.83 = 73.83dB \tag{43}$$

As we see in the formula above, our Carrier Power of -73dBW is much higher than a typical noise power. The noise power calculation was done using boltzmann's constant of -228.6dB for k. Tsys was calculated using 300K which is just an approximate temperature of a normal outside day in central Florida. A usual downlink Tsys in a textbook problem is a lot less since the earth station satellite is pointed up towards a cold space. In decibel calculations there is not a big difference, so we are comfortable using such an approximation. Our noise bandwidth was done using 500kHz which is the largest bandwidth that our SX1278 transmitter uses. This C/N value should be more than enough to allow our transmission at 500 meters.

Our Earth Station is going to be set up with a duplicate transmitter receiver as to that within the CubeSat. The Earth Station version will be the down link receiver for the sensor measurements and then send back the cease transmissions signal when requested. If this project had an unlimited budget we would be able to manufacture a PCB for the receiving Earth Station as well as what is being done in the CubeSat. Since we are not on an unlimited budget, and because the transmission and receiving is not our primary focus, the mock Earth Station is going to remain a testing circuit connected by bread board. This decision saves some money and, considering our need to remain distant and remote as a team, allows easier testing by multiple team members. If there were only one manufactured receiving station, then we would be limited to one team member doing any and all testing.

7 System Testing and Demonstration

As of 12/10/2020, many parts are not yet received and only some proof of concept testing can be done.

7.1 Control Circuit

Figure 69 presents the circuit responsible for directing power to the various subsystems that are used in the satellite. This is the Power Management and Distribution system.

Figure 70 shows the circuit which takes the current produced from the photodiode in the optode sensor and converting it to a voltage that the A/D converter in the MCU can read. The photodiode is reverse-biased and the output current is sent across a shunt resistor to create a voltage for the op-amp. The resistors in the op-amp are tuned to the specific current output of the photodiode, but determining that value is going to require testing. Given that we have not received the photodiode and therefore cannot test it, we have not finalized the resistance values in this schematic. Figure 71 shows a similar approach, but with the PSD for the refractometer. The PSD will also be reverse biased.

The primary method to direct power in the PMAD system is through a series of N-type MOSFETs acting as digital switches for power direction. The MOSFETs will be connected to individual LEDs as well as some of the other subsystems such that we will be able to minimize the light interference between the camera LEDs, Optode LEDs, and the Refractometer laser. Since all of these systems emit light and rely on said light for their measurements, the reduction of interference between these subsystems is important for clean readings.

The MSP430G2553 has an A/D input voltage range of 0.3-3.0 V, so the amplifiers for the sensors must output a voltage within that range. The output from the amplifying circuits is sent to the A/D inputs on the MSP430G2553, which processes that data and sends it to the Raspberry Pi through the UART interface.

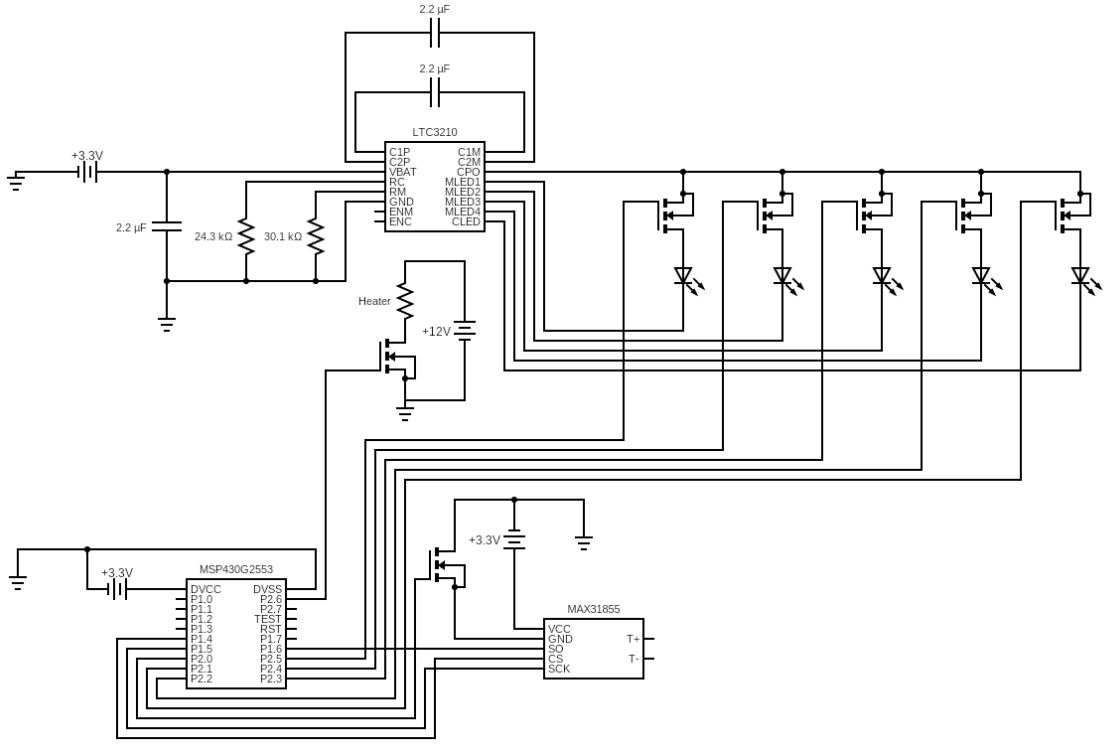

Figure 69: Power Management and Distribution System Schematic

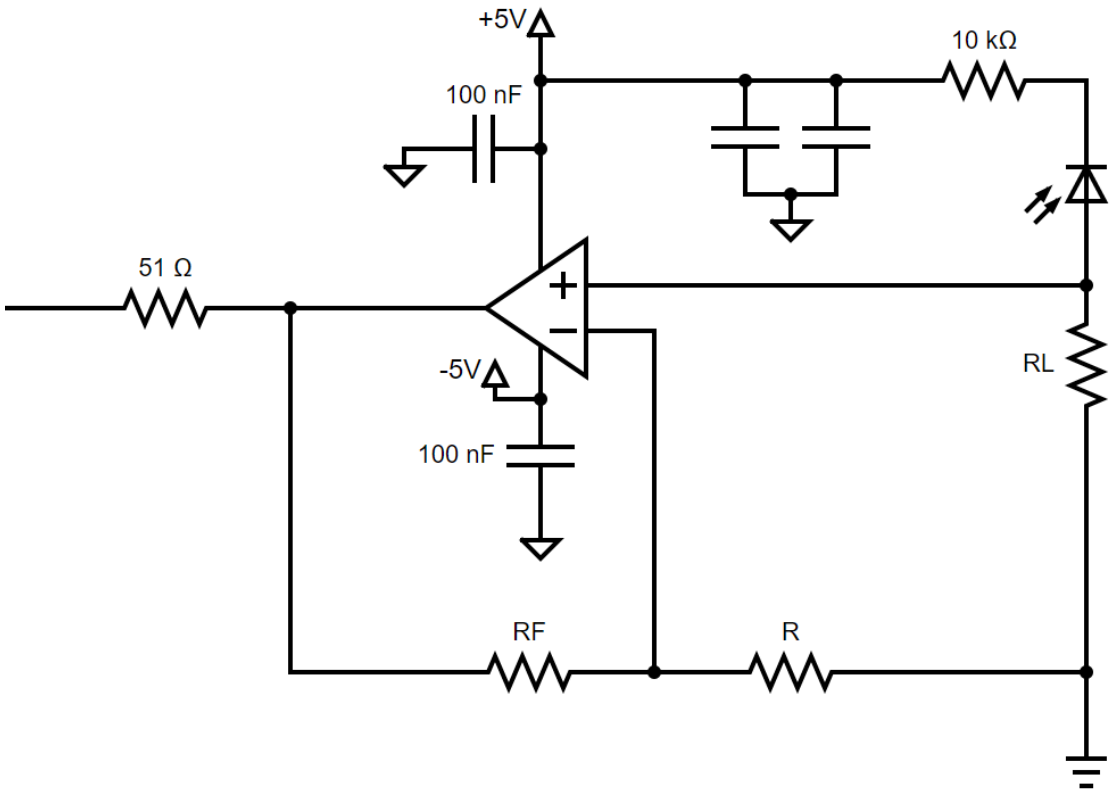

Figure 70: Optode Analog Output Circuit

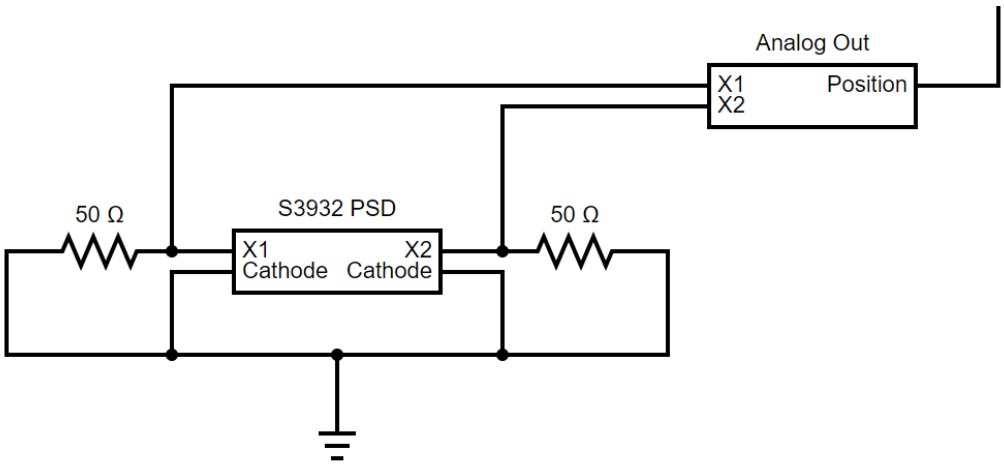

Figure 71: Refractometer Analog Output Circuit

7.2 Preliminary Refractometer Test

An experiment was devised with a tank of water, a cheap glass prism, and a 532nm laser. The goal was to fill the tank with freshwater, measure beam displacement, then

repeat with saltwater instead.

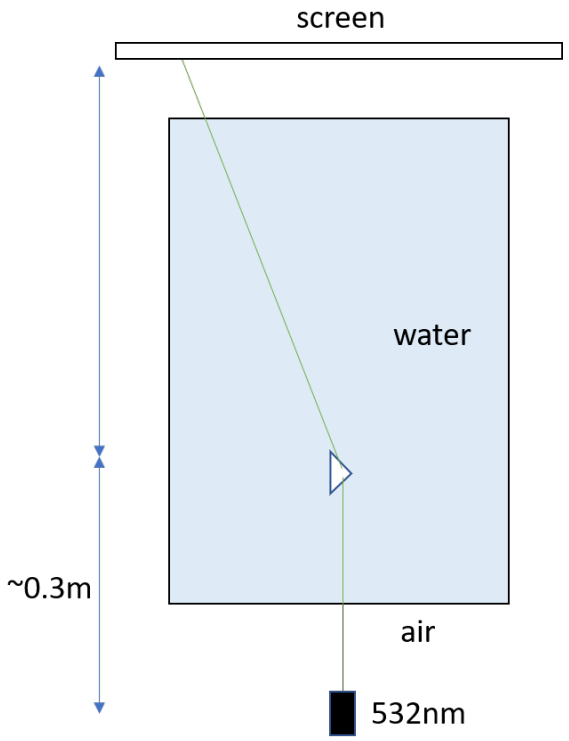

Figure 72: Layout for preliminary refractometer experiment.

The beam was marked with freshwater in the tank. With saltwater in the tank, the beam was also marked. After repeating the experiment a few times, inconsistent results were found. The largest beam displacement came on the first experiment attempt, and was in the wrong direction. This reduced confidence in the refractometer. From this experiment, we learned that there are other dominant factors at play. Particles in the water greatly affect the beams profile and the measurement.

Figure 73: Visual of experiment in progress.

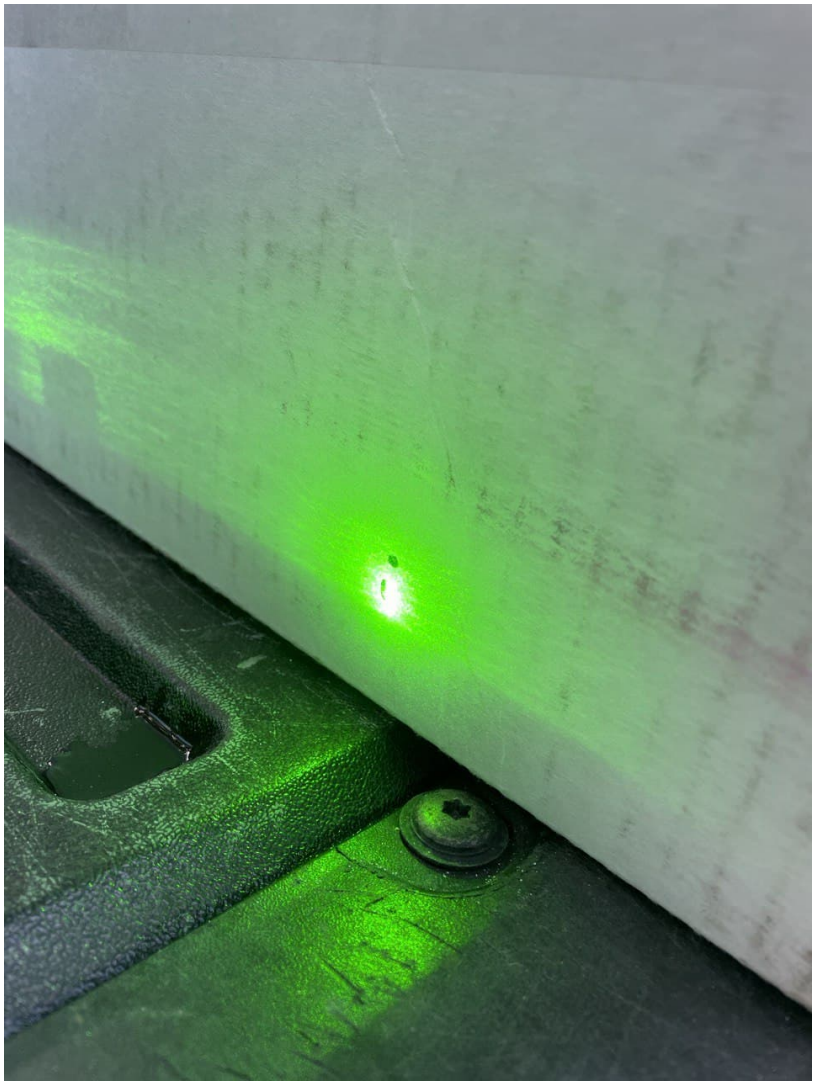

Figure 74: Beam displacement in an unexpected direction. The freshwaster beam deviation is marked by the sharpie dot.

The refractive index change between freshwater and salt water was calculated to be approximately 0.006. Over the meter this experiment was conducted, we expected to see a lateral deviation of 4.145mm. Strangely enough, we saw a vertical deviation of about that much.
From this preliminary experiment, confidence in the refractometer was reduced. It caused a design change to be implemented. A laser with a small spot size, a prism with a high refractive index, and a small distance traveled (in hopes of avoiding particles) is now necessary. A double prism configuration was certainly necessary if this single prism test was indicative of anything. This design rework was reflected in the part selection section of 3.6.5. Additionally, the expectations for the final demonstration were lowered.

7.3 Transmission Testing

We began with a goal of transmitting our data over a distance of 500 meters. Several locations were scouted out around the UCF campus at distances of 3 meters, 100 meters, and 500 meters. The 3 and 100 meter distances were measured across the top of Parking Garage C in order to get base measurements of signal strength, settings, and bit rate we were able to use. Our 500 meter test was done with the transmitting side on top of Garage C and the receiving side on the top of Garage H. Since our main goal was transmitting with as little power consumption as possible, we wanted to get a high bit rate, in order to reduce the air time, along with a small transmit power. We can see the ideal setting we found below. Transmission across 500 meters took approximately eight times the power to transmit as our 3 meter base. While this was a larger factor increase, it still succeeded as an extremely low power transmission, more than capable of transmitting sensor readings on a battery powered device.

3m Ideal Settings	
SF	7
BW (kHz)	500
Power (dB)	13
Consumption (mA)	31
RSSI AVG (dB)	-45.875
Air Time (ms)	12.86
Rb (kbps)	13.67188
Any Error %	20

100m Ideal Settings	
SF	7
BW (kHz)	125
Power (dB)	13
Consumption (mA)	31
RSSI AVG (dB)	-75.125
Air Time (ms)	51.46
Rb (kbps)	3.41797
Any Error %	20
Power Increase	4.001555

500m Ideal Settings	
SF	8
BW (kHz)	125
Power (dB)	13
Consumption (mA)	31
RSSI AVG (dB)	-79.5
Air Time (ms)	102.91
Rb (kbps)	1.95313
Any Error %	0
Power Increase	1.999806

Figure 75: Measured Signal Strength and Bit Rate of Chosen LoRa Settings.

8 Administration

We consider the administrative work associated with our project, including the budget, funding with NASA, and the timeline in which we have set due dates to complete certain parts of the project by.

8.1 Financial Considerations

Our group has submitted a proposal to NASA and been approved for a budget of $2,000. This budget comes through the FSGC which requires an overhead of 10% leaving us a remaining $1,800. Our collaboration with NASA includes trips to the Kennedy Space Center and so we want to allow a travel budget of $50 per group member which is $200 total. Our remaining budget of $1,600 is to be used on developing, prototyping and building our final device. Table 1 below is our current estimation of how our budget will be spent.

In order to not create a tedious itemized budget, each section of the below table has been over priced. This added padding in the budget estimation will include all of

the electrical and mechanical components needed for it to operate. This may include smaller items such as casing, resistors, screws, or any other component that is required to connect our devices together.

Product Description	Quantity	Price Estimate
Optode Sensor	1	$250
Refractometer	1	$200
Colorimeter	1	$200
Thermometer	1	$25
Ammonia Alert	1	$35
Heater	1	$70
Camera	1	$100
Aerator	1	$30
Thermal Camera	1	$150
Turbidity	1	$50
Computer	1	$90
Antenna	1	$100
Battery	1	$150
Chassis	1	$150
Total Cost Approximation		$1,600

Figure 76: Proposed Budget

8.1.1 Cost Analysis of manufacturing the Optode

In totaling the expenses associated with the materials needed to fabricate and assemble the oxygen optode, without considering the opportunity cost associated with the labor required to fabricate and assemble the device, or the cost of tools that are already available for use, the following tables have been created. It should be noted, however, that we borrowed toluene in order to fabricate our optode sensing layer, so the cost of toluene was not included in our total expenditures for this project.

Component	Quantity/Purchase	Quantity/Device	Multiples	Cost/Purchase	Cost/Device
PtTFPP	100 mg	3 mg	33	$203	$6.09
Toluene	100 mL	2 mL	50	$41.4	$0.828
Polystyrene ($m_w = 250,000$)	25 g	.2 g	125	$15.54	$0.12
Sterile Single-use Syringes	100	1	100	$13	$0.13
25x25 mm Hach Cover Slips	124	1	124	$38.52	$0.31

Table 26: Materials Required for the Optode Sensing Layer

Component	Quantity/Purchase	Quantity/Device	Multiples	Cost/Purchase	Cost/Device
Hamamatsu S5973 Si PD	1	1	1	$28.16	$28.16
TSHG5510 Vishay, 830nm LED	5	1	5	$7.56	$1.51
UV5TZ-395-30 Bivar UV LED	2	1	2	$4.65	$2.32
SCHOTT OG-570 Longpass Filter	1	1	1	$15.3	$15.3

Table 27: Optode Source and Detection Components

Total cost of materials for sensing layer (not including toluene) = $311.46
Per-device cost of materials for sensing layer (not including toluene) = **$7.48**
Total cost of source & detection components = $55.67
Per-device cost of source & detection components = **$47.29**
Total Cost of one Optode = $54.77

8.2 Timeline of Project

Here we describe the schedule that we will follow in completing certain milestones associated with this project, as planned ahead of time. Since this project spans two semesters, that is the time frame we are looking at here.

8.2.1 Senior Design I

This is a two semester project. The first semester is the design and purchasing phase which occurs in Senior Design 1. This first phase consists of the research, outline, proposals, and part selection. Purchasing of the selected parts should be completed by the end of the semester in December of 2020. This allows the winter break before the second semester to be a buffer for any shipping delays or out of stock conveniences. As this project was selected in partnership with NASA and FSGC, there were extra steps involved in submitting proposals and budget requests through the UCF Office of Research. This was accomplished by the middle of October 2020 and the project was approved by Dr. Mukherjee at the Florida Space Grant Council in conjunction with the Kennedy Space Center senior design project liaisons. After this approval, our team will receive guidance from the KSC as we develop further into our work. Teaming up with KSC in this way has also allowed us to have a much higher budget than a typical senior design project. More parties involved will of course add delays as we communicate back and forth on different schedules, but the guidance and infusion of extra funding more than makes up for it.

The initial development stage will be spent determining the possible constraints pertaining to the technical and economic feasibility of our design. We plan to take inspiration from preexisting sensor suites that are utilized on earth based CELSS models for our design. We will adapt our prototype as needed to account for the additional challenges of operating with in-space radiation and various levels of gravity. Employing a photonics-based approach, we will demonstrate the usefulness of optode sensors and refractometry in this sensor package.

The beginning of our Fall 2020 semester through the end of the 2020 calendar year will

be spent on research for our proposal and prototyping of the optode, refractometer, and imaging system. Initially, the group will develop a plan for resource allocation and logistics to fit into our budget. Modeling will be done in preparation for actual construction that will follow. The second semester of our project, ranging from January through April of 2021 will be spent building the designed prototype, testing it, and finally demonstrating its feasibility.

8.2.2 NASA Proposals

As this Senior Design project was presented to us as part of a NASA competition within the listed possible project ideas, we had to follow along with some extra steps and requirements that would not normally be required. One of these requirements was the need for extra documentation and proposals to be written and sent to the NASA Florida Space Grant Consortium. There were some projects that could win up to $500 and in the case of our project, deemed a NASA Competition, up to $1000 for a one semester project or $2000 for our two semester project. The only requirement was for all of our members to be US citizens which we are.

We chose the project titled: "Development of a standard Small Satellite (e.g. CubeSat range) research platform for Life Sciences research - Ecosphere."
This project had the following description: Development of a standard Small Satellite (e.g. CubeSat range) platform for researching a closed self-sustaining closed ecological environment consisting of active micro-organisms, small shrimp, algae and bacteria (e.g., build your own or commercially available). NASA is seeking ideas on what capabilities are technically and economically feasible and how several common system elements can be assembled for keeping this ecosystem thermally balanced so it can be observed, as well as what sensor package is able to characterize the survival of an enclosed eco-system and how it reacts to the in-space radiation environment.

On September 11, 2020 we submitted to following proposal to Dr. Mukherjee:

Our project will be to develop a sensor suite to monitor a self-sustaining, hypersaline, closed ecological environment (CES) of brine shrimp, algae, and possibly other microorganisms. This suite will use electronic and optical sensors to observe the pH, dissolved oxygen, specific gravity, NO3-, NO2-, NH3, average temperature, and algae color for the purposes of maintaining thermal balance in order to characterize the survivability of the CES. The initial development stage will be spent determining the possible constraints pertaining to the technical and economic feasibility of our design. We plan to take inspiration from preexisting sensor suites on earth based CES models for our design. We will adapt our prototype as needed to account for the additional challenges of operating with in-space radiation and various levels of gravity. Employing a photonics-based approach, we will demonstrate the usefulness of optode sensors and UV spectrophotometry in this sensor package.

For our project to succeed at being useful for NASA, the overall size and body of the package will be designed to fit the dimensions of a typical CubeSat range small satellite. Image processing will be done to consider the color, particulate settling, bubbles, and culture medium transparency in an effort to infer the state of the system and the changes to the health of the aquarium while exposed to the off world radiation environment. The data will be collectively monitored to determine whether the sustainability is being affected by in-house dependency of the various water quality parameters or the external factors of the new gravitational and radiation environment. Upon completion of our project we hope the information obtained will give a better baseline of what research needs to be done to develop a sustainable and thriving closed microalgal-based microcosm that can be used by astronauts.

The beginning of our Fall 2020 semester, through the end of the 2020 calendar year, will be spent on research and design of our proposal. Initially, the group will develop a plan for resource allocation and logistics to fit into our budget. Modeling and simulations will be done in preparation for actual construction and testing that follows. The second semester of our project, ranging from January through April of 2021 will be spent building the designed prototype, testing it, and finally demonstrating its feasibility.

On the same day, Dr. Mukherjee responded that our project was approved and could move on to the second step which was due by October 16, 2020. This second step required finding a Faculty Advisor. We did so and Dr. Hagan the Interim Dean and Director of CREOL agreed to take on that role. At that point we contacted the UCF Office of Research (ORC). Through the UCF ORC we submitted the required administrative paperwork to Dr. Mukherjee and a funding account was set up for this project.

SENIOR DESIGN I	Responsible	Begin	Finish	Status
Familiarize ourselves with the project	Group 9	9/2/2020	9/11/2020	Completed
Role Assignments	Group 9	9/2/2020	9/18/2020	Completed
Identify Parts	Group 9	9/2/2020	9/18/2020	Completed
NASA and FSGC Proposals				
First Step	Group 9	9/2/2020	9/11/2020	Completed
Second Step	Group 9	9/11/2020	10/16/2020	Completed
Project Report				
Initial Project Document D&C	Group 9	8/27/2020	9/18/2020	Completed
Updated D&C	Group 9	8/27/2020	9/18/2020	Completed
Updated D&C V2	Group 9	9/21/2020	10/2/2020	Completed
60 Page Draft	Group 9	10/26/2020	11/13/2020	Completed
100 Page Draft	Group 9	11/9/2020	11/27/2020	Completed
Final Document Due	Group 9	11/23/2020	12/8/2020	In Progress
Research, Documentation, & Design				
Optode Sensor	John	9/18/2020	11/1/2020	Completed
Refractometer	Brandon	9/18/2020	11/1/2020	Completed
Colorimeter	John	9/18/2020	11/1/2020	Completed
Thermometer	John	9/18/2020	11/1/2020	Completed
Ammonia Alert	Brandon	9/18/2020	11/1/2020	Completed
Heater	Nicholas	9/18/2020	11/1/2020	Completed
Camera	Jennifer	9/18/2020	11/1/2020	Completed
Aerator	John	9/18/2020	11/1/2020	Completed
Thermal Camera	Brandon	9/18/2020	11/1/2020	Completed
Turbidity	John	9/18/2020	11/1/2020	Completed
Computer	Jennifer	9/18/2020	11/1/2020	Completed
Antenna	Nicholas	9/18/2020	11/1/2020	Completed
Battery	Nicholas	9/18/2020	11/1/2020	Completed
Chassis	Group 9	9/18/2020	11/1/2020	Completed
Order and Test Parts	Group 9			In Progress

Figure 77: Senior Design I Milestones

8.2.3 Senior Design II

Senior Design II beginning in January of 2021 starts the actual building and testing of the prototype itself. As we begin to put the selected parts together, we will try to adhere to all of our project goals and constraints. There will surely be plenty of redesigns and adjustments made as combining so many different components into a

single prototype invites a lot of room for error. As we get into that second stage of development in 2021, the guidance from our KSC and UCF advisors will definitely be invaluable. The application of what we have learned in our classes at UCF will be put to the test in a real world scenario. Since our group does not include any mechanical engineering students, we hope to be able to work with our peers from that department at UCF who are also working on similar projects. Since the mechanical and aerospace engineering students are less focused on the sensors, which are our primary focus, and more involved in developing the housing and chasis of the cubesat, we plan to coordinate with them for any welding that might be needed. The end of Senior Design II will include presentations and demos of the prototype. Unfortunately for our modern times we must learn to deal with a world wide pandemic and so demonstration of our project has added complexity. As live, in person demonstrations are not possible, we plan on creating different scenarios that can be recorded. These recordings will have to be included in our final presentations that will be done remotely through video conference.

SENIOR DESIGN II			
Build Prototype		4-Feb	Completed
Testing and Redesign		26-Feb	Completed
Finalize Prototype		29-Mar	Completed
Peer Presentation		5-Mar	Completed
Final Report		9-Apr	Completed
Final Presentation		20-Apr	Completed

Figure 78: Senior Design II Milestones

9 Conclusion

The Standard Small Satellite Research Platform for Life Sciences Research proved to be an instructive challenge in coordinating ideas between different platforms and disciplines. The nature of this project is interdisciplinary and requires a thoughtful effort from all of our team members to conquer the electrical, computer, and photonic elements of this project. The project provided for an open-ended approach to be taken, and our group had to show initiative in studying the biology of these aquatic systems to be able to provide a suitable solution for our customer, NASA.

Our research into Artemia and aquatic environments, gave us a list of prospective measurements to take to characterize the system. An engineering analysis was done to determine which of these measurements were feasible to characterize. ultimately, we decided on five parameters: dissolved oxygen, salinity, ammonia, temperature, and algae color. This lead to the development of five sensors, each being projects of their own. The dissolved oxygen and salinity measurements resulted in the design and development of photonic-integrated modules: an optode and a refractometer, respectively.

The project's modular design required an extra effort to be made at communication between our team members, and our projects components. It is a project in and of its own to design all the sensors, it is another to make them all communicate, work automatically, and transmit their meaningful data wirelessly. This project had many goals and individual features, ultimately, we hope to demonstrate that our platform can take the measurements we deemed to be essential to characterizing an aquatic system, record the data from those measurements, and transmit that data.

We recognize the importance in our work in that it serves as a learning tool for us and the customers interested in our project. We will take away that openness in communication and collaboration between disciplines is not only important, but necessary for any project that seeks to do something extraordinary. It can be extremely difficult to have many people effectively communicate on a complex project, that is why it is so important to adhere to the engineering standards, communication, and ethic techniques that we have been taught. Besides this great learning experience, we feel that we have largely accomplished our goal of designing a complex system, that is very modular in nature, into an integrated system that will hopefully give us a great building block to start from in senior design II.We hope that our project serves as an educational basis for a more refined platform to actually conduct life-form research in zero gravity environments for NASA.

10 Appendices

10.1 Copyright Permissions

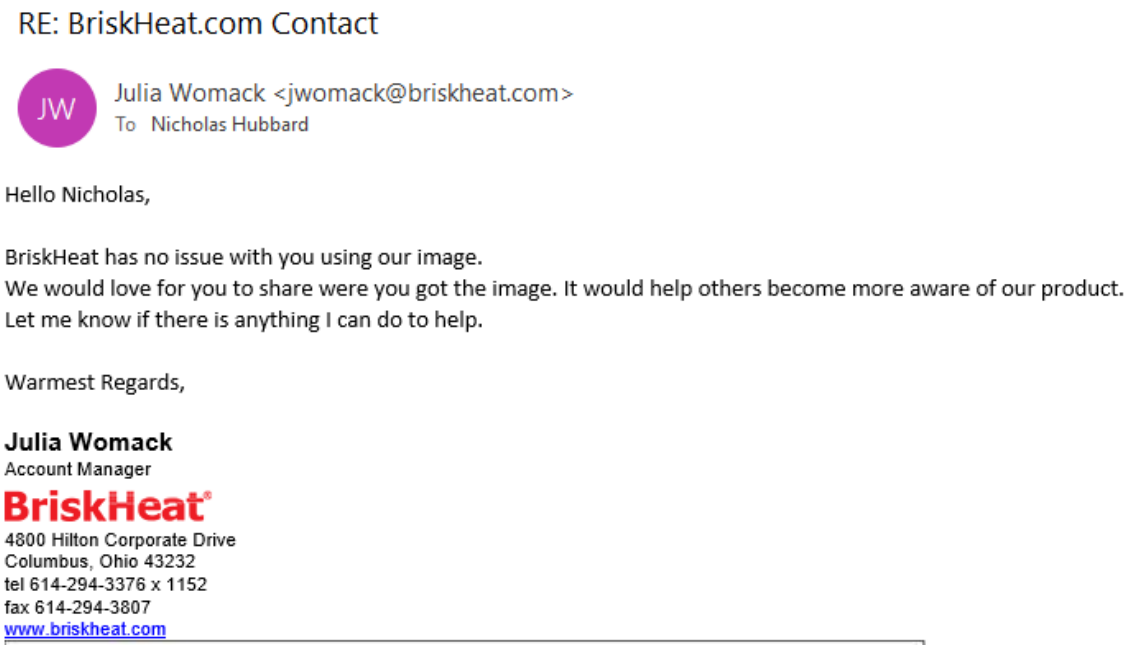

RE: BriskHeat.com Contact

JW

Julia Womack <jwomack@briskheat.com>
To Nicholas Hubbard

Hello Nicholas,

BriskHeat has no issue with you using our image.
We would love for you to share were you got the image. It would help others become more aware of our product.
Let me know if there is anything I can do to help.

Warmest Regards,

Julia Womack
Account Manager
BriskHeat
4800 Hilton Corporate Drive
Columbus, Ohio 43232
tel 614-294-3376 x 1152
fax 614-294-3807
www.briskheat.com

Figure 79: BriskHeat.com

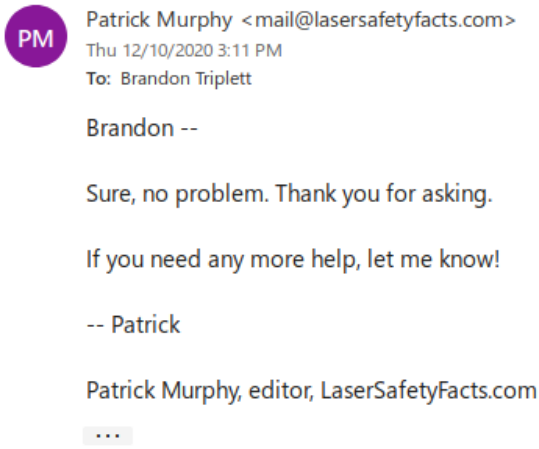

PM

Patrick Murphy <mail@lasersafetyfacts.com>
Thu 12/10/2020 3:11 PM
To: Brandon Triplett

Brandon --

Sure, no problem. Thank you for asking.

If you need any more help, let me know!

-- Patrick

Patrick Murphy, editor, LaserSafetyFacts.com

...

Figure 80: Laser safety classification table permission to use as seen in figure: 44

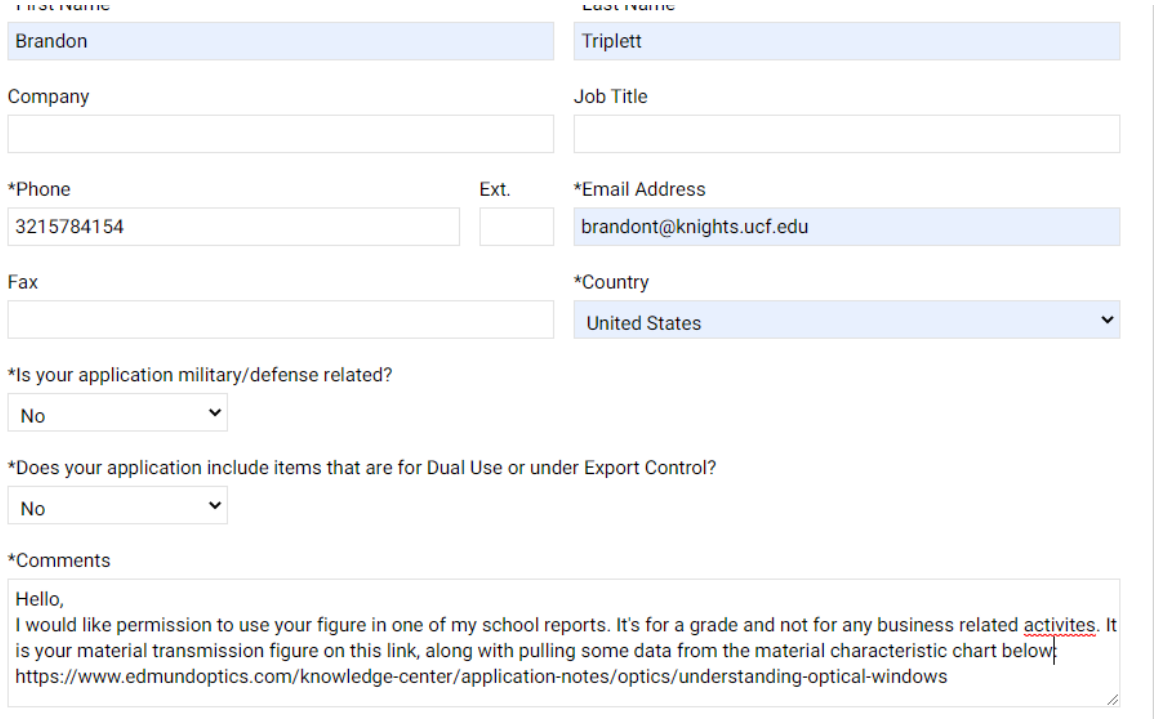

Figure 81: Edmonds IR window transmission charts and material characterization data I used. Figures: 13 12 29

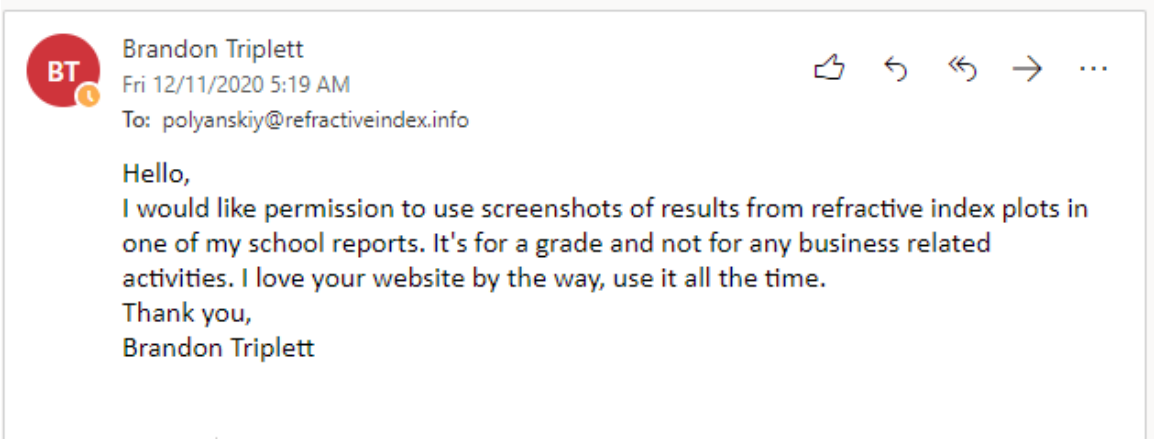

Figure 82: Screenshots of refractive index charts of optical materials considered for the prism. Figures: 16 15 14

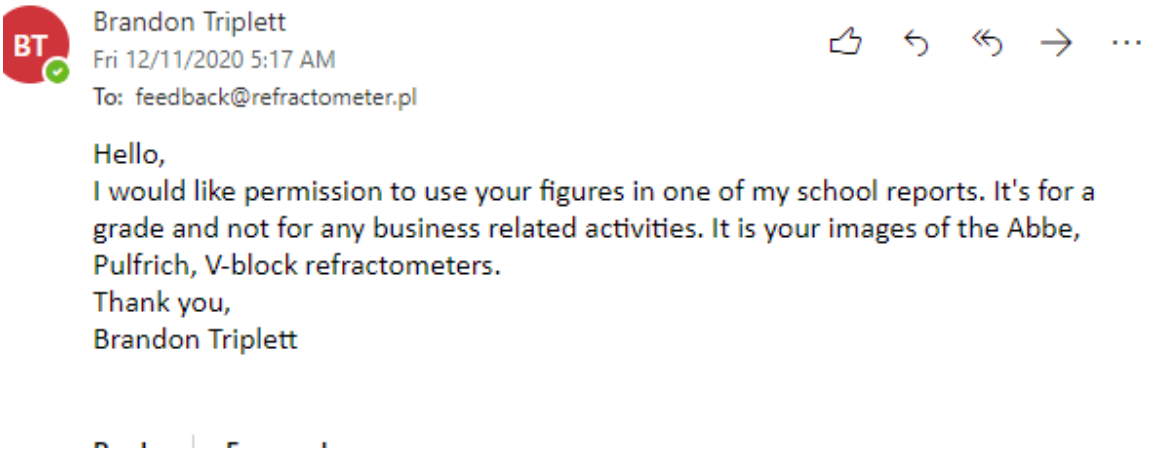

Figure 83: Abbe, pulfrich, vblock refractometer figures: 9 10 11

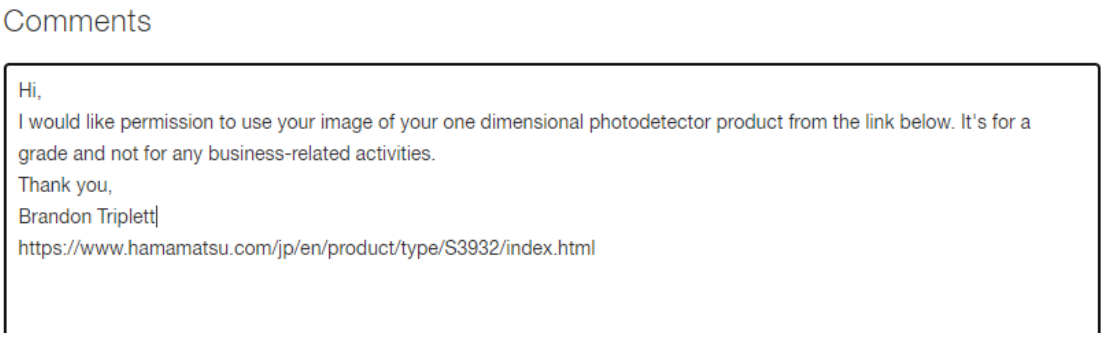

Figure 84: Chart and image from this website for photodiode array [1]

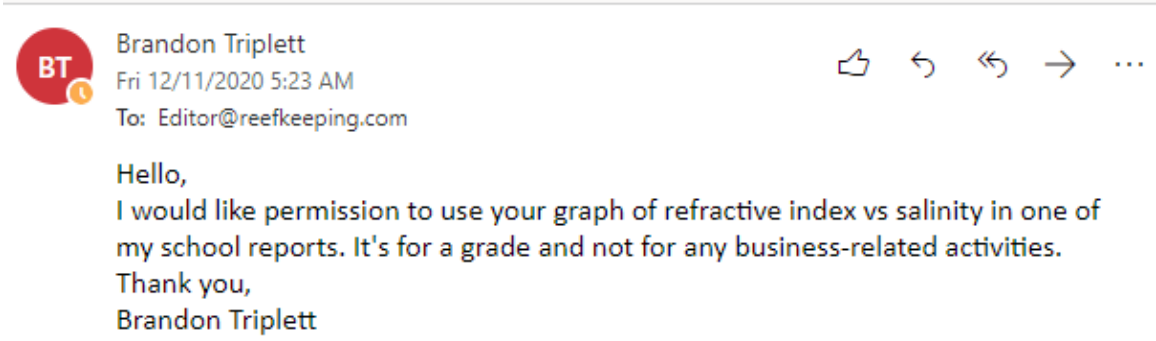

Figure 85: Chart for refractive index vs salinity as seen in figure: 12

References

[1] Mitsubishi electric(1/ 3)as of nov. '04ml1xx25 series mitsubishi laser diodesfor optical information systems. Technical Report ML101J25, Mitsubishi, November 2004.

[2] General requirements. Standard, Occupational Safety and Health Association, Geneva, CH, March 2020.

[3] Eye and face protection. Standard, Occupational Safety and Health Association, Geneva, CH, March 2020.

[4] Sigma Aldrich. 5,10,15,20-tetrakis(pentafluorophenyl)-21h,23h-porphine palladium(ii). `https://www.sigmaaldrich.com/catalog/product/aldrich/673587?lang=en&region=US`, 2020. Accessed: 2020-09-17.

[5] Francisco Amat. Utilización de artemia en acuicultura. 1985.

[6] Alireza Asem, Amin Eimanifar, Gilbert Van Stappen, and Shi-Chun Sun. The impact of one-decade ecological disturbance on genetic changes: a study on the brine shrimp artemia urmiana from urmia lake, iran. *PeerJ*, 7:e7190, 2019.

[7] Atmel. *8-bit Atmel Microcontroller with 16/32/64KB In-System Programmable Flash*, 2014.

[8] Roswell W Austin and George Halikas. The index of refraction of seawater. 1976.

[9] T Bharathidasan, Bhavana Rikhari, Dijo Prasannan, V Dinesh Kumar, RPS Chakradhar, and Bharathibai J Basu. Studies on the fabrication and characterization of optical sensor coatings for aerodynamic applications. *Journal of Applied Sciences(Faisalabad)*, 12(16):1646–1650, 2012.

[10] Santa Cruz Biotechnology. Tris(4,7-diphenyl-1,10-phenanthroline)ruthenium(ii) bis(hexafluorophosphate) complex. `https://www.scbt.com/p/tris-4-7-diphenyl-1-10-phenanthroline-ruthenium-ii-bis-hexafluorophosphate-co` `lang=en&cur=usd`, 2020. Accessed: 2020-09-17.

[11] BIVAR. *UV5TZ-XXX-XX*, 4 2009.

[12] Christian Blaise. Microbiotesting: An expanding field in aquatic toxicology. *Ecotoxicology and Environmental Safety*, 40(1-2):115–119, 1998.

[13] Combi Blocks. 5,10,15,20-tetrakis(pentafluorophenyl)-21h,23h-porphine palladium(ii). `http://www.combi-blocks.com/cgi-bin/find.cgi?QC-3460`, 2020. Accessed: 2020-09-17.

[14] Sergey M Borisov and Ingo Klimant. Ultrabright oxygen optodes based on cyclometalated iridium (iii) coumarin complexes. *Analytical Chemistry*, 79(19):7501–7509, 2007.

[15] RA Browne and G Wanigasekera. Combined effects of salinity and temperature on survival and reproduction of five species of artemia. *Journal of experimental marine biology and ecology*, 244(1):29–44, 2000.

[16] Cyril Buttay. Buck chronogram, 2006.

[17] Cyril Buttay. Buck conventions, 2006.

[18] Cyril Buttay and Alessio Damato. Boost continuous discontinuous, 2006.

[19] Reef Central. Refractive index and salinity. `http://reefkeeping.com/issues/2006-12/rhf/#3`, 2020. Accessed: 2020-11-13.

[20] Chemistry LibreTexts. *17.5: Batteries and Fuel Cells*, 2020.

[21] Chun-Shan Chen, Tsung-Han Tsai, and Ming-Ta Chou. Optical image lens system, Nov 2016.

[22] Federal Communications Commission et al. Guidance on obtaining licenses for small satellites. *FCC Public Notice*, 5, 2013.

[23] Wikimedia Commons. Measuring principle v2.png. `https://commons.wikimedia.org/wiki/File:Measuring_Principle_v2.png`, 2020. Accessed: 2020-11-13.

[24] National Research Council et al. *Prudent practices in the laboratory: Handling and disposal of chemicals*. National Academies Press, 1995.

[25] Refractive Index Database. Optical constants of ag (silver). `https://refractiveindex.info/`, 2020. Accessed: 2020-11-13.

[26] Constant C Delwiche. The nitrogen cycle. *Scientific American*, 223(3):136–147, 1970.

[27] James N Demas, BA DeGraff, and Patricia B Coleman. Peer reviewed: Oxygen sensors based on luminescence quenching. *Analytical Chemistry*, 71(23):793A–800A, 1999.

[28] Eustace L Dereniak and Teresa D Dereniak. Geometric and trigonometric optics. 2008.

[29] Robert J. Diaz. Overview of hypoxia around the world. *Journal of Environmental Quality*, 30(2):275–281, 2001.

[30] Robert J Diaz. Overview of hypoxia around the world. *Journal of environmental quality*, 30(2):275–281, 2001.

[31] Alexander Doroshkin, Alexander Zadorozhny, Oleg Kus, Vitaliy Prokopyev, and Yuri Prokopyev. Laboratory testing of lora modulation for cubesat radio communications. In *MATEC Web of Conferences*, volume 158, page 01008. EDP Sciences, 2018.

[32] Gregorio Drayer and Ayanna Howard. Ecophysiological models in simulations of an aquatic habitat for closed-loop life support research. In *42nd International Conference on Environmental Systems*, page 3524, 2012.

[33] Edmonds Optics Worldwide. *The Correct Material for Infrared (IR) Applications*, N/A.

[34] Laser Saftey Facts. Laser classification table. `https://www.lasersafetyfacts.com/laserclasses.html`, 2020. Accessed: 2020-11-29.

[35] FCC. 47 cfr § 97.301 - authorized frequency bands. *Electronic Code of Federal Regulations*, Telecommunication, 2020.

[36] FCC. *Federal Register*, 2020.

[37] Robert Edward Fischer, Biljana Tadic-Galeb, Paul R Yoder, Ranko Galeb, Bernard C Kress, Stephen C McClain, Tom Baur, Richard Plympton, Bob Wiederhold, and Bob Grant Alastair J. *Optical system design*, volume 599. Citeseer, 2000.

[38] Fisher Scientific. *Material Safety Data Sheet (Toluene)*, 2 2008.

[39] Fluorophores.org. Pttfpp. `http://www.fluorophores.tugraz.at/substance/61`, 2020. Accessed: 2020-12-11.

[40] Gonzalo M Gajardo and John A Beardmore. The brine shrimp artemia: adapted to critical life conditions. *Frontiers in physiology*, 3:185, 2012.

[41] Barbara M Gilchrist. Haemoglobin in artemia. *Proceedings of the Royal Society of London. Series B-Biological Sciences*, 143(910):136–146, 1954.

[42] HAMAMATSU. *One-dimensional PSD*, 4 2011.

[43] HAMAMATSU. *High-speed photodiodes (S5973 series: 1 GHz)*, 11 2015.

[44] JA Hellebusi. Osmoregulation. *Annual Review of Plant Physiology*, 27(1):485–505, 1976.

[45] Safety of laser products - part 1: Equipment classification and requirements. Standard, International Electrotechnical comission, Geneva, CH, May 2014.

[46] NASA CubeSat Launch Initiative et al. Cubesat 101: basic concepts and processes for first-time cubesat developers. *no. October*, page 96, 2017.

[47] Programming languages — c. Standard, International Organization for Standardization, Geneva, CH, April 2017.

[48] Ingo Klimant, Michael Kühl, Ronnie N Glud, and Gerhard Holst. Optical measurement of oxygen and temperature in microscale: strategies and biological applications. *Sensors and Actuators B: Chemical*, 38(1-3):29–37, 1997.

[49] Ingo Klimant and Otto S Wolfbeis. Oxygen-sensitive luminescent materials based on silicone-soluble ruthenium diimine complexes. *Analytical chemistry*, 67(18):3160–3166, 1995.

[50] Sunil J Kulkarni. A review on research and studies on dissolved oxygen and its affecting parameters. *International Journal of Research and Review*, 3(8):18–22, 2016.

[51] Joseph R Lakowicz. *Principles of fluorescence spectroscopy*. Springer science & business media, 2013.

[52] Chad A Larson and Gary E Belovsky. Salinity and nutrients influence species richness and evenness of phytoplankton communities in microcosm experiments from great salt lake, utah, usa. *Journal of plankton research*, 35(5):1154–1166, 2013.

[53] Sang-Kyung Lee and Ichiro Okura. Photostable optical oxygen sensing material: Platinumtetrakis (pentafluorophenyl) porphyrin immobilized in polystyrene. *Analytical Communications*, 34(6):185–188, 1997.

[54] Ph Léger, DA Bengtson, KL Simpson, and Pi Sorgeloos. The use and nutritional value of artemia as a food source. *Oceanogr. Mar. Biol. Ann. Rev*, 24:521–623, 1986.

[55] Philipp Lehner, Christoph Larndorfer, Emilio Garcia-Robledo, Morten Larsen, Sergey M Borisov, Niels-Peter Revsbech, Ronnie N Glud, Donald E Canfield, and Ingo Klimant. Lumos-a sensitive and reliable optode system for measuring dissolved oxygen in the nanomolar range. *PLoS One*, 10(6):e0128125, 2015.

[56] Ying Ting Liu. *REVIEW AND DESIGN A MOBILE PHONE CAMERA LENS FOR 21.4 MEGA*. PhD thesis, University of Arizona, 2017.

[57] Thomas H MacRae. Molecular chaperones, stress resistance and development in artemia franciscana. In *Seminars in cell & developmental biology*, volume 14, pages 251–258. Elsevier, 2003.

[58] Thomas H MacRae. Stress tolerance during diapause and quiescence of the brine shrimp, artemia. *Cell Stress and Chaperones*, 21(1):9–18, 2016.

[59] Microchip. *megaAVR® Data Sheet*, 2020.

[60] Fereidun Mohebbi. The brine shrimp artemia and hypersaline environments microalgal composition: a mutual interaction. *Int. J. of Aquatic Science*, 1(1):19–27, 2010.

[61] E. Moreels, C. de Greef, and R. Finsy. Laser light refractometer. *Appl. Opt.*, 23(17):3010–3013, Sep 1984.

[62] NASA. Spectrum guidance for nasa small satellite missions. *NASA Spectrum Management Program*, Version 1.0 (2015.08.27, 2015.

[63] NASA. *Power*, 2020.

[64] NASA. *Thermal Control*, 2020.

[65] Bruno S Nunes, Félix D Carvalho, Lúcia M Guilhermino, and Gilbert Van Stappen. Use of the genus artemia in ecotoxicity testing. *Environmental pollution*, 144(2):453–462, 2006.

[66] Open-Source. *Quantum Chemistry*. LibreText, 2020.

[67] Edmund Optics. Schott og-570. `https://www.edmundoptics.com/p/og-570-125mm-dia-longpass-filter/11325/`, 2020. Accessed: 2020-12-11.

[68] Charles Perrow. *Normal accidents: Living with high risk technologies-Updated edition*. Princeton university press, 2011.

[69] J. Petajajarvi, K. Mikhaylov, A. Roivainen, T. Hanninen, and M. Pettissalo. On the coverage of lpwans: range evaluation and channel attenuation model for lora technology. In *2015 14th International Conference on ITS Telecommunications (ITST)*, pages 55–59, 2015.

[70] Donald B Porcella and J Anne Holman. Nutrients, algal growth, and culture of brine shrimp in the southern great salt lake. *The Great Salt Lake and Utah's water resources. Utah Water Research Laboratory, Logan, Utah, USA*, pages 142–155, 1972.

[71] PorphyChem. *Material Safety Data Sheet (PtTFPP)*, 10 2020.

[72] Yu Qian, Yong Zhao, Qi-lu Wu, and Yang Yang. Review of salinity measurement technology based on optical fiber sensor. *Sensors and Actuators B: Chemical*, 260:86–105, 2018.

[73] Michela Quaranta, Sergey M Borisov, and Ingo Klimant. Indicators for optical oxygen sensors. *Bioanalytical reviews*, 4(2-4):115–157, 2012.

[74] refractometer.pl. Abbe refractometer. `http://www.refractometer.pl/Abbe-refractometer`, 2020. Accessed: 2020-11-13.

[75] refractometer.pl. Block refractometer. http://www.refractometer.pl/V-block-refractometer, 2020. Accessed: 2020-11-13.

[76] refractometer.pl. Pulfrich refractometer. http://www.refractometer.pl/Pulfrich-refractometer, 2020. Accessed: 2020-11-13.

[77] James R Rosowski and Aris A Efting. Growth of the brine shrimp aremia franciscana kellogg (anostracoda) in the materials dispersion apparatus as a sealed microcosm. 1992.

[78] Chet Sandberg, N Robert Rafferty, Marcus Kleinehanding, and Juan Jose Hernandez. Electrical heat tracing: international harmonization-now and in the future. *IEEE industry applications magazine*, 8(3):50–56, 2002.

[79] Seachem. Ammonia alert. https://e-lss.jp/seachem/ammonia-alert.php, 2020. Accessed: 2020-12-11.

[80] A SEMTECH and Modulation Basics. An1200. 22. *LoRa Modulation Basics*, 46, 2015.

[81] Anders Tengberg, Jostein Hovdenes, Henrik Johan Andersson, Olivier Brocandel, Robert Diaz, David Hebert, Tony Arnerich, Christian Huber, Arne Körtzinger, Alexis Khripounoff, et al. Evaluation of a lifetime-based optode to measure oxygen in aquatic systems. *Limnology and Oceanography: Methods*, 4(2):7–17, 2006.

[82] Anders Tengberg, Jostein Hovdenes, Dennis Barranger, Olivier Brocandel, Robert Diaz, Juha Sarkkula, Christian Huber, and Achim Stangelmayer. Optodes to measure oxygen in the aquatic environment-dr. anders tengberg (goteborg university), jostein hovdenes (aanderaa instruments a/s), dennis barranger, olivier brocandel (nereides), dr. *Sea Technology*, 44(2):10–16, 2003.

[83] Øyvind Aasen Tengesdal. Measurement of seawater refractive index and salinity by means of optical refraction. Master's thesis, The University of Bergen, 2012.

[84] Texas Instruments. *MSP430G2x53, MSP430G2x13 Mixed-Signal Microcontrollers (Rev. C)*, 2013.

[85] Laura Torrentera and Stanley I Dodson. Ecology of the brine shrimp artemia in the yucatan, mexico, salterns. *Journal of plankton research*, 26(6):617–624, 2004.

[86] Laura Torrentera-Blanco. Ecology and evolution of yucatan peninsula. *Artemia. Doctor Thesis, University of Wisconsin, Wisconsin, EEUU*, 1993.

[87] Ivo Vertat and Ales Vobornik. Efficient and reliable solar panels for small cubesat picosatellites. *International Journal of Photoenergy*, 2014, 2014.

[88] VISHAY. *High Speed Infrared Emitting Diode, 830 nm, GaAlAs Double Hetero*, 10 2012.

[89] Xu-dong Wang and Otto S Wolfbeis. Optical methods for sensing and imaging oxygen: materials, spectroscopies and applications. *Chemical Society Reviews*, 43(10):3666–3761, 2014.

[90] Paul Westgate, Karen Kohlmann, Richard Hendrickson, and Michael R Ladisch. Bioprocessing in space. *Enzyme and microbial technology*, 14(1):76–79, 1992.

[91] Wikipedia. Refractometer. `https://en.wikipedia.org/wiki/Refractometer`, 2020. Accessed: 2020-11-13.

[92] Rachel L Yung, Mark A Gouthro, and James R Rosowski. The brine shrimp artemia franciscana in closed microalgal-based microcosms (biospheres). 1999.